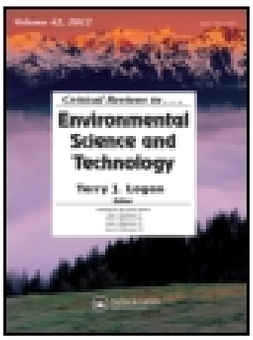

Critical Reviews in Environmental Science and Technology

ISSN: 1064-3389 (Print) 1547-6537 (Online) Journal homepage: http://www.tandfonline.com/loi/best20

Analysis of Fundamentals of Two-Phase Flow in Porous Media Using Dynamic Pore-Network Models: A Review

V. Joekar-Niasar & S. M. Hassanizadeh

To cite this article: V. Joekar-Niasar & S. M. Hassanizadeh (2012) Analysis of Fundamentals of Two-Phase Flow in Porous Media Using Dynamic Pore-Network Models: A Review, Critical Reviews in Environmental Science and Technology, 42:18, 1895-1976, DOI: 10.1080/10643389.2011.574101

To link to this article: http://dx.doi.org/10.1080/10643389.2011.574101

Accepted author version posted online: 20 Mar 2012.

Critical Reviews in Environmental Science and Technology, 42:1895–1976, 2012

ISSN: 1064-3389 print / 1547-6537 online
DOI: 10.1080/10643389.2011.574101

Analysis of Fundamentals of Two-Phase Flow in Porous Media Using Dynamic Pore-Network Models: A Review

V. JOEKAR-NIASAR and S. M. HASSANIZADEH
Earth Sciences Department, Utrecht University, Utrecht, the Netherlands

In this literature survey, different aspects of dynamics of two-phase flow in porous media are discussed. This review is based on the results of developed dynamic pore-network models and their applications. Thus, those concepts of dynamics of two-phase systems are addressed that have been already discussed in previous studies. Since it is not always possible to study different aspects of laboratory experiments, dynamic pore-network models were developed to gain new insights into the process. This characteristic is the major advantage of pore-network models, which give a better understanding of the physics of a process at pore scale as well as at the scale of representative elementary volume. Dynamic pore-network models are reviewed under different classifications; structure, computational algorithm, and local rules and applications.

KEY WORDS: dynamic pore-network model, ganglia, interfacial area, nonequilibrium effects, pressure field, relative permeability

1. INTRODUCTION

1.1. Two-Phase Flow

Everybody has seen the flow of water into a piece of cloth when it comes into contact with water or the flow of coffee into a sugar cube. All these phenomena involve movement of two or more immiscible fluids in a porous material, which is referred to as *multiphase flow in porous media*. We can also find two-phase flow in porous media in many technical applications such as fuel cells, paper pulp drying, food industry, oil recovery, textile industry,

Address correspondence to S. M. Hassanizadeh, Earth Sciences Department, Utrecht University, Budapestlaah 4, 3584CD, Utrecht, the Netherlands. E-mail: hassanizadeh@geo.uu.nl

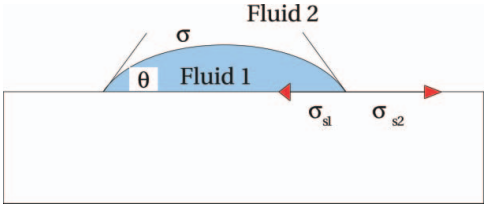

FIGURE 1. Fluid drop in contact with a solid surface. The contact between surface and fluids 1 and 2 is characterized by surface tensions σ_{s1} and σ_{s2} (Color figure available online).

and biomedical technology. These cover a wide range of applications, from large-scale applications such as oil recovery (10^3–10^5m) to very small-scale applications such as biological systems (10^{-5}–10^{-3}m).

In all of these systems, there is a moving interface between the fluids. The force acting on the interface between two immiscible fluids is referred to as the *capillary force*. The interfacial tension between two fluids relates the surface tension of each fluid with the solid phase through the following equation based on Figure 1.

$$\sigma_{s2} - \sigma_{s1} = \sigma^{nw} \cos\theta \tag{1}$$

From the contact angle, one can determine which fluid is the wetting phase and which fluid is the nonwetting fluid (relative to the solid). In Figure 1 since $\theta < \pi/2$, fluid 1 is the wetting phase and fluid 2 is the nonwetting one. Figure 2 shows definition of the fluids depending on the contact angle.

If the nonwetting fluid displaces the wetting fluid, it is referred to as *drainage* and the flow in opposite sequence is referred to as *imbibition*. It has been found that dynamic properties of a system can control the macroscopic pattern of the moving interface between the fluids (Lenormand, 1990; Lenormand et al., 1988). Dynamic properties of a system can be described by two parameters, namely viscosity ratio (M) and capillary number (Ca).

Viscosity ratio (M) is defined as a ratio of viscosity of invading fluid to the receding one. It is referred to as favorable if it is larger than 1 and as unfavorable if it is smaller than 1. Capillary number (Ca) is a dimensionless number, which illustrates the ratio of viscous forces to capillary forces:

$$Ca = \frac{\mu_{inv.} q_{inv.}}{\sigma^{nw}} \tag{2}$$

Here, $\mu_{inv.}$ $[ML^{-1}T^{-1}]$ is viscosity of the invading phase, $q_{inv.}[LT^{-1}]$ is total Darcy velocity (volume flowing per unit area per unit time) of the invading phase, and σ^{nw} is the interfacial tension $[MT^{-2}]$. If Ca is zero or very small, capillary forces dominate.

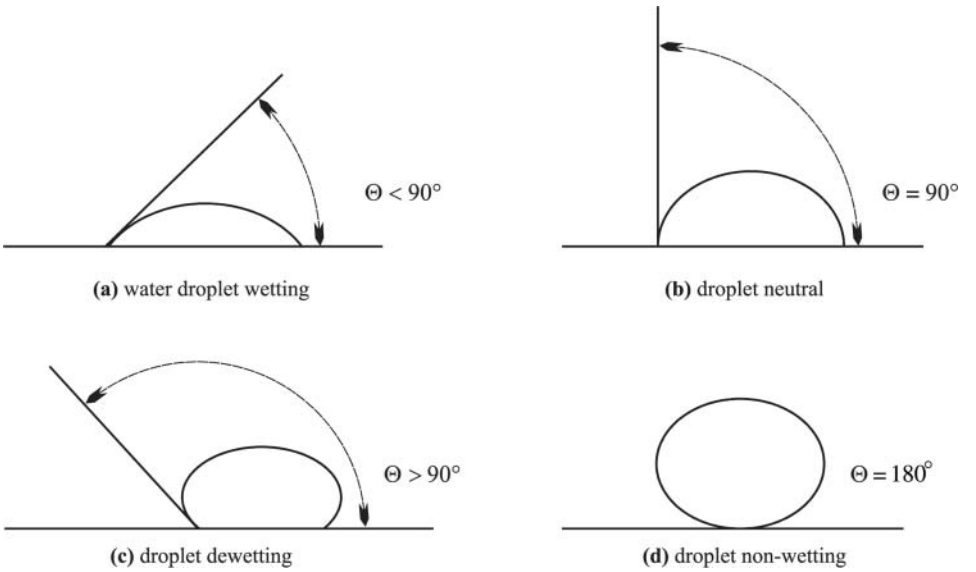

FIGURE 2. Definition of the wettability based on the contact angle.

Capillary number is a macroscopic parameter, which cannot be applied at pore scale. These pore-scale interface velocities depend on the global capillary pressure, interfacial tension, pore size, and viscosity ratio. For example, Lu et al. (1995) found that for ethanol-air system with a viscosity of 0.0119 Pa.s, in a pore with radius of 0.05 cm, the velocity of capillary rise can reach 20 cm/s at the moment of invasion into a pore. So, these velocities are not really representative of macroscopic phase velocity and pore-scale capillary number will be very different from macroscopic capillary number. Furthermore, it should be noted that Equation 2 is applied for a two-phase system. In a three-phase system (oil-water-gas), this definition can be applied to any pair of the fluids. But, since it is based on the velocity of a fluid, this definition by itself cannot give any information about the stagnant disconnected fluids.

Viscosity ratio is essential in development of the flow pattern and trapping of fluids. Lenormand et al. (1988) presented a phase diagram, which shows flow pattern under different capillary numbers and viscosity ratios, as shown in Figure 3. For favorable viscosity ratios, two flow patterns are possible depending on capillary number. If capillary number is very small (Figure 3a), capillary fingering is observed; if capillary number is large enough (Figure 3c), a stable displacement front occurs. Generally, if the capillary number is less than 10^{-6}, the viscous pressure drop in a phase is negligible and fluids movement is controlled by capillary forces. It means that, for this regime, intrinsic properties of the medium (pore size distribution) control the invasion. However, for unfavorable viscosity ratios, independent of how

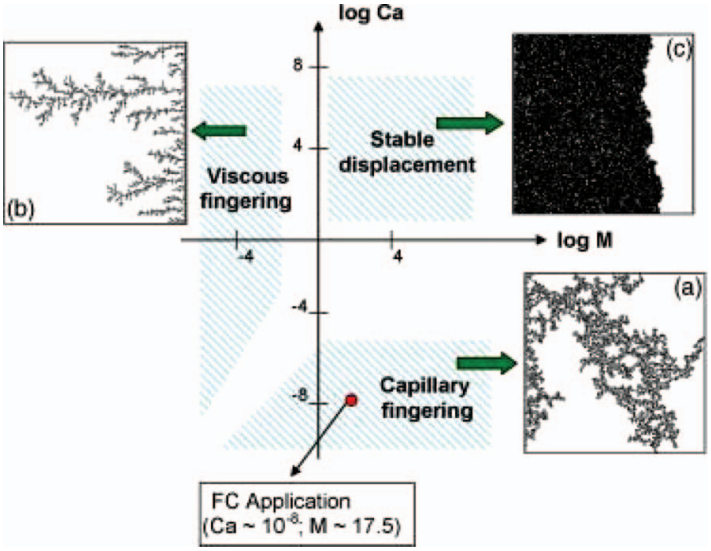

FIGURE 3. Schematic presentation of flow pattern under different capillary numbers (*Ca*) and viscosity ratios (*M*) based on Lenormand (1990) and Lenormand et al. (1988), courtesy of Sinha and Wang (2007) (Color figure available online).

large the viscous forces are, viscous fingering (Figure 3b) occurs and larger pressure gradient cannot stabilize the invasion front (Vizika et al., 1994).

1.2. Numerical Models for Two-Phase Flow

The two-phase processes have been investigated using various theoretical, computational, and experimental methodologies. Despite the enormous value of experimental work, often it cannot be used to its full potential due to several limitations such as complexity of processes, difficulty of measuring certain quantities, or uncertainty in results of measurements. Moreover, experiments are commonly expensive and time-consuming. Thus, theoretical and computational approaches can be used as complementary, and sometimes as a substitute tool to gain a more detailed understanding of processes. They can also be used to aid with a more effective design of experiments (see Joekar-Niasar et al., 2009).

In general, computational methods applied for studying two-phase flow systems can be classified into conventional continuum-scale numerical models and pore-scale models.

Continuum-scale models cannot explain the physical processes at pore scale, and its consequence at macroscale. For instance, classical macroscopic two-phase flow simulators cannot physically represent viscous fingering very well, since pore space geometry and topology as well as fluid properties are both important that create such invasion mechanism. To understand the

physics of multiphase flow under effect of capillary, viscous, and gravity forces, pore-scale simulators are of great importance.

In pore-scale simulators, one attempts to represent pore-scale geometry and topology of the medium and to solve the pore-scale equations within the given domain. Conventional pore-scale models may be subdivided into five different groups: Lattice-Boltzmann (LB), models (e.g., Knutson et al., 2001; Martys and Hagedorn, 2002), smoothed particle hydrodynamics approach (e.g., Liu et al., 2006; Tartakovsky and Meakin, 2005), level-set models (e.g., Prodanović and Bryant, 2006), percolation models (e.g., Wilkinson, 1984), and pore-network models (e.g., Blunt et al., 2002; Fatt, 1956; Held and Celia, 2001; Joekar-Niasar et al., 2008, 2009; Payatakes, 1982; Payatakes et al., 1980; Reeves and Celia, 1996). Among these methods, percolation models cannot provide any information about the transient processes. Other methods, compared to pore-network modeling, are more expensive due to differences in discretization of physical domain as well as the governing equations.

Pore-network models can be divided into two major classes: quasistatic pore-network models (see reviews by Blunt, 2001; Celia et al., 1995; Dullien, 1992) and dynamic pore-network models. Similar to invasion-percolation models, quasistatic pore-network models can be used for simulating equilibrium states of the capillary-dominated systems, where the dynamic effects in fluid distribution in absent. These models are based on the fact that the displacement of fluids is controlled by entry capillary pressure of individual pores. Quasistatic pore-network models can simulate equilibrium states of drainage and imbibition processes only. Flow conditions between equilibrium states are not modeled. For these models to be applicable, it is essential to remain close to equilibrium. Therefore, incremental changes in global pressure differences should be applied to go from one equilibrium to another equilibrium state. The comparison between quasistatic pore-network models and experiments show that these models can be used successfully for predictive purposes for capillary pressure-saturation, relative permeability curves (e.g., Blunt et al., 2002; Lerdahl et al., 2000; Øren et al., 1998), as well as interfacial area-saturation curves (e.g., Joekar-Niasar et al., 2009).

Under dynamic conditions, both viscous and capillary forces have to be included at the pore scale. Invasion at the pore scale is determined by the entry capillary pressure of network elements (e.g. pore throats) and time-rate of invasion is determined by local viscous and capillary forces. Thus, transient behavior of multi phase flow systems can be studied using dynamic pore-network models. Clearly, these models require much more complicated coding, robust solution methods, and efficient algorithms. Problems of numerical convergence and instabilities may cause major difficulties. Also, due to the highly non linear nature of the coupling between viscous forces and capillary forces, simulations are much more time-consuming and memory-demanding (Al-Gharbi and Blunt, 2005).

Among the dynamic pore-scale simulators, dynamic pore-network models are computationally less demanding. They have been used extensively, mostly for two-phase flow, but also for drying process (see Figus et al., 1999; Prat, 2007), gas nucleation and heavy oil depressurization (e.g., Bondino et al., 2009; Du and Yortsos, 1999), and three-phase flow (e.g., Pereira et al., 1996) in porous media. In contrast, LB method, which solves Navier-Stokes–type equation on a full voxel-based void domain, is computationally too expensive and memory demanding. Furthermore, in contrast to pore-network modeling, it requires postprocessing of the simulations. For instance, Porter et al. (2009) recently used LB method to simulate air-water flow in glass beads with physical domain size of less than 500 pores, which was discretized into 207 × 207 × 166 voxels. At a flux of 0.00008 muts^{-1} (mass unit per time step), approximately 50,000 *ts* were required to obtain only a 5% change in saturation, which took about 1.25 days to run on four amd64 CPU (2.8 GHz) machines in parallel. Roughly speaking, for their given specifications of domain and fluids, a full drainage simulation would take more than 100 days with a single processor. In another study, Pan et al. (2004) stated that computational limitations are of great concern when applying LB simulations for multiphase porous medium systems, even using large-scale parallel computing. They could not afford to simulate domains with sizes close to a reprensentative elementary volume (REV). The advantage of LB method, however, is that it can solve equations in an arbitrary pore space geometry and topology without simplification. In contrast, in pore-network modeling, the porous medium should be idealized to some simple geometries, such that essential features are adequately represented (Celia et al., 1995). This idealization can lead to loss of geometrical and topological information. Also, information on temporal changes within a single pore in pore-network models is not as detailed as in LB simulations, since every single pore is usually assumed as only one computational node. Nevertheless, simplifications in pore-network modeling allow us to simulate much larger domains and with much less computational effort; this is a major advantage.

1.3. Overview

This review is restricted to the computational aspects of dynamic pore-network modeling for two-phase systems and their application in investigation of dynamics of two-phase flow. We review geometrical and topological properties of the networks (section 2) as well as the computational algorithms employed in solving a two-phase system (section 3). Advantages and disadvantages of these algorithms as well as the numerical complexities are discussed in detail.

Furthermore, various applications of these models, which give new insights into the physics of two-phase flow, are discussed. Understanding

the dependencies of residual saturation (trapping) is important especially in reservoir engineering applications. Effect of geometrical and dynamic parameters on residual saturation in two-phase systems is discussed in detail in section 4. Section 5 covers the pressure field evolution under different viscosity ratios as well as nonequilibrium capillarity effects. Pore-network modeling has been employed to analyze the dependencies of nonequilibrium capillarity coefficient, which was proposed in the nonequilibrium capillarity theory (section 5.2).

Dynamic pore-network models have been extensively used to investigate topological property of the invasion front. The scaling of the interface as a fractal object under unfavourable viscosity ratios as well as the crossing over from invasion-percolation system to diffusion-limited aggregation and compact flow invasion are discussed in section 6. Furthermore, nonequilibrium effects on interfacial area are illustrated.

Section 7 discusses the disconnected flow (ganglia flow) regimes under effect of dynamic parameters. The discussion covers the use of pore-scale information to obtain a probability kernel to include the effect of ganglia flow regime in macroscopic simulators. Finally, it has been observed in the experiments that under ganglia flow regime, such as gas-liquid flow, there are nonequilibrium effects on relative permeability curves. These effects are discussed in section 8.

2. NETWORK STRUCTURE

Interstitial spaces in granular porous media are typically very irregular in shape and size. At the pore scale, there are larger void spaces as well as bottlenecks. To mimic the geometrical features of these interstitial spaces, pore-network models typically consist of pore bodies (larger voids) connected to each other by pore throats (narrow voids). However, the geometry of void spaces is not the only important factor to be considered in a representing a porous medium. Vogel and Roth (2001) showed that connectivity of the pore space, in addition to the pore geometry, plays an important role in soil hydraulic properties. The topological and geometrical properties of the dynamic pore-network models are discussed subsequently.

2.1. Network Topology

Mathematically network topology is based on the spatial properties of a network that are preserved under continuous deformations of network elements, without creating or deleting connections. Two porous media with the same topology can have very different hydraulic properties if the geometries are different (Joekar-Niasar et al., 2010b). The main topological characteristics of a network are (a) the spatial location of pore bodies and (b) the

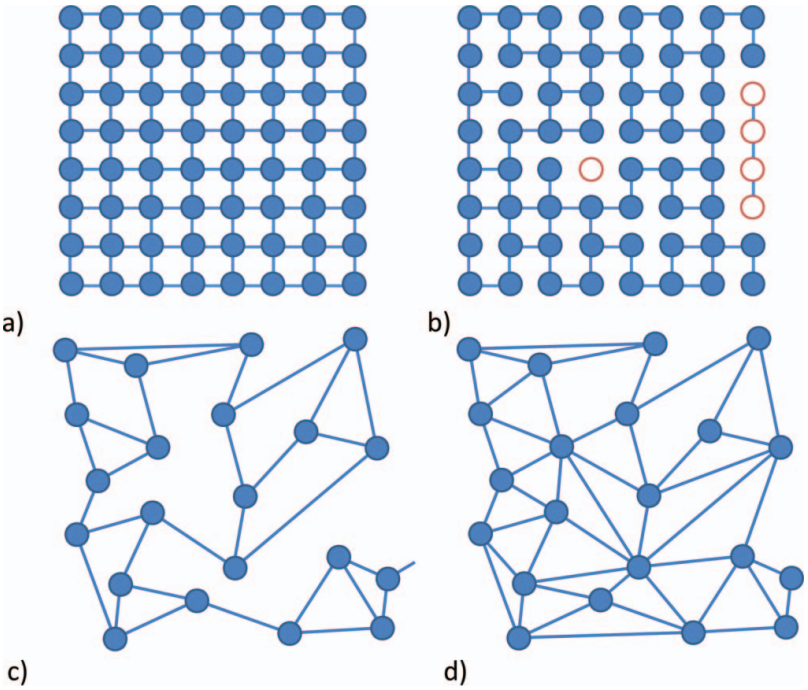

FIGURE 4. Classifications of pore networks: (a) structured regular, (b) structured irregular (red color illustrates isolated pores), (c) unstructured regular, and (d) unstructured irregular (Color figure available online).

connectivity of pore elements. The first property illustrates that the network is a structured or unstructured lattice. The second property is defined by coordination number, which is the number of pore throats connected to a pore body.

The simplest network structures are two-dimensional or three-dimensional regular lattices with square or cubic unit cells, respectively. We refer to each of these structures as a *regular structured network*. In such a network, pore bodies are located at the lattice nodes, which are all equally spaced, and pore throats are lined up along the lattice coordinates. In a regular structured network, the coordination number is equal to four for a two-dimensional network and six for a three-dimensional network. In a real porous medium, the centers of large pore spaces are not located on lattice points. Also, the number of pore throats connected to large pores is not the same for all pores. Therefore, unstructured pore-network models have been developed to mimic this feature of a real porous medium.

Based on these two characteristics of topology, pore-network models can be classified into four groups: structured regular, structured irregular, unstructured regular, and unstructured irregular networks (Figure 4). Up to now almost all dynamic pore-network models, except those developed by

King (1987), Blunt and King (1991), and Koplik and Lasseter (1985), have been structured. King (1987) and Blunt and King (1991) developed unstructured regular networks, and only in models developed by Koplik and Lasseter (1985) and Mogensen and Stenby (1998) was coordination number variable. Mogensen and Stenby (1998) developed a model with a variable coordination number up to a maximum of 26. To our knowledge, no unstructured irregular dynamic pore-network model has been developed untill now. Although up to now few irregular dynamic pore-network models have been developed, variation of coordination number in all of them has been selected arbitrarily and is not related to the pore geometry. To relate the network topology to pore geometry, Vogel and Roth (2001) adopted the so-called Euler characteristic, χ_v.

In case the structure is partitioned into convex volume elements each defined by a number of vertices, edges and faces, the Euler number may be calculated according to the classical Euler formula of graph theory as follows:

$$\chi_v = v - E + F - V \tag{3}$$

in which, v, E, F, and V denote number of vertices, number of edges, number of faces, and number of volumes, respectively. This equation can be used for any pore size larger than a threshold size of i. As a result for each category of pore size larger or equal than i, χ_v^i can be calculated, which shows the contribution of topology to the geometry for a given medium. However, network topology has not been considered as a design parameter in constructing dynamic pore-network models, since most of them have been developed for a generic and not specific porous medium.

2.2. Network Geometry

Network geometry is related to the geometrical shape and size of pore bodies and pore throats. Commonly, pore bodies are assumed to be cubic (e.g., Joekar-Niasar et al., 2010a) or spherical (Koplik and Lasseter, 1985) in shape. An exception is the work of Joekar-Niasar and Hassanizadeh (2011), who considered the pore bodies to be truncated octahedrons. For pore throats, however, a variety of geometrical shapes for the cross sections have been considered, as shown in Figure 5.

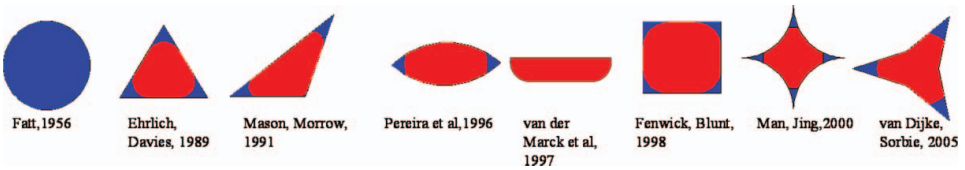

FIGURE 5. Various cross-sectional shapes used for pore throats in pore-network models (Color figure available online).

Angular cross sections allow for the existence of corner flow along the edges. This feature can allow simulating simultaneous flow of two phases within a pore throat. In a real porous medium, the wetting phase usually fills the corners and grooves, and the corner flow has a significant effect on flow mechanism at pore scale especially during imbibition. Therefore, researchers who have developed a pore-network model for simulating experiments generally assign angular cross sections to pore throats; see for example Van der Marck et al. (1997), who simulated micro-model experiments. Another example can be the quasi static model developed by Joekar-Niasar et al. (2010b), who considered hyperbolic polygonal cross sections for pore throats to simulated air-water P^c-S^w curves in glass beads. Existence of corner flow will allow phase continuity for the two fluids in a pore throat. Thus, the governing equation for the pressure field will be different from that for circular cross sections.

Many of dynamic pore-network models have pore throats with circular cross sections (e.g., Dias and Payatakes, 1986a, 1986b; Koplik and Lasseter, 1985), but there are few models with angular cross sections such as Al-Gharbi and Blunt (2005), who assumed triangular cross sections. Also, Hughes and Blunt (2000); Joekar-Niasar et al. (2010a); Mogensen and Stenby (1998); Singh and Mohanty (2003) used cubic pore bodies, and parallelepiped pore throats.

There are some other pore-network models, which do not explicitly consider pore bodies and pore throats. In these models, it is assumed that pore elements have varying cross sections; the narrowest part is located in the middle and it diverges toward both ends, which may be considered to play the role of a pore body (e.g., Aker et al., 1998a, 1998b; Al-Gharbi and Blunt, 2005; Knudsen et al., 2002; Knudsen and Hansen, 2002; Valvanides et al., 1998). But, no specific geometry or configuration has been assumed at the connection point of these pore elements. In this article, these pore elements are referred to as *composite pores*.

Another important geometrical parameter is the ratio of pore body diameter to pore throat diameter, referred to as *aspect ratio*. This parameter plays an important role in snap-off, which can influence trapping during imbibition. For example, Joekar-Niasar et al. (2009) did not find any trapped nonwetting phase at the end of imbibition in a high-porosity domain with small aspect ratio. Effect of aspect ratio on residual saturation is discussed in detail in section 4.3.

3. COMPUTATIONAL ALGORITHMS

Continuum-scale equations of two-phase flow in porous media are usually solved for the pressure and the saturation of wetting or nonwetting phases. Ignoring gravity effect, the following system of equations for a rigid porous medium and incompressible immiscible nonreactive fluids should be

solved:

$$\phi \frac{\partial S^\alpha}{\partial t} = -\nabla \cdot \mathbf{u}^\alpha, \quad \alpha = n, w$$

$$\mathbf{u}^\alpha = -\frac{1}{\mu^\alpha} k^\alpha \mathbf{K} \nabla P^\alpha, \quad \alpha = n, w$$

$$S^w + S^n = 1$$

$$P^c = P^n - P^w = f(S^w) \tag{4}$$

where ϕ is the porosity, μ^α is the viscosity of phase α, S^α is saturation of phase α, $\mathbf{u}^\alpha$ is the velocity of phase α, $\mathbf{K}$ is the intrinsic permeability tensor, k^α is the relative permeability of phase α, P^α is the pressure of phase α, P^c is the capillary pressure, and w and n refer to the wetting and nonwetting phases, respectively. Obviously, these equations do not apply at the pore scale. A different, but somewhat similar, set of equations needs to be formulated at the pore scale. The form of these equations depends on how the fluid pressure fields are handled. Two general approaches exist: single-pressure and two-pressure algorithms, which are described in detail subsequently. These approaches are based on the following general assumptions:

- Fluids are assumed immiscible and incompressible, and the solid matrix is assumed to be rigid.
- Flow in the pore throats is assumed to have low Reynolds number such that inertial effects can be neglected. This allows us to use Washburn equation for fluid fluxes through pores. However, inertial term can be added as employed by Sorbie et al. (1995) in a single tube, and by Ridgway et al. (2002) in a network model with cylindrical pore throats. Ridgway et al. (2002) employed Bosanquet equation (Bosanquet, 1923), which includes inertial effects. According to Sorbie et al. (1995), under capillary forces flow in narrow pore throats could be faster than in large pore throats at shorter times, which disagrees with the Washburn equation.

3.1. Single-Pressure Algorithm

In this algorithm, regardless of the fluid occupancy of pore bodies, a single pressure is assigned to each pore body. This single-pressure algorithm is generally based on one of following three assumptions:

1. It is assumed that each pore body or pore throat can be occupied by only one fluid at any given time. This is generally applied to networks with circular cross sections (e.g., Aker et al., 1998a, 1998b, Van der Marck et al., 1997).

2. It is assumed that both fluids can be present within a pore body but not within a pore throat. Also, a major assumption is made that the local capillary pressure in pore bodies is negligible. Therefore, to each pore a single pressure is assigned (e.g., Blunt and King, 1990; Gielen et al., 2005).
3. It is assumed that pore bodies and pore throats may be occupied by both fluids. But then, an equivalent fluid is defined (averaged conductivities using the electric resistors concept); with an equivalent single pressure assigned to each pore body and an equivalent conductivity assigned to each pore throat (e.g., Al-Gharbi and Blunt, 2005; Mogensen and Stenby, 1998).

In all three cases, the volumetric fluxes through pore throats is calculated using an analog of Washburn equation. The complete system of the equations using single-pressure algorithm may be written as follows for a pore body i connected to a neighboring pore body j by a pore throat ij:

$$\begin{aligned} V_i \frac{\partial S_i^w}{\partial t} + \sum_{j=1}^{N_i} Q_{ij} S_{ij}^w &= 0 \\ Q_{ij} &= K_{ij} \Delta_{ij} \\ S_i^w + S_i^n &= 1 \\ \Delta_{ij} &= f\left(P_i^n, P_j^n, S_i^w, S_j^w, P_{ij}^c\right) \\ P_{ij}^c &= f(r_{ij}) \end{aligned} \tag{5}$$

where Q_{ij} is the total volumetric flux from pore body i to pore body j, N_i is the number of pore throats connected to the pore body i, P_{ij}^c $[ML^{-1}T^{-2}]$ is the entry capillary pressure of pore throat ij, P_i^α $[ML^{-1}T^{-2}]$ is the pressure of the phase α in the pore body i that can be wetting or nonwetting, S_i^w is the saturation in pore body i, r_{ij} is the radius of pore throat ij, and K_{ij} $[M^{-1}L^4T]$ is the equivalent hydraulic conductivity as a function of the pore throat radius, pore throat length and fluid viscosities. Please note that in every pore, only nonwetting or wetting phase pressure can be defined and superscript n and w does not mean that both pressures have been defined at the same time in a pore.

An important issue in single-pressure algorithm is how the equivalent pressure drop, Δ_{ij}, is related to the capillary forces in pore throat ij and it is related to fluid pressures at neighboring pore bodies. Two different formulations, proposed by Koplik and Lasseter (1985) and Van der Marck et al. (1997), are discussed here.

Based on fluids configurations in Figure 6, Koplik and Lasseter (1985) considered eight combinations of fluid occupancies in pore bodies i and j,

TABLE 1. Defining Δ_{ij} (Equation 5) based on fluid configurations in two neighboring pore bodies and a pore throat (Koplik and Lasseter, 1985), P_i^{α} is the pressure of α phase in pore body i, superscripts w and n denote wetting and nonwetting fluids, respectively.

Case	Fluid occupancy in pore body i	Fluid occupancy in pore body j	Δ_{ij}
1	nonwetting	nonwetting	$P_i^n - P_j^n$
2	wetting	wetting	$P_i^w - P_j^w = P_i^n - P_j^n - P_i^c + P_j^c$
3	nonwetting	wetting	$P_i^n - P_j^w - P_{ij}^c = P_i^n - P_j^n + P_j^c - P_{ij}^c$
4	wetting	nonwetting	$P_i^w - P_j^n + P_{ij}^c = P_i^n - P_j^n - P_i^c + P_{ij}^c$
5	meniscus at pore, nonwetting	nonwetting	$P_i^n - P_j^n$
6	meniscus at pore, wetting	nonwetting	$P_i^w - P_j^n + P_i^c = P_i^n - P_j^n$
7	wetting	meniscus at pore, nonwetting	$P_i^w - P_j^n + P_j^c = P_i^n - P_j^n - P_i^c + P_j^c$
8	wetting	meniscus at pore, wetting	$P_i^w - P_j^w = P_i^n - P_j^n - P_i^c + P_j^c$
	General form		$\Delta_{ij} = P_i^n - P_j^n + S_i^w(P_{ij}^c - P_i^c) - S_j^w(P_{ij}^c - P_j^c)$

as shown in Table 1. They assumed that up to two interfaces may exist in a pore throat *ij*. Based on these eight possibilities Koplik and Lasseter (1985) proposed following general form for Δ_{ij}, which covers all the options using saturations at pore bodies (Table 1).

$$\Delta_{ij} = P_i^n - P_j^n + S_i^w\left(P_{ij}^c - P_i^c\right) - S_j^w\left(P_{ij}^c - P_j^c\right), \tag{6}$$

in which S_i^w and S_j^w are the wetting saturations in pore bodies i and j.

Van der Marck et al. (1997) modeled a system similar to what Koplik and Lasseter (1985) used. Van der Marck et al. (1997) simulated drainage process and Koplik and Lasseter (1985) simulated imbibition process in circular cross sections, where corner flow is absent. They assumed pore throats to have a negligible volume compared with pore bodies. Therefore, the interface was

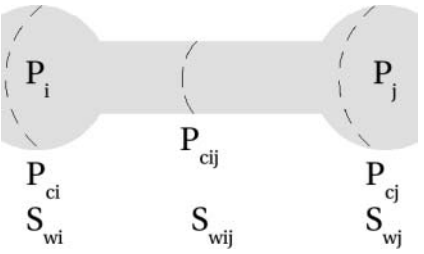

FIGURE 6. Schematic presentation of pore bodies i and j and pore throat ij and corresponding capillary pressures and saturations. Based on the occupancy of the pore bodies and interface location, pressure drop rules have been defined in Table 1.

TABLE 2. Defining Δ_{ij} based on fluid configurations in two neighboring pore bodies and a pore throat (Van der Marck et al., 1997)

Fluid occupancy in pore body i	Fluid occupancy in pore body j	Δ_{ij}
nonwetting	nonwetting	χ_{ij}
wetting	wetting	χ_{ij}
nonwetting	wetting	$\theta[\chi_{ij} - P^c_{e_{ij}}](\chi_{ij} - P^c_{e_{ij}}) + \theta[\chi_{ij}]\chi_{ij}$
wetting	nonwetting	$\theta[\chi_{ji} - P^c_{e_{ij}}](\chi_{ij} + P^c_{e_{ij}}) + \theta[\chi_{ij}]\chi_{ij}$
meniscus at pore, nonwetting	meniscus at pore nonwetting	$\theta[\chi_{ij} - P^c_{e_{ij}}](\chi_{ij} - P^c_{e_{ij}}) + \theta[\chi_{ji} - P^c_{e_{ij}}](\chi_{ij} + P^c_{e_{ij}})$

not tracked within the pore throat (i.e., spontaneous filling of a pore throat at the moment of invasion was assumed). Van der Marck et al. (1997) also assumed that up to two interfaces can exist in a single pore throat, one at each end. They included the gravity effects in the pore-network model. For a pore throat connecting pore body i to pore body j, and filled with a fluid with density ρ_{ij} $[ML^{-3}]$, a variable χ_{ij} was defined as follows:

$$\chi_{ij} = P_i - P_j - \rho_{ij} g(x_i - x_j) \tag{7}$$

Assuming a dummy variable x, Van der Marck et al. (1997) also defined a step-wise function, $\theta[x]$, as follows.

$$\theta[x] = \begin{cases} 1 & \text{if } x > 0 \\ 0 & \text{otherwise} \end{cases} \tag{8}$$

Considering definitions of χ_{ij} and $\theta[x]$, Δ_{ij} in Equation 5 was defined for different cases as shown in Table 2. The entry capillary pressure for pore throat ij was denoted by $P^c_{e_{ij}}$.

A similar formulation was also used by Dias and Payatakes (1986a, 1986b), Vizika et al. (1994), and Knudsen et al. (2002) with some modifications. Application of Δ_{ij} formulations in Equation 5 results in a nonlinear system of equations that has been solved with a combination of overrelaxation and dampened Newton-Raphson methods.

Obviously, corner flow is not included in the original Washburn equation (single-pressure approach). Nevertheless, this equation has been modified and used for angular cross sections, using the concept of equivalent phase described in situation 3 previously. The equivalent conductivity of a pore throat K^{eq}_{ij} is defined as the average of conductivities of phases using the rule of equivalent resistor for electrical resistor circuits. Thus, instead of solving for two pressure fields, one can solve for a single pressure field (see Al-Gharbi and Blunt, 2005; Bravo et al., 2007; Mogensen and Stenby, 1998).

The advantage of single-pressure approach is that it simplifies the problem significantly, and it can reduce computational effort. But, it has the

limitation that it cannot be used for angular cross sections properly. Al-Gharbi and Blunt (2005) have shown that single-pressure approach in angular cross sections can lead to inconsistent results in fluids occupancy in the network. If we use the same contact angle in static and dynamic simulations, one would expect that during drainage the same equilibrium fluid occupancy to be obtained from a quasistatic pore-network model and a dynamic pore-network model for the same boundary conditions. However, Al-Gharbi and Blunt (2005) showed that when employing the concept of equivalent phase pressure, snapshots of fluid occupancy obtained from quasistatic and dynamic pore-network models with the same boundary conditions are not the same.

3.2. Two-Pressure Algorithm

In this algorithm, when a pore body is filled with two fluids, each fluid is assumed to have its own pressure. Therefore, a local capillary pressure exists in a pore body. The complete system of the equations for the two-pressure algorithm may be written as follows:

$$\begin{aligned} V_i \frac{\partial S_i^\alpha}{\partial t} + \sum_{j=1}^{N_i} Q_{ij}^\alpha &= 0, \quad \alpha = n, w \\ Q_{ij}^\alpha &= K_{ij}^\alpha \left(P_i^\alpha - P_j^\alpha\right) \\ S_i^w + S_i^n &= 1 \\ P_i^c &= P_i^n - P_i^w = f\left(S_i^w\right) \\ K_{ij}^\alpha &= f\left(P_{ij}^c\right), \quad \alpha = n, w \end{aligned} \tag{9}$$

where K_{ij}^α is the hydraulic conductivity for phase α, and V_i is the volume of pore body i. This formulation was used initially by Thompson (2002) to investigate the imbibition process in fibrous materials for water-air system (favorable viscosity ratio). He solved pressure fields for each phase separately, including local capillary pressure. The local capillary pressure in each pore body was defined through the local interface curvature, corresponding to a given local saturation. This formulation provides the possibility to include mechanisms related to the variations of local capillary pressure (e.g., snap-off, counter-current flow) in simulations. In addition, numerical formulation of this approach is easier to implement compared with the single-pressure approach. However, similar to Equation 5, in capillary-dominated regimes, this equation shows a highly nonlinear behavior that should be treated carefully. Thompson (2002) stated that he could not find a good agreement between results of a slow dynamic simulation and a quasistatic simulation. Also, the model could not be used for very small capillary numbers. Later on, Joekar-Niasar et al. (2010a) and

Joekar-Niasar and Hassanizadeh (2011) used two-pressure algorithm with some numerical improvements in the pressure solver. They investigated nonequilibrium effects in capillary pressure and fluid-fluid interfacial area.

3.3. Numerical Difficulties

When capillary forces are comparable with viscous forces, there is a competition between them that creates high nonlinearities in pressure field at pore scale. Handling these nonlinearities in simulations is not trivial and equations should be treated carefully, especially in capillary-dominated flow.

The numerical problem in dynamic pore-network modeling was reported for the first time by Koplik and Lasseter (1985), who observed that saturations in two neighboring pore bodies were oscillating between 1 and 0 continuously. They referred to this as capillary pinning problem. This is due to the employment of decoupled scheme for calculation of pressure field and saturation. The decoupled scheme does not lead to a serious problem for viscous-dominated flow (i.e., large capillary numbers), since the pressure gradient in fluids (viscous forces) are much larger than the local capillary pressure imposed by pore geometry. Consequently, the nonlinearity of the problem at pore scale decreases. At low flow rates, local capillary forces are comparable with viscous forces. Thus, the fluid occupancy in pore throats will change in an on and off fashion in consecutive time steps and oscillation of saturations between two neighboring pores will be resulted (capillary pinning).

To overcome this problem, Koplik and Lasseter (1985) linearized the system using a constrained set of equations. For linearization, they defined a criterion to check whether local saturation in a pore body oscillated from 1 to 0 in three successive iterations. If this condition occurred, a no-flow condition was assigned to that pore body (dead-end pore body). Then, the pressure field was solved again. At each time step, validity of the local no-flow pore body (and pore throat) was also checked. However, this algorithm was extremely time-consuming.

The capillary pinning problem was also observed in other pore-network models, where no geometry was assigned to the connections of pore throats (i.e., no pore bodies were defined) as in Dias and Payatakes (1986a), Aker et al. (1998 1998b,a), and Knudsen et al. (2002). When an interface moving in a pore throat reaches a connection point (a node), new interfaces should be created in the connecting pore throats (see Figure 7). So, when a meniscus reaches the end of a pore throat (position 1), it is removed and three new menisci are created at position (δ) in the neighboring pore throats (position 2). When a new interface is created, a capillary pressure is assigned to it. If capillary forces are comparable with viscous forces, they can cause the interface to move back and forth within a pore throat in successive time

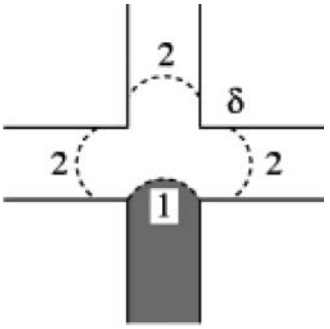

FIGURE 7. The motion of the menisci at a node. The nonwetting fluid (shaded) reaches the end of the tube (position 1) and moves a distance δ into the neighboring tubes (position 2). A proper time is recorded due to the small movement (Aker et al., 1998a).

steps. To overcome this problem, a part of all pore throat (denoted by δ in Figure 7) is defined as the pore body region. They forced the capillary pressure in a pore throat to change from P_{ij}^c to zero in the connection points of pore throat. This change of capillary pressure occurs in the range shown by δ. This region prevents immediate disappearing of menisci at position 2 and moving back to the initial position 1 in tubes (Figure 7). Dias and Payatakes (1986a, 1986b) assumed to have a δ_{ij} equal to 15% of the total length of pore throat *ij*. Aker et al. (1998 1998b,a) and Løvoll et al. (2005) assumed that δ_{ij} has a length equal to 1–5% of the length of pore throat *ij*.

In the two-pressure algorithm, Joekar-Niasar et al. (2010a) and Joekar-Niasar and Hassanizadeh (2011) proposed a semi-implicit saturation update, instead of explicit saturation update. Based on their approach, the discretized form of Equation 9 results in

$$V_i \frac{\left(S_i^w\right)^{k+1} - \left(S_i^w\right)^k}{\Delta t} - \sum_{j=1}^{N_i} \left(\frac{K_{ij}^n}{K_{ij}^{tot}} Q_{ij}^{tot} + \frac{K_{ij}^w K_{ij}^n}{K_{ij}^{tot}} \frac{\partial P_{ij}^c}{\partial S_{ij}^w} \left(\left(S_i^w\right)^{k+1} - \left(S_j^w\right)^{k+1} \right) \right) = 0 \tag{10}$$

in which local capillary pressure P_i^c is a function of radius of curvature of interface in the pore body. However, for simplicity, they related the radius of curvature of the interface to the local saturation. As a result, they approximated the local capillary pressure as a smoothed function of local saturation. This formulation includes a term related to viscous forces and another term related to capillary forces. They showed that it worked successfully for both unfavorable and favorable viscosity ratios for very small and large capillary numbers. Based on this formulation, they could

model very small capillary numbers for drainage and they found a precise agreement between quasistatic and dynamic simulations.

3.4. Boundary Conditions

Boundary conditions commonly considered in dynamic pore-network models are either constant pressure (*Dirichlet*) or constant flux. Implementing constant pressures at boundaries is numerically quite straight forward. However, since pore-network models have been mostly used to study two-phase flow for prescribed capillary numbers, constant flux boundary conditions have been applied more frequently. Applying constant flow rate in pore-network modeling is not trivial. At pore scale, the pressure field is sensitive to the local capillary pressure and this causes small fluctuations in flow rate in successive time steps. The constant flux boundary conditions have been implemented in various ways. A common approach is what Al-Gharbi and Blunt (2005) used. They specified a constant injection rate at the upstream boundary and a constant pressure at the downstream boundary. Although at each time step, fluid configuration and consequently pressure field might change, they assumed that the change in pressure drop required to maintain a constant injection rate between two consecutive time steps was small. But, it seems that this assumption was not valid for their network where the lattice size was only 9×9 pores. They selected a small time step to calculate the next pressure step and finally the discharge rate. Vizika et al. (1994) considered very narrow (high-resistivity) pore throats at the downstream boundary, and applied a constant flux at the upstream boundary. Applying narrow pore throats at downstream boundary can regulate the flux only during drainage. During imbibition, applying very fine pore throats at downstream can increase probability of the snap-off at the boundary that will result in large amount of trapped nonwetting fluid.

Aker et al. (1998 1998b) implemented the constant flux boundary conditions differently. Considering the Washburn equation, they suggested that for two-phase flow, total flux (Q) over the whole domain may be written in terms of the global pressure difference and capillary pressure:

$$Q = f_1(\Delta P) + f_2(P^c) \tag{11}$$

where ΔP is the difference between the pressures at upstream and downstream boundaries. Assuming a linear relationship, Aker et al. (1998 1998b) suggested the following equation:

$$Q(S^w) = A(S^w)\Delta P + B(S^w, P^c) \tag{12}$$

Clearly, $A(S^w)$ and $B(S^w, P^c)$ depend on two-phase fluid configurations. Thus, to calculate $A(S^w)$ and $B(S^w, P^c)$ for a given fluid saturation

(S^w), two equations are required. For a given fluid configuration, two different pressure drops can be imposed at the boundaries. Thus, two different flux rates can be calculated, which both should be consistent with Equation 12. So, two equations are resulted. By solving these two equations, $A(S^w)$ and $B(S^w, P^c)$ can be calculated. Knowing parameters $A(S^w)$ and $B(S^w, P^c)$, and knowing the desired injection rate (Q), proper pressure drop can be estimated. Since, $A(S^w)$ and $B(S^w, P^c)$ are dependent on the fluid configuration, they should be calculated at each time step, with the change of fluid configuration. This makes the problem computationally too expensive.

To investigate steady-state flow conditions, Constantinides and Payatakes (1996) and later Knudsen et al. (2002); Knudsen and Hansen (2002) defined periodic boundary conditions for saturation at inlet and outlet. Side boundaries were assumed to be periodic. In this approach, the amount of $\alpha-$phase that exits the domain is introduced from the corresponding pore throat at inlet. Thus, saturation of the whole domain does not change with time, and it is possible to simulate the steady-state conditions. However, to prevent simulation results being biased by initial conditions, simulations should be continued until the average values of pressure becomes constant.

3.5. Geometry and Conductivity Assumptions

Assumptions on the pore-network structure have a major influence on the complexity of computations and computational time. Major assumptions regard the volume as well as the resistance of pore elements. In many models (see Blunt and King, 1991; Blunt et al., 1992; Bravo et al., 2007; Gielen et al., 2004, 2005; Koplik and Lasseter, 1985; Touboul et al., 1987; Van der Marck et al., 1997), it is assumed that the volume of pore throats is negligible compared to the volume of pore bodies. At the same time, resistance of pore bodies has been considered to be negligible compared to that of pore throats. In some models, since no specific geometry was assigned to the connections (no pore body), volume and resistance were both assigned to the pore throats (e.g., Aker et al., 1998 1998b,a; Dahle and Celia, 1999; Knudsen et al., 2002; Knudsen and Hansen, 2002; Løvoll et al., 2005). The only case, where volume and resistance were assigned to both pore bodies and pore throats, is the work of Mogensen and Stenby (1998). Using the harmonic averaging, they calculated the effective resistance of a pore unit, composed of a pore throat and connected pore bodies. If a pore (body or throat) is considered to have resistance and volume at the same time, the fluid-fluid interfaces should be tracked inside that pore (body or throat), which is computationally expensive. However, the practical advantages of this model compared to the other ones have not been discussed.

3.6. Local Rules

In addition to the general equations required for simulating dynamics of two-phase flow in a pore-network model (Equations 5 or 9), some local rules should be defined as well. The local rules are applied to each and every single pore and they should be updated in every time step during simulations. General local rules, usually needed for the development of a dynamic pore-network model, are as follows:

- *Entry capillary pressure*: Nowetting phase can invade a pore-throat only when the local capillary pressure is larger than the entry capillary pressure of that pore throat. Entry capillary pressure can be calculated by writing balance of forces for a specific cross section (geometry) and based on contact angle and interfacial tension. The most common approach for calculating entry capillary pressure is the Mayer-Stowe-Princen (MS-P) method suggested by Ma et al. (1996); Mayer and Stowe (1965); Princen (1969a, 1969b, 1970), which is based on balance of forces for contact lines at the moment of invasion. Using this method, entry capillary pressures for different cross sections such as irregular triangular (Mason and Morrow, 1991), square (Fenwick and Blunt, 1998; Joekar-Niasar et al., 2010a), rectangular (Joekar-Niasar et al., 2009), star-shape (van Dijke and Sorbie, 2006), irregular hyperbolic triangular (Joekar-Niasar et al., 2010b), and regular hyperbolic polygonal (Joekar-Niasar et al., 2010b) have been calculated. The suggested relationships for the entry capillary pressure have been employed for both quasistatic and dynamic pore-network models. Furthermore, since the entry capillary pressure depends on the contact angle, one may include change of contact angle due to flow rate to use the same relationships.
- *Local conductivities*: Assuming Poiseuille equation to be valid in a pore element, its conductivity can be determined in terms of its geometry (cross section, length) and fluid property (viscosity, contact angle). In the case of pores with angular cross section, the conductivity for each phase will be a function of local saturation and thus local capillary pressure. Solving Navier-Stokes equation in pore throats with triangular and square cross sections, some algebraic equations for conductivities have been suggested (Patzek and Silin, 2001; Ransohoff and Radke, 1988; Zhou et al., 1997). Since in a dynamic process, the radius of curvature of interface is variable, local fluid conductivities should be calculated in every single time step to account for change of phase permeability with time.
- *Snap-off*: Generally, there are two mechanisms that regulate fluids displacement at pore scale: snap-off and piston-like displacement. The phenomenon in which wetting phase in the corners pinches off the nonwetting phase in the middle of pore throat (Figures 8 and 9) is referred to as *snap-off*. Snap-off can occur under both drainage and imbibition, but only

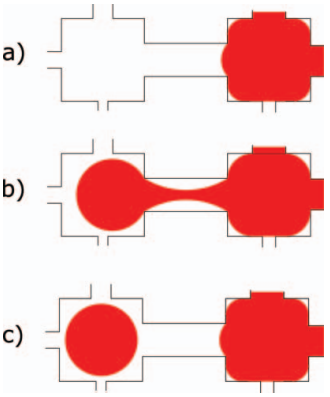

FIGURE 8. Schematic presentation of snap-off sequence during drainage (Color figure available online).

in a pore throat with wetting corner flow. Moreover, since under drainage nonwetting fluid is the invading phase, fluid interfaces are sandwiched to the corners and capillary pressure within pore throats builds up gradually. Thus, the possibility of snap-off decreases compared imbibition.

Under drainage, when the nonwetting phase saturation in a pore body increases, the local capillary pressure in that pore body builds up. It continues until it can invade a pore throat (Figure 8a). When the invasion occurs, if the nonwetting phase cannot fill the next pore body rapidly (Figure 8b) and cannot keep the capillary pressure in the pore throat high enough, it will be snappedoff by the wetting phase, which remains in the pore throat. After snap-off, there will be a disconnected blob of nonwetting phase in the second pore body (Figure 8c). Then, after capillary pressure builds up further in the first pore body, the nonwetting phase will invade the pore throat again. If the nonwetting phase does not fill up the second pore body, it will get disconnected again. This process continues intermittently until the second pore body is filled up and the nonwetting phase in both pore bodies can stay connected without snap-off.

Under imbibition, the wetting phase will first fill small pores, crevices, and grooves. If the wetting fluid is already present in the porous medium, it tends to flow through the films already present in the corners. Thus, a swelling of the wetting film during imbibition will happen (Figure 9b). As the injection of the wetting fluid continues, the filling grows so that eventually the wetting fluid is able to fill the pore throat (Figure 9c). This snap-off or choke-off mechanism was proposed for the first time by Roof (1970).

Similar to entry capillary pressure, capillary pressure at which snap-off occurs is a function of pore geometry, contact angle, and interfacial tension, as well as fluid occupancy in the neighboring pores (e.g., Vidales et al., 1998). The snap-off capillary pressure should be checked in the

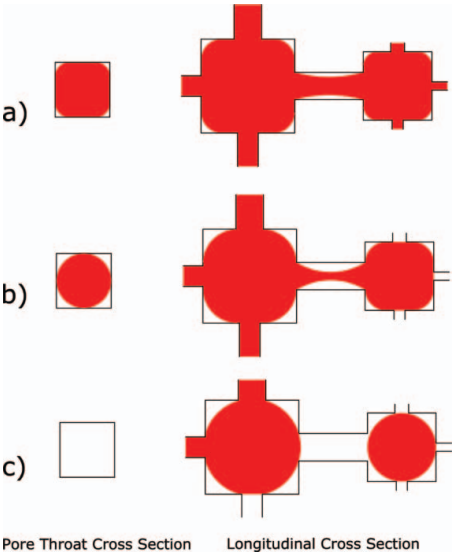

FIGURE 9. Schematic presentation of snap-off sequence during imbibition. With the decrease of local capillary pressure, the wetting phase in the corners of a pore throat swell until snap-off occurs (Color figure available online).

pores occupied by the nonwetting fluid, at each time step, to reconsider the fluid occupancy in them. Since this criterion depends on the fluid occupancy of the neighboring pores, dynamics of the system can influence significantly the snap-off occurrence. More detailed explanations about the dynamic effects on snap-off rate are given in the next section.

- *Piston-like movement*: If the invading fluid can completely sweep the receding fluid in a pore element, the displacement is referred to as piston-like movement. In absence of corner flow, only piston-like movement can occur. In general, piston-like movement and snap-off are mutually exclusive mechanisms. As Blunt et al. (1992) stated, snap-off can happen only when a piston-like movement is topologically impossible.

  If the capillary number is very small, snap-off is dominant and with the increase of capillary number, the possibility of snap-off decreases. Using a pore-network model, Mogensen and Stenby (1998) found that for capillary numbers between 10^{-8} and 10^{-7}, there was a transition from snap-off movement to piston-like movement. In general, the longer the pores aspect ratio (i.e., for relatively small pore throats), the higher the possibility of snap-off is, and vice versa. For instance, Joekar-Niasar et al. (2009) did not observe any snap-off in a micromodel experiment even for very small capillary numbers due to small aspect ratio (relatively large pore throats) and high porosity of the domain.
- *Trapping*: If the receding phase forms clusters that are disconnected from the moving part (which is commonly connected to its boundary

reservoir), it is considered to be trapped. In a water-wet porous medium, trapping of the nonwetting phase during imbibition is more probable than during drainage, since the wetting phase can be connected to its boundary reservoir through the corners. Since phase trapping (residual saturation) depends significantly on dynamic parameters, the degree of trapping are very different in dynamic and quasistatic simulations. In order to identify whether local disconnection causes larger groups of pores to get disconnected from their boundary reservoir, a search algorithm (such as *depth-first search*) in a tree structure is required (Cormen et al., 2009).

Search algorithm for checking the trapping of phases in pore-network models has been employed by Al-Futaisi and Patzek (2003), which can be applied either in quasistatic or dynamic pore-network models.

4. MACROSCOPIC RESIDUAL SATURATION

4.1. Factors Affecting Residual Saturation

When the receding fluid has fully disconnected from its corresponding boundary reservoir and cannot be expelled out of the domain, the corresponding saturation is referred to as residual saturation. In oil recovery, a major concern is to reduce the residual saturation of the oil (nonwetting fluid). There are many factors such as capillary number, viscosity ratio, aspect ratio, interfacial tension, and contact angle that influence the residual saturation significantly. The residual saturation can be reduced in two different ways: suppressing snap-off and mobilizing disconnected blobs. These are described subsequently.

- Suppressing the snap-off at pore scale, which results in reducing residual macroscale saturation. As explained before, under imbibition, snap-off causes the entrapment of the nonwetting fluid. However, the rate of snap-off is highly dependent on fluid properties as well as dynamic conditions. Snap-off mechanism can be suppressed by decreasing the capillary forces in comparison with viscous forces. Thus, by increasing the capillary number, decreasing the interfacial tension, and decreasing wettability, snap-off probability can be decreased and consequently the residual saturation will be reduced (Dias and Payatakes, 1986a, 1986b; Hughes and Blunt, 2000; Mogensen and Stenby, 1998; Vizika et al., 1994).
- Mobilization of the disconnected phase, even when it has been disconnected from the reservoir. Ng and Payatakes (1980) calculated at which capillary number the main terminal interfaces of a trapped ganglion might move. Main terminal interfaces are shown in Figure 10 by thick curves separating the blank pore space and the hatched pore space. When ganglia are trapped in a porous medium, under no-flow conditions, i.e. $\nabla P = 0$, neglecting gravity effects, the curvatures of the menisci should all be equal.

Imposing pressure gradient on the wetting phase, the pressure within the ganglion (P_o), the pressure in the water decreases along the ganglion in the flow direction. Thus, assuming that the pressure inside the ganglion is uniform, capillary pressure at downstream interface will be larger than that of the upstream interface.

Under this condition, there are backward forces on the ganglion due to capillary pressure and forward forces due to external pressure difference. The two forces may cancel each other so that the ganglion remains immobile. However, with the increase of the wetting phase pressure gradient to a critical value, menisci can move if at least one of its main terminal interfaces can cause drainage and back menisci allows imbibition (Figure 10). Once, this criterion is met, the ganglion cannot resist mobilization any longer. This displacement is referred to as a *rheon* (Ng and Payatakes, 1980). During the rheon, oil invades one of the downstream chambers and this displacement is referred to as *xeron*. Furthermore, the aqueous phase invades one of the upstream chambers that used to be occupied by the oil. This displacement is referred to as *hygron*. In porous media with very irregular geometry, it is possible that if the xeron occurs in an unusually large chamber, two (or more) hygrons may be necessary to supply enough oil for the xeron. The reverse may also occur. Finally, if proper conditions for a hygron develop at a site (where the ganglion is one chamber long), the ganglion may fission into two daughter ganglia.

Thus, to develop displacement criterion for the mobilization of oil ganglia in quasistatic pore-network models, menisci locations should be identified in calculations. Based on the schematic presentation shown in Figure 11, Ng and Payatakes (1980) assumed that all interfaces were locked in their unit cells, except for two; one downstream with index I and one upstream with index K. For this particular pair of menisci locations, there is a critical pressure gradient that may cause mobilization. By repeating this calculation for all possible pairs, one can identify the particular pair (i = I, k = K) for which the required pressure gradient is minimum. If the mobilization is to occur, it will proceed through the I^{th} and K^{th} menisci. This analysis is equivalent to determining the maximum mobility factor (β_{KI}), namely

$$\beta_{KI} = \Delta L_{KI} \cos\theta_{KI} / \left[J_{dr,I}\left(\theta_r^o\right) - J_{im,K}\left(\theta_a^o\right) \right] \tag{13}$$

in which, ΔL_{KI} is the distance between menisci K and I, θ_{KI} is the angle between the line connecting throats K and I and the macroscopic flow direction, $J_{dr,I}$ is the drainage curvature in the downstream meniscus I, $J_{im,K}$ is imbibition curvature in the upstream meniscus K, estimated as $J_{j,i} = \frac{4\cos\theta_j}{d_i}$, in which d_i is diameter of pore i with circular cross section.

Finally, Ng and Payatakes (1980) defined the following mobilization and stranding criterion:

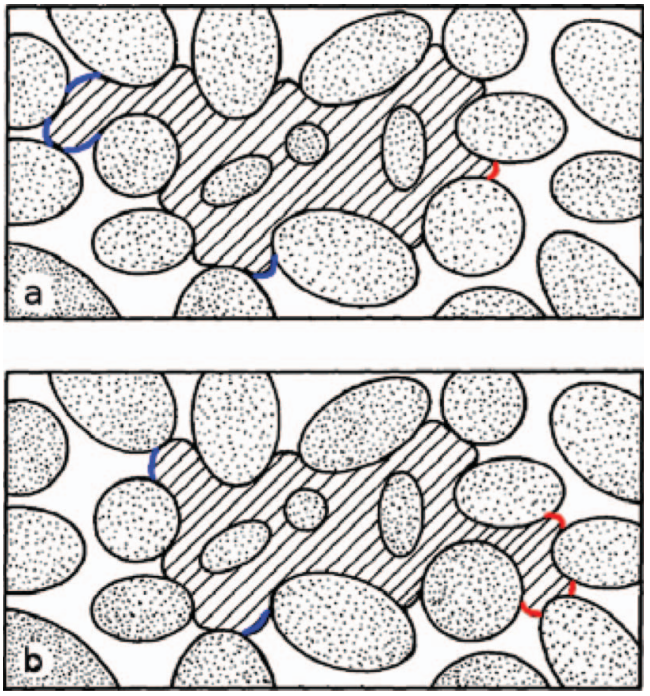

FIGURE 10. Schematic presentation of a ganglia movement showing drainage menisci and imbibition menisci. Flow direction is from left to right (Payatakes, 1982) (Color figure available online).

If $\beta_{KI}|\nabla P|/\gamma_{ow} \geq 1$, mobilization occurs.
If $\beta_{KI}|\nabla P|/\gamma_{ow} < 1$, stranding occurs.

Obviously, parameters influencing the snap-off rate can influence mobilization process as well. In the following section, effects of different parameters on residual saturation are discussed in detail. One should note that the mobilization of ganglia have been included only in dynamic network models developed by Payatakes and coworkers and Al-Gharbi and Blunt (2005).

4.2. Effect of Contact Angle

Contact angle can influence the possibility of snap-off especially during imbibition. Hughes and Blunt (2000) simulated the effect of flow rate and contact angle on snap-off and piston-like movement using a pore-network model. They showed that with the decrease of contact angle, possibility of snap-off increases. Thus, more disconnection of the nonwetting phase would happen, leading to more trapping of the phase. This is evident from Figure 12 where

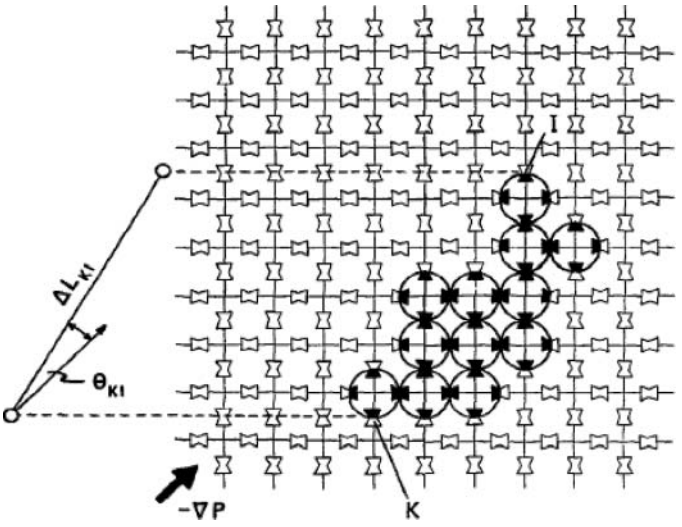

FIGURE 11. Concepts involved in the quasistatic criterion for mobilization (Payatakes, 1982)

residual oil saturation is shown to increase with the decrease in contact angle. They found that more than 50% of pore throats in their simulation were affected by snap-off when the flow rate was very low and contact angle was zero.

Constantinides and Payatakes (2000) modeled the effect of wetting films on snap-off during imbibition using a pore-network model. Their simulations showed that the wetting film could cause significant disconnection and entrapment of nonwetting phase during imbibition. This was specially so when contact angle as well as capillary number were small for unfavorable viscosity ratios.

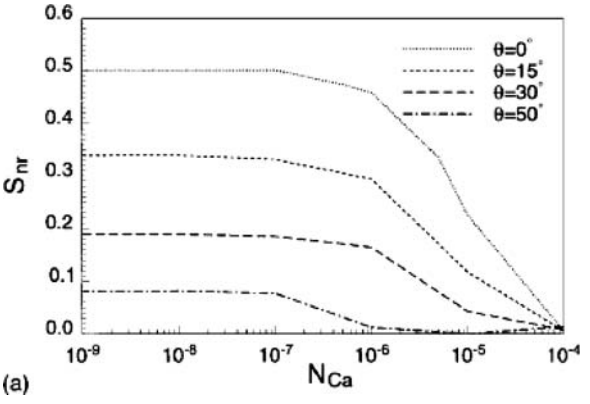

FIGURE 12. Effect of capillary number and contact angle on residual nonwetting saturation. Mobilization has not been included (Hughes and Blunt, 2000).

4.3. Effect of Aspect Ratio and Coordination Number

As explained earlier, capillary number and viscosity ratio are the main parameters that control the invasion mechanism and trapping. However, under some conditions, porous media topology and geometry can be so important that could suppress effect of dynamic parameters. For instance, in micromodel experiments, Joekar-Niasar et al. (2009) observed zero snap-off and consequently zero residual nonwetting phase saturation during imbibition. They simulated two-phase flow experiments with nitrogen and decane in a two-dimensional micro-model with 68-72% porosity and very small aspect ratio.

As explained in Section 2.2, the main geometrical and topological characteristics of pore networks are aspect ratio and coordination number, respectively. Some researchers have looked into the effect of structural simplification of porous media on qualitative results from pore-network models. Mogensen and Stenby (1998) investigated the effect of coordination number and aspect ratio on the residual nonwetting saturation (imbibition), using a pore-network model, which had variable coordination numbers up to 26. They found that, for high capillary numbers, the effect of coordination number on residual nonwetting phase saturation was minor compared to the aspect ratio, contact angle, and capillary number. However, for small capillary numbers, where snap-off movement may be more dominant than piston-like movement, effect of coordination number is significant. For example, for $Ca = 10^{-6}$, with the decrease of coordination number from 4 to 3 in a 40×40 two-dimensional network, residual nonwetting phase saturation increased from 13.3% to 29.4%. However, in general, effects of contact angle, aspect ratio and capillary number on residual saturation are more significant than the effect of coordination number.

Aspect ratio, which is a measure of the contrast between pore body and pore throat size distributions, can magnify the response of the system to the dynamic parameters under different conditions. For instance, there is a transition zone between snap-off-dominated and piston-dominated flow, as shown in Figure 13. For large aspect ratios, the transition is more abrupt than for small aspect ratios.

In another study, Chaouche et al. (1994) studied the effect of heterogeneity (by increasing the variance of pore sizes) on saturation distribution during drainage. They compared results of a continuum model and a pore-network model with their experiments. They did not find a good agreement between continuum and pore-network model results, which might be due to the small size of their pore-network model. Their model was based on the algorithm by Blunt and King (1991) for a two-dimensional network. Capillary number in the pore-network model varied between 1.5×10^{-6} and 1.5×10^{-3}, and three viscosity ratios were selected equal to 0.1, 1, and 10.

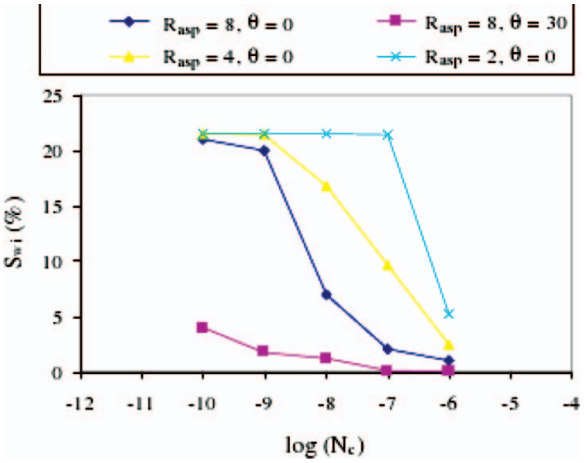

FIGURE 13. Effect of aspect ratio, contact angle, and capillary number on the amount of wetting fluid accumulating in the corners, Z = 6 (Mogensen and Stenby, 1998) (Color figure available online).

The nonwetting phase saturation rose as the low permeable region was approached, but then it decreased substantially as it entered the low permeable region.

Under favorable viscosity ratios during drainage, homogeneous displacement was compact in all regions (low and high permeability). Thus, high saturation values and high sweeping efficiency were resulted. Variation of saturation in a highly permeable region (with small capillarity effect) was insignificant. In contrast, for an unfavorable viscosity ratio, displacement was much less efficient and heterogeneity effects were quite pronounced in the saturation profile.

4.4. Effect of *Ca* and Viscosity Ratio

Many researchers have focused on the effect of dynamic parameters—capillary number and viscosity ratio—on residual oil saturation during imbibition. Koplik and Lasseter (1985) simulated the imbibition process with a viscosity ratio of unity. They showed that capillary number significantly influences the fluids distribution under imbibition. They studied the distribution of blob sizes remained in the pore network at the end of the imbibition experiment for different capillary numbers. They found that with the increase of capillary number, the size of trapped blobs decreased, but the number of trapped blobs increased. This is because viscous forces tend to fragment residual oil into small parts. Under low capillary number conditions, the size of trapped blobs got larger, but number of trapped blobs decreased compared to high capillary number conditions.

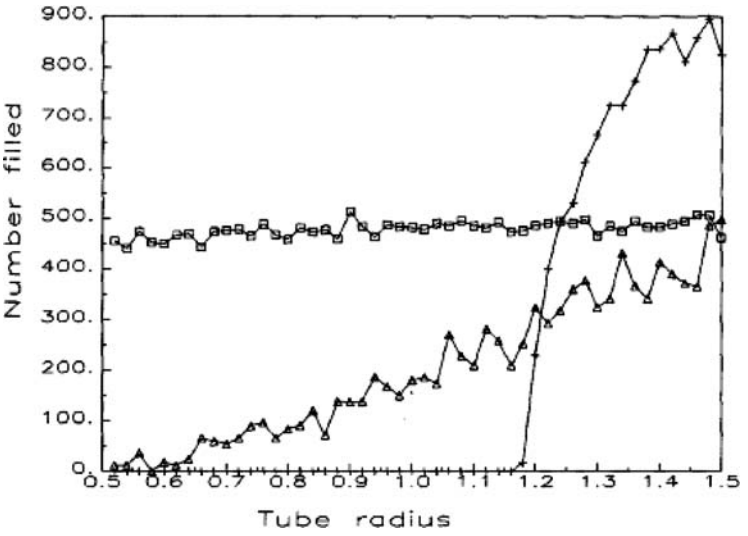

FIGURE 14. Number of pore throats filled with the nonwetting fluid versus the radii of pore throats for $M = 0.1$. Crosses $Ca = 0$; triangles $Ca = 0.5$, squares $Ca = \infty$ (zero entry capillary pressure). Notice that for $Ca = 0$, none of the pore throats with entry capillary pressure larger than the percolation threshold are filled (Blunt and King, 1991).

Blunt and King (1991) studied distribution of nonwetting phase–filled pores at breakthrough during drainage for different viscosity ratios. They showed that when capillary number was high, a uniform distribution of filled pores was resulted. But at low capillary numbers, only large pores were invaded. This effect has been illustrated in Figure 14 by showing number of pore throats filled with the nonwetting fluid versus radius of pore throats. The horizonal curve with square symbol shows that at very large capillary number (where only viscous forces are important), pore throat occupancy for different pore throat radii is constant. But, if capillary forces are dominant ($Ca \approx 0$), mostly large pore throats are filled (curve with cross symbols). For an intermediate capillary number (triangle symbols), large pore throats are more probable to be filled by the nonwetting fluid and this probability decreases with decrease of pore throat radii. This is similar to the conclusion by Koplik and Lasseter (1985); at low capillary number, there is more possibility for trapping and larger blobs are expected.

Dias and Payatakes (1986a), Vizika et al. (1994), Blunt and Scher (1995), Mogensen and Stenby (1998), Hughes and Blunt (2000), DiCarlo (2006), and Nguyen et al. (2006) also showed that during imbibition, with the increase of capillary number and viscosity ratio, less trapping of the nonwetting phase (oil) during imbibition would happen. This is due to the suppression of snap-off at high flow rates. Dias and Payatakes (1986a) showed the effect

of capillary number on residual oil saturation for different viscosity ratios (Figure 15). It should be noted that κ in Figure 15 is the inverse of M. Thus, with increase of κ, M will decrease. As it can be seen, during imbibition, residual oil saturation remains virtually constant (around 50%) for smaller capillary numbers. From $Ca \approx 10^{-5}$, it starts to decrease drastically with increasing Ca. For viscosity ratios smaller than 1 (unfavorable conditions), residual oil saturation remains constant up to $Ca \leq 10^{-7}$ and in range of $10^{-7} \leq Ca \leq 5 \times 10^{-5}$, it increases slightly. Then, it decreases rapidly for $Ca \geq 10^{-4}$. This figure shows that the effect of capillary number on residual saturation decreases with decrease of viscosity ratio (M). Hashemi et al. (1999) and Hughes and Blunt (2000) presented a curve qualitatively similar to Figure 15.

Vizika et al. (1994) investigated the effect of viscosity ratio in more detail for different capillary numbers using three-dimensional pore-network models and also micromodel experiments. They concluded that the viscosity ratio affects the residual oil saturation during imbibition even at low Ca. But when the capillary forces decrease (for example with increase of contact angle), effect of viscosity ratio on residual oil saturation is less pronounced. Their interpretation is that local pressure gradients, which are created by the advance of a single meniscus or a wetting film, may be sufficiently large to make viscous stresses locally important, even if the local overall flow rate

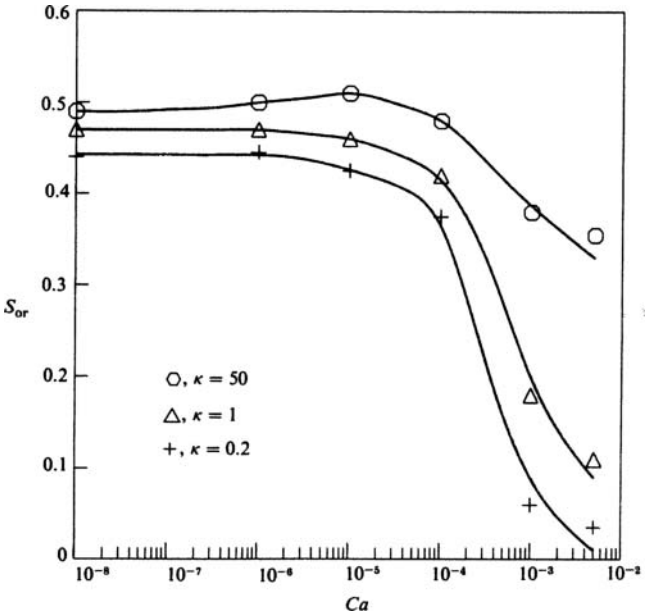

FIGURE 15. Residual oil saturation (S_{or}) versus the capillary number, Ca, for imbibition simulation on a 15 × 30 network for various values of inverse viscosity ratio ($\kappa = 1/M$; Dias and Payatakes, 1986a).

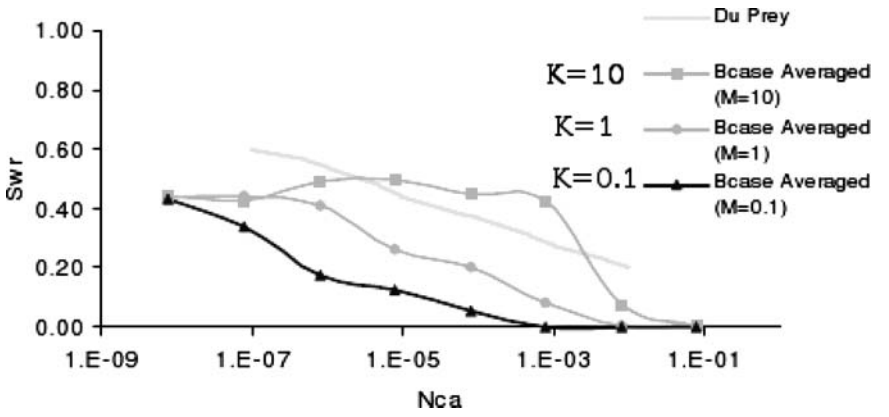

FIGURE 16. Capillary desaturation curves for different viscosity ratios, due to Singh and Mohanty (2003). Each data point represents an average value over three realizations. Data from Lefebvre du Prey (1973) are also plotted for comparison. It should be noted that $\kappa = \frac{\mu_{receding}}{\mu_{invading}}$.

is very small. The gradual accumulation of local viscous effects may lead to substantial macroscopic effects.

Although due to the industrial applications in reservoir engineering residual nonwetting phase saturation is generally of more interest, some researchers have also investigated the trapped wetting phase during drainage. Singh and Mohanty (2003), and Al-Gharbi and Blunt (2005) have studied residual water saturation during drainage for constant flow rates. Singh and Mohanty (2003) showed that in almost all cases of drainage (including high and low capillary numbers, favorable and unfavorable viscosity ratios), an increase of viscous forces (large *Ca*) can lead to a decrease of residual water saturation. However, as it can be observed in Figure 16, for unfavorable viscosity ratio it does not monotonically decrease. They conjecture that the peak values are related to the change of behavior from viscosity fingering to capillary fingering. Once again, it should be noted that κ is defined as the ratio of receding phase viscosity to invading phase viscosity.

5. FLUIDS PRESSURE FIELDS DEVELOPMENT

To understand complexities in multiphase flow, it is essential to investigate pressure field evolution as well as capillarity effects under nonequilibrium conditions. Such information will be needed for investigating the validity of the extended Darcy's law for multiphase flow. Van der Marck et al. (1997), Aker et al. (1998 1998b,a), Gielen et al. (2004, 2005), and Joekar-Niasar et al. (2010a) studied temporal evolution of fluids pressure

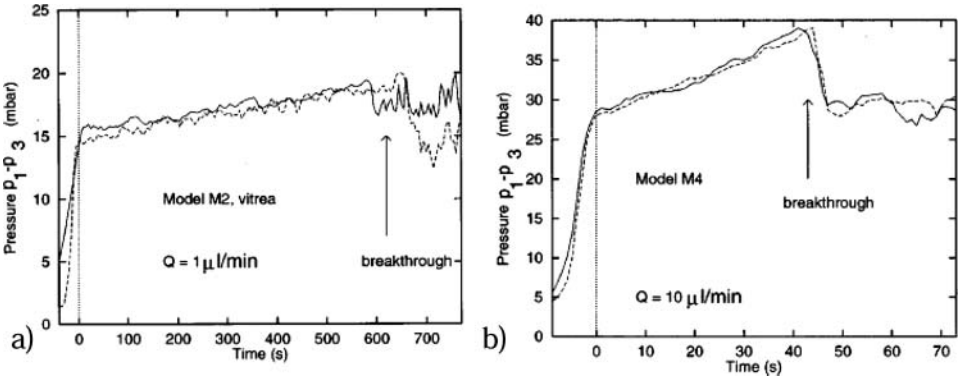

FIGURE 17. An experimental pressure curve for drainage experiment showing pressure drop after breakthrough. (a) High-conductivity network, $M = 12$. (b) Low-conductivity network $M = 1$ (Van der Marck et al., 1997)

fields using pore-network models in order to gain a better insight into macroscopic pressure field behavior. They investigated pressure field evolution under the effect of viscosity ratio and capillary number in drainage simulations.

5.1. Boundary Pressure Difference Versus Capillary Pressure

Van der Marck et al. (1997) compared pore-network model results with micro-model experimental data. The experiments, performed in one-, two-, and three-layer micromodels, were designed to investigate the effect of gravity for two different viscosity ratios: equal to 1 and larger than 1. They measured pressures at the inlet and outlet during drainage experiments under constant flow rate. Agreement between their model results and experimental results decreased for viscosity ratios larger than one and at high capillary numbers. Obviously, with the invasion of nonwetting phase, for $M > 1$, the pressure difference between inlet and outlet increased due to increasing viscous energy dissipation, as shown in Figure 17. At first, the nonwetting phase pressure had to increase to reach the entry pressure of the model. After nonwetting phase invaded the model, its pressure built up slowly as more and more nonwetting fluid (with higher viscosity) was injected at a constant flow rate. Capillary blockage of channels and the resulting decrease in the flow conductance of the micromodel were the main reasons for the pressure buildup. However, after breakthrough of the nonwetting fluid, its pressure dropped significantly under the influence of the outlet chamber (see Figure 17). This pressure drop was also simulated in gas migration problem by Impey et al. (1997) using a pore-network model. They showed that at the moment of breakthrough of gas, its pressure drops

down and at a blockage, there is a build-up in gas pressure. Van der Marck et al. (1997) had chosen a large outlet chamber for their micromodel, which had a negligible influence on flow conductance and capillary pressures. This had the disadvantage that the nonwetting phase that entered the outlet chamber could remain connected or snapped off, under the influence of processes occurring outside the microflow model and were hard to control. They did not include these effects in their pore-network model. Thus, their simulations' results after breakthrough deviated from the experimental measurements.

Aker et al. (1998a) investigated the effect of capillary forces for different viscosity ratios and capillary numbers using a two-dimensional pore-network model. They related the macroscopic flux in two-phase flow to two separate terms related to viscous forces and capillary forces. This formulation was selected in analogy to pore-scale Washburn equation (Equation 5, and Table 1). In single-phase flow and ignoring the gravity effect, there is a linear relationship between the flux and global pressure drop (between the two boundaries $\Delta P = P_{ent} - P_{ex}$), written as $Q = A_0 \Delta P$, where A_0 is a constant. But, in two-phase flow, we have: $Q = A\Delta P + B$, where A and B are functions of saturation. The term B is due to capillary pressure acting across the fluid-fluid interfaces. This linear relationship can be written as

$$\Delta P = \frac{Q}{A} - \frac{B}{A} \tag{14}$$

Under drainage conditions, new interfaces will be created as the nonwetting phase invades a domain. Aker et al. (1998a) divided interfaces into two groups: cluster menisci, surrounding the trapped clusters of receding fluid, and the front menisci located at the front between the invading and receding fluids. Variation of capillary pressure associated with theses interfaces can be different. So, Aker et al. (1998a) introduced two different capillary pressures: global capillary pressure: (P_g^c), which contributes to all menisci, and front capillary pressure (P_f^c), which is the average capillary pressure associated with the front menisci. Based on the analogy between global pressure drop and pore-scale pressure drop, the second term in Equation 14 was assumed to be equal to the global capillary pressure (P_g^c).

$$P_g^c = -\frac{B}{A} \tag{15}$$

Using simple arithmetic averaging, the front capillary pressure was given as

$$P_f^c = \frac{1}{N} \sum_{i=1}^{N} \left| P_i^c \right| \tag{16}$$

Based on several drainage simulation they investigated trends of ΔP, A, and B under different capillary numbers, and viscosity ratios, as described subsequently.

Unfavorable viscosity ratio: First, Aker et al. (1998a) performed drainage simulations with unfavorable viscosity ratio ($M = 0.001$) for different capillary numbers (3.5×10^{-4} to 1.1×10^{-2}) and different sizes of network. Thus, they could observe capillary fingering as well as viscous fingering. The largest network had 60×80 nodes. They studied the trends of ΔP, global capillary pressure (P_g^c), and average front capillary pressure (P_f^c). According to the results for $M = 0.001$, ΔP decreased with the invasion of nonwetting fluid. They observed some fluctuations of ΔP, which were due to fluctuations in P_g^c, as menisci invaded into or retreated from tubes. Their simulation results showed that for small capillary numbers (less than 3.5×10^{-4}), there is no significant difference between global capillary pressure (P_g^c) and average front capillary pressure (P_f^c). Under slow flow conditions, the viscous pressure gradient vanishes and fluids pressure difference would be equal to the global capillary pressure P_g^c. In fact, the global capillary pressure becomes equal to the front capillary pressure: $P_f^c \approx P_g^c$. Therefore, for $M \ll 1$ or at low injection rates, the effect of the clusters became negligible, and P_g^c reduces to the local capillary of the invading menisci along the front.

Favorable viscosity ratio: When viscosity ratio is larger than 1, the pressure drop, ΔP, increases with the invasion of high viscosity fluid. This pressure drop increases linearly at high flow rates but the linearity of the trend decreases if unstable displacement develops. Aker et al. (1998a) performed a series of pore-network model simulations and determined variations of the ratio A_0/A, ΔP, and P_g^c with time, for four different capillary numbers and $M = 100$. According to their results with the increase of nonwetting phase saturation, A_0/A increased (starting from zero). For small flow rates, where capillary forces are dominant, the effect of viscous forces disappeared and small values for A were obtained. Thus, the ratio A_0/A was to be found smaller in fast flow than in slow flow. Initially, P_g^c should be negligible, since the domain is filled by one fluid. With the invasion of the nonwetting phase, the share of global capillary pressure in the total pressure drop (ΔP) increases.

Although Aker et al. (1998a) showed that nonlinearities created by viscous forces and capillary forces are highly dependent on capillary number and viscosity ratio, they did not define sound theoretical background for their conjecture. Finally they did not propose a formulation to relate the nonequilibrium effects to the dynamic conditions of the system. Hassanizadeh and Gray (1990) proposed a relationship, which relates viscous forces and capillary forces to the dynamic conditions of

a system. These conjecture and the relevant studies discussed in detail in the following section.

5.2. Nonequilibrium Capillarity Effects

A central equation in theories of two-phase flow in porous media is the so-called capillary pressure-saturation relationship, which is commonly written as

$$P^n - P^w = P^c(S^w) \tag{17}$$

In fact, there are two major assumptions in this equation: capillary pressure is a function of wetting phase saturation, and fluids pressure difference is equal to capillary pressure (at all times and under all conditions).

Regarding the second assumption underlying Equation 17, it is now an established fact that $P^n - P^w$ is equal to capillary pressure but only under equilibrium conditions (see Hassanizadeh et al., 2002, for an extended review of experimental evidences). According to Entov (1980), capillary pressure-saturation relationship is not unique and, even though it is obtained under equilibrium conditions, it is a function of the history of fluids movements. In fact, it depends not only on the volume fraction of each phase, but also on their microscale distribution and change of saturation with time. Nonequilibrium effects in capillary pressure can be of significant importance whenever, gradients of fluids pressure and fluids velocities are large (Lewalle et al., 1994). For nonequilibrium conditions, the following equation for the difference in fluids pressure has been suggested (Hassanizadeh and Gray, 1990; Kalaydjian and Marle, 1987; Stauffer, 1978):

$$P^n - P^w = P^c - \tau \frac{\partial S^w}{\partial t} \tag{18}$$

where τ ($ML^{-1}T^{-1}$) is a material property that may still be a function of saturation.

Equation 18 has been the subject of many studies in recent years, computationally using Darcy-scale models (see Das et al., 2006; Manthey et al., 2005), and pore-scale models (see Dahle et al., 2005; Gielen et al., 2005; Joekar-Niasar et al., 2010a; Joekar-Niasar and Hassanizadeh, 2011) as well as experimentally (see Berentsen and Hassanizadeh, 2006; Bottero, 2009; Bottero and Hassanizadeh, 2006; Camps-Roach et al., 2010; Hassanizadeh et al., 2004; O'Carroll et al., 2005; Oung et al., 2005). Hassanizadeh et al. (2002) reviewed extensively the experimental works in which non-equilibrium effects have been observed.

Dahle et al. (2005) developed a bundle-of-tube model to investigate the variation of τ with variance of radii distribution and with saturation under

drainage process. They found that τ increases with decrease of wetting fluid saturation and with increase of variance.

Gielen et al. (2004, 2005), and Gielen (2007) developed a dynamic pore-network model based on the model developed by Blunt and King (1991). They assumed that the capillary pressure in pore bodies was negligible. They implemented simulations for viscosity ratios of 1 and 10; therefore a stable front was dominant in their simulations. They found that τ value increased with decrease of wetting phase saturation. Since the employed pore-network model had a simplified geometry (circular cross sections), many physical processes such as snap-off, capillary diffusion, and local countercurrent flow could not be observed in simulations. In addition, all simulations were for the case of $M = 1$ and 10, where stable front invasion occurred.

Joekar-Niasar et al. (2010a) and Joekar-Niasar and Hassanizadeh (2011) investigated functionality of nonequilibrium capillarity coefficient using a dynamic pore-network model with angular cross sections for three different viscosity ratios $M = 10, 1, 0.1$. However, Joekar-Niasar and Hassanizadeh (2011) investigated uniqueness of this coefficients under primary and main drainage and main imbibition as well. Figure 18 shows the relationship between τ and saturation for a $35 \times 35 \times 35$ network for different viscosity ratios (Joekar-Niasar et al., 2010a). Two different aspects of these data are important: (a) order of magnitude of the non-equilibrium capillarity coefficient τ and (b) its variation with saturation for different viscosity ratios.

Values of τ found by Joekar-Niasar et al. (2010a) ranged from 100 to 1000 Pa.s for $M = 1.0$. These values are in agreement with results obtained in other pore-network modeling studies, mentioned previously.

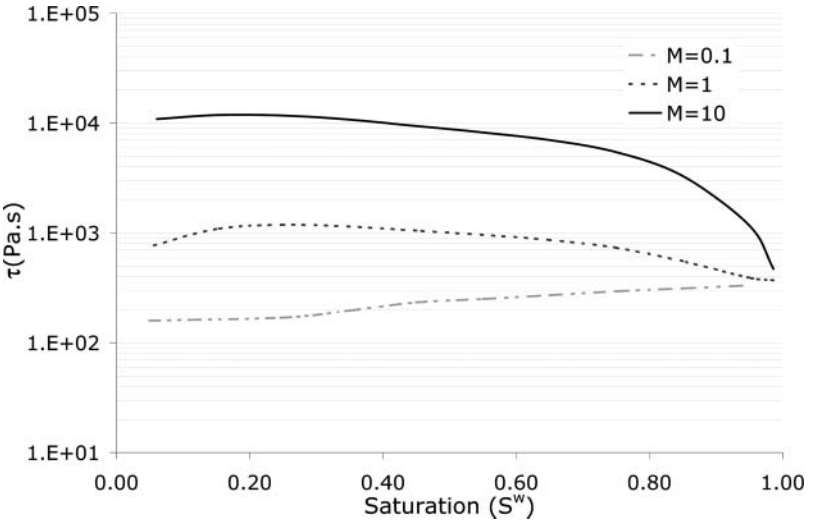

FIGURE 18. τ as a function of saturation and viscosity ratio for a $35 \times 35 \times 35$ network (Joekar-Niasar et al., 2010a).

The dimensions of their network corresponded to a porous medium sample size of $1.9 \times 1.9 \times 1.9\,\mathrm{mm}^3$, which is very small. The intrinsic permeability was $1.43 \times 10^{-12}\,\mathrm{m}^2$, which corresponds to permeability of a fine sand. The general understanding is that the magnitude of τ increases with the size of the observation or averaging window and is inversely correlated with permeability. Dahle et al. (2005), using a bundle-of-tube model, concluded that τ value can be proportional to L^2, where L is the length of averaging window. A similar result was found by Manthey et al. (2005) based on simulations at continuum scale.

In laboratory experiments by Hassanizadeh et al. (2004), the value of τ for a fine sand sample of 3 cm in height was found to be 5×10^5Pa.s. The pressure measurements were actually done by transducers with a diameter of around 1 cm. Using similar transducers in experiments with the same fine sand, Bottero and Hassanizadeh (2006) found a τ -value of around 10^5 Pa.s. But, when Bottero (2009) upscaled the results to the column scale (18 cm), the average τvalue was found to be around 10^6 Pa.s. Table 3 presents a summary of experimental and computational works for determining τ in different porous media.

Figure 18 shows that the dynamic effect is stronger for larger viscosity ratios when wetting phase viscosity is constant ($\tau(M = 10) > \tau(M = 1) > \tau(M = 0.1)$). This trend is in agreement with the explanation given by Barenblatt et al. (2003), who stated that dynamic effect in capillary pressure is related to the finite time required for the fluids in the pore structure to rearrange themselves. Indeed, for larger effective viscosity values, more time is required for fluids to reach the equilibrium condition, which corresponds to a larger τ value. Entov (1980) reported that $\tau \propto \frac{\mu l^2}{k\Delta P^c}$, in which k is the permeability, μ is the (effective) viscosity, l is the length of the averaging domain, and ΔP^c is the deviation from the equilibrium capillary pressure for a given saturation. Joekar-Niasar and Hassanizadeh (2011) only investigated effect of fluid property on nonequilibrium capillarity coefficient. They showed that by dividing τ by effective viscosity over the domain, the curves for different viscosity ratios would collapse on each other. Effective viscosity is defined simply as $\mu_{eff} = \mu^n S^n + \mu^w S^w$.

Figure 18 shows that for $M \geq 1$, nonequilibrium capillarity coefficient increases with the decrease of wetting fluid saturation, which is similar to most findings as reported in the literature. For $M < 1$, an slightly reverse trend is observed: namely, τ decreases with the decrease of wetting fluid saturation. An empirical formula relating τ to medium and fluid properties was proposed by Stauffer (1978). In that formula, however, no dependence on saturation was included. We propose to modify the Stauffer formula as follows:

$$\tau = \frac{\alpha \epsilon \mu_{eff}}{\lambda k} \left(\frac{P_d^c}{\rho g} \right)^2 \tag{19}$$

TABLE 3. Values of τ in literature for computational and experimental works.

Reference	Exp. Type	Process	Fluids	M	P^d(kPa)	K (m^2) $\times 10^{-12}$	$\frac{\partial \tau}{\partial S^w}$	τ (Pa.s)	Domain Dimensions (cm)
Dahle et al. (2005)	BTM	Drain	—	1	0.8	4.7	274	$\ll 0$	0.1 (L)
Gielen et al. (2005) Gielen (2007)	PNM	Drain	Oil-water	10	5	—	1.2×10^5	< 0	$0.3 \times 0.3 \times 1$
Joekar-Niasar et al. (2010a)	PNM	Drain	—	1,10	4	150	900,2750	$\ll 0$	$0.5 \times 0.5 \times 0.5$
Joekar-Niasar et al. (2010a)	PNM	Drain	—	0.1	4	150	350	$\gg 0$	$0.5 \times 0.5 \times 0.5$
Das et al. (2007)	CM	Drain	Oil-PCE-Water	>0.6	1.2	5	10^5 to 10^7	$\ll 0$	
Manthey et al. (2004)	Lab	Drain	PCE-Water	0.9	5.58	3	2 to 7×10^4	< 0 >0	—
O'Carroll et al. (2005)	Lab	Drain	PCE-Water	0.8	2.1	15.8	5.64×10^7	$\ll 0$	5.07(D),9.62(L)
O'Carroll et al. (2005)	Lab	Drain	PCE-Water	0.8	2.4	12.6	1.99×10^7	$\ll 0$	5.07(D),9.62(L)
Bottero and Hassanizadeh (2006) Bottero (2009)	Lab	Drain	PCE-Water	0.9	6	—	10^5 to 10^7	$\ll 0$	9.8 (D),19(L)
Camps-Roach et al. (2010)	Lab	Drain	Air-Water	0.02	2.2	53	2×10^5to10^6	$\gg 0$	10 (D),20(L)
Camps-Roach et al. (2010)	Lab	Drain	Air-Water	0.02	4.6	14.7	10^5to8×10^5	$\gg 0$	10 (D),20(L)

BTM: Bundle of tubes, PNM: Pore-network model, CM: Continuum model, Lab: Laboratory experiment D: Diameter, L: Length.

where α is a constant, ϵ is porosity, λ and P_d^c are the coefficients in Brooks-Corey formula (Brooks and Corey, 1964), k is the saturated permeability, ρ is the water mass density, and g is the gravity. Compared to the original Stauffer formula, we have replaced μ by μ_{eff}.

Equation 19 suggests that the change of τ with saturation is proportional to the change of μ_{eff} with saturation. Recalling the simple linear algebraic equation for μ_{eff}, we can write

$$\frac{\partial \mu_{eff}}{\partial S^w} = \mu^w - \mu^n \tag{20}$$

which means that $\frac{\partial \tau}{\partial S^w}$ ($\propto \frac{\partial \mu_{eff}}{\partial S^w}$) should be negative for $M > 1$ and positive for $M < 1$:

$$\frac{\partial \tau}{\partial S^w} \propto \begin{cases} \mu^w - \mu^n \leq 0, & M \geq 1 \\ \mu^w - \mu^n > 0, & M < 1 \end{cases}$$

One should note that the effective viscosity defined previously is assuming that the fluids are behaving similar to resistors in series. Thus, it does not include nonlinearities related to viscous and capillary fingering in the invasion process. However, the general trend in variation of τ with saturation is in full agreement with the observations reported in the literature. This was found in Mirzaei and Das (2007) in column-scale drainage simulations, in Joekar-Niasar et al. (2010a) in pore-network model simulations, and in Bottero and Hassanizadeh (2006) in PCE-water experiments ($M \approx 0.9$), where τ increased with the decrease of wetting fluid saturation. For $M = 0.1$, an opposite trend of τ as a function of saturation has been reported in air-water experiments by Camps-Roach et al. (2010), and as shown in Figure 18.

6. MACROSCOPIC INTERFACE DYNAMICS

As shown in Figure 3, depending on M and Ca, the invasion front can be classified into three different classes: capillary fingering, viscous fingering, and stable displacement. In these invasion regimes, macroscopic front topology is one of the major features that is related to the system dynamic parameters. Due to the versatility and rather inexpensive computational cost of dynamic pore-network models, they have been used extensively to investigate scaling of capillary fingering and viscous fingering regimes for different viscosity ratios. Furthermore, velocity of macroscopic interfaces and dynamics of interfacial area have been analyzed. Understanding the dynamics of interfacial area can be useful in interface-related topics such as mass exchange over the interfaces.

Chen and Wilkinson (1985) investigated the effect of randomness of the porous medium structure on viscous fingering using experimental

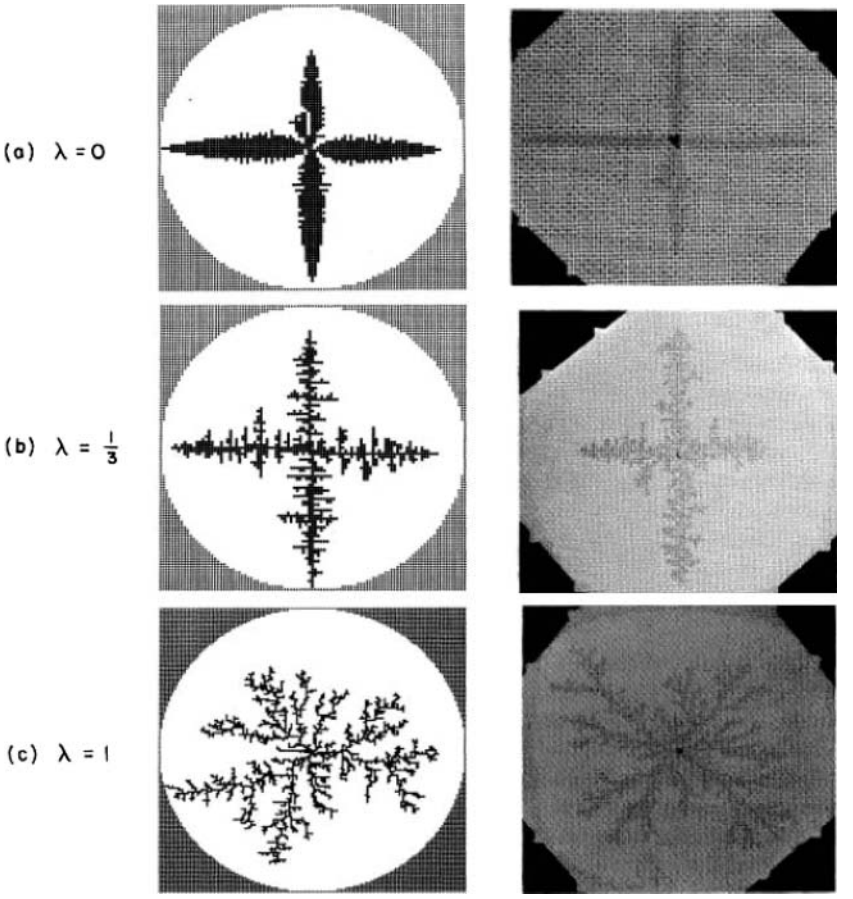

FIGURE 19. Viscous fingering invasion pattern for different randomness in porous media structure. Left column shows modeling results for different randomness factor (λ) and right column shows the experimental results in a two-dimensional micromodel with injection point in the center. These two columns should not be compared with each other quantitatively (Chen and Wilkinson, 1985).

and modeling approaches. In the experiments oil was injected into a two-dimensional micro-model initially filled by glycerin ($M = \frac{1}{1200}$). As seen in the imaged from the experiments, shown in the right column of Figure 19, fingers developed. The size and pattern of fingers were found to depend on pore size distribution. This was also shown using a two-dimensional pore-network model with a single-pressure algorithm. Radii of the pores were generated in the interval $[1-\lambda, 1+\lambda]r$, where r is the mean radius and λ is a randomness factor changing from 0 to 1. In both experiments and modeling results, they observed that for a narrow size distribution of the tubes (small λ), fingers formed almost ordered patterns and grew along the injection direction (Figure 19a). But, for a wider range of distribution, fingers formed in a chaotic fashion (Figure 19c).

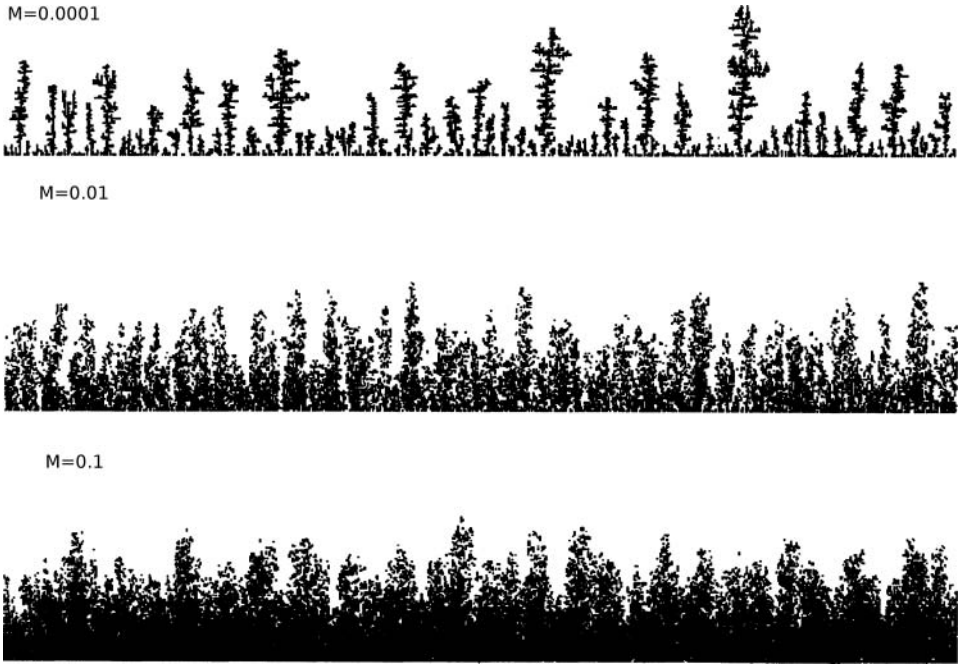

FIGURE 20. Near breakthrough flow patterns for three different unfavorable viscosity ratios. With increase of viscosity ratio the flow pattern crosses over from DLA-type ($M = 0.0001$) to compact flow ($M = 0.1$; Ferer and Smith, 1994).

Although there was no quantitative agreement between experiments and model results, the effect of pore size randomness was visible in their results.

Although randomness of the medium is an important intrinsic property in finger formation, dimension and topology of the fingers can also change based on capillary number and viscosity contrast. The behavior of the fingers has been investigated using empirical scaling of the results of dynamic network models. Under unfavorable conditions, there is crossover from diffusion limited aggregation–type (DLA) flow to compact flow with increasing viscosity ratio, as shown in Figure 20. The effect of viscosity ratio has been investigated using pore-network models (e.g., Ferer et al., 1993; King, 1987).

Fractal dimension (D_f) is the major parameter that has been used to characterize the fingers resulted from pore-network models. It is a statistical quantity that gives an indication of how completely a fractal fills the space, as one zooms down to finer and finer scales. The fractal dimension is:

$$D_f = \frac{\log N(l)}{\log l} \tag{21}$$

in which l is the grid size (length of pore unit) and $N(l)$ is the number of grids (pore units) filled with the front. A cubic grid with the minimum grid size of network spacing distance can be mapped onto the network and the number of grid cells can be counted consequently. For instance, Chen and Wilkinson (1985) found that fractal dimension in their random two-dimensional simulations (Figure 19c) was about 1.72. Later, King (1987) also used a pore-network model to investigate the fractal behavior of fingering in different finite viscosity ratios in a two-phase system. He investigated the surface fractal dimension (D_s), which was assigned to the fingers at the front of the compact flow. He showed that surface of finger follows a fractal phenomenon and the fractal dimension does not depend on the disorder of porous medium structure. Instead, it is highly dependent on the viscosity ratio: fractal dimension decreases with the increase of viscosity ratio (limited to unity). They found the following formula by fitting to their simulations results:

$$D_s = 1 + \frac{2}{3}\left(\frac{1-M}{1+M}\right)^2 \quad M = \frac{\mu^{inv}}{\mu^{rec}} \tag{22}$$

For equal viscosities, the surface fractal dimension will reach 1.

Ferer et al. (1993) investigated crossover from DLA-type flow (for $M = 0$) to compact flow (for $M = 0.1$) using a pore-network model without capillary forces to suppress the capillary pinning. The simulation results illustrate that for all viscosity ratios, the initial flows had an unstable, fractal behavior that crossed over to compact flow on a time scale. The time scale increases with decrease of viscosity ratio. Furthermore, fitting of results allows an empirical relation for crossover length scale and crossover time scale defined as

$$\Lambda = M^{\phi_l} \quad \phi_l = 0.24 \pm 0.06 \tag{23}$$

$$\tau = M^{\phi_t} \quad \phi_t = 0.17 \pm 0.03 \tag{24}$$

More detailed pore-network simulations have been performed by Aker et al. (1998a); Blunt and King (1991); Vizika et al. (1994), and Singh and Mohanty (2003). Blunt and King (1990) also studied fractal behavior of an invading phase in relation to the structure spacing. Fractal dimension in their network increased from 1.82 in a two-dimensional network to 2.44 in a three-dimensional network.

Furthermore, with increasing the capillary number for constant viscosities, there is a crossover from capillary fingering system (invasion-percolation) to viscous fingering system or even to compact flow regime. Wilkinson (1986) investigated the crossover of fractal flow described by invasion-percolation with trapping (IPWT) to the compact linear flow given by Buckley-Levrett flow using fractal analysis. He found out that the

crossover from fractal to compact flow occurs on a length scale (Λ) given by

$$\Lambda = Ca^{-\alpha} \tag{25}$$

and in a two-dimensional domain α is given equal to 0.38. Generality of this relation for all capillary numbers suggests scaling functions for average position and width of the macroscopic interface. Ferer et al. (2005) simulated drainage process in a two-dimensional lattice pore network with circular cross sections. They analyzed their results and show that there are scaling functions, which provide closed form expressions for the dependence of average position and interfacial width upon capillary number and time.

In another study Fernández et al. (1991) showed that crossover from capillary fingering given by IPWT to the viscous fingering given by DLA flow occurs on a length scale (Λ) given by

$$\Lambda = Ca^{-2/(2+D_s)} = Ca^{-0.6} \tag{26}$$

where D_s is a the surface fractal dimension of the capillary fingers ($D_s = 1.33$). Ferer et al. (2004) analyzed this scaling using two-dimensional air-water flow cell experiments. They found that the volume of the injected air initially scales with its average position (as given by IPWT) and then crosses over to DLA-type flow at the characteristic length, which decreases with increase of capillary number.

Results of a pore-network model by Dias and Payatakes (1986a) showed that although the effect of capillary number on displacement is essential, but at high and moderate *Ca*, the effect of viscosity ratio is more important, acting as a pivotal factor. This was also shown by Touboul et al. (1987). They showed that at large capillary numbers (when viscous forces dominate the flow), depending on the viscosity ratio, either viscous fingering or stable displacement would occur (Figure 3). If the viscosity ratio is larger than 1, stable displacement will occur, as also shown by Singh and Mohanty (2003) and DiCarlo (2006). Using a two-dimensional pore-network model, Aker et al. (1998 1998b) showed that at $Ca = 4.6 \times 10^{-3}$ for $M = 1.0 \times 10^{-3}$ and 1.0×10^{2}, two different displacements can be observed. If $M < 1$, at high capillary number, viscous fingering was observed, while for $M > 1$ stable displacement was reported. With decreasing the flow rate, front moved from viscous fingering to capillary fingering. For instance, for $M = 0.1$ at high flow rate, nonwetting front was stable and compact. For very low flow rates, capillary fingering was observed. Thus, one would expect to have less flooding efficiency for $M < 1$ compared with the favorable conditions. Dias and Payatakes (1986a) showed that for unfavorable viscosity ratio ($M < 1$), flooding efficiency begins to improve only for capillary numbers larger than 5×10^{-4}, and it is substantially inferior to the achieved values with $M > 1$ with the same *Ca*.

Vizika et al. (1994) showed that at any flow rate, under unfavorable conditions, microfingering can happen and cause macrofingering. In addition, they found that for favorable displacements ($M > 1$), the extent of microfingering decreased with increasing Ca and for unfavorable displacements ($M < 1$), the extent of microfingering increased slightly with increasing Ca for $10^{-6} \leq Ca \leq 10^{-5}$.

Investigation of width of the invasion front under different conditions is another aspect of macroscopic interface dynamics, which has been studied by Aker et al. (1998a) for applications in reservoir engineering and by Lam and Horváth (2000) for application of paper wetting process. Aker et al. (1998a), Lam and Horváth (2000) and Løvoll et al. (2005) have studied development of the front width with time using a pore-network model with circular cross sections for pore throats. Aker et al. (1998a) used different terminologies:

- Front width: During the invasion of nonwetting phase, there will be some pores on the invasion front, referred to as front pores. Front width (w) is defined as the standard deviation of the distance between all front pores and the centroid of the front.
- Saturation width: Denoted by w_s, it is defined as the standard deviation of the distance between all pores filled with the invading phase and the centroid of part of the domain saturated with the invading phase.
- Saturation time: Denoted by t_s, it is defined as the time in which saturation width (w_s) is equal to the front width.

Aker et al. (1998a) calculated front width for different capillary numbers, including $2.3 \times (10^{-3}, 10^{-4})$, $4.6 \times (10^{-4}, 10^{-5})$ and $9.2 \times (10^{-4}, 10^{-5})$, as shown in Figure 21.

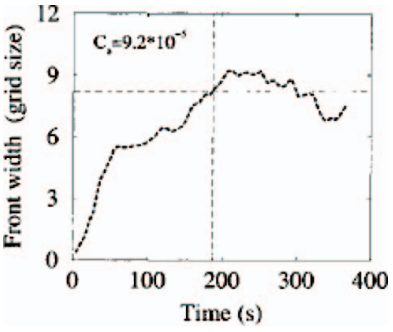

FIGURE 21. The front width (w) as a function of time for $Ca = 9.2 \times 10^{-5}$. The horizontal dashed line indicates the saturations width (w_s) and the vertical dashed line indicates the saturation time, t_s (Aker et al., 1998a).

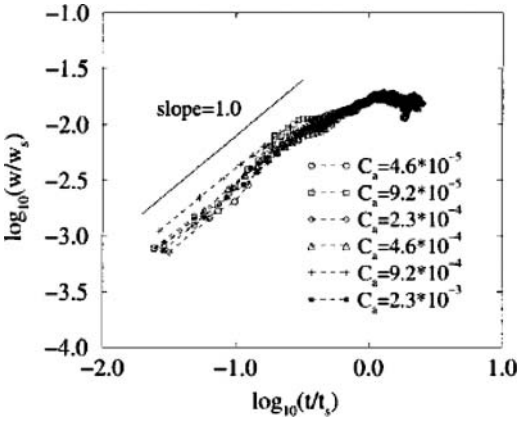

FIGURE 22. Data collapse for the front width. β is given by the slope when $t/t_s < 1$ and was estimated to $\beta = 1.0 \pm 0.1$ (Aker et al., 1998a).

They used the simulation results to show scaling of the front width for $t < t_s$. They found that data points collapsed onto a more or less single curve when $\log w/w_s$ was plotted against t/t_s (Figure 22). For this curve, they assumed the following relationship for $t \ll t_s$:

$$\frac{w}{w_s} = \left(\frac{t}{t_s}\right)^{\beta} \tag{27}$$

They found a good agreement between their results and experimental data of Frette et al. (1997), who found $\beta = 0.8 \pm 0.3$. Furthermore, they found that saturation front width (w_s), and saturation time (t_s) are only functions of capillary number. The results of Aker et al. (1998a) related to the drainage process only. Lam and Horváth (2000) showed temporal and spatial correlation for fronts during imbibition process. In a series of experiments by Horváth and Stanley (1995), a paper sheet was moved continuously downward into a water container at constant speed v. Imbibition front evolution was investigated for various different dynamic conditions (different values of v) and a stationary experiment ($v = 0$). Lam and Horváth (2000) simulated imbibition experiments using a pore-network model with circular cross sections. They found $\beta = 0.29 \pm 0.01$. Due to the large viscosity ratio ($M \sim 100$), they solved the pressure field only in the wetting phase (water), and ignored the pressure drop in air phase.

In another study by Løvoll et al. (2005), the effect of gravity and viscous forces on front width evolution with time was studied. They performed drainage experiments in a two-dimensional micro-mode of 35 × 35 cm^2. The nonwetting phase was air and the wetting phase was a mix of glycerol and water. Planar porosity was about 0.63 and permeability was 0.0189 × 10^{-3}cm^2. The nonwetting phase viscosity was much smaller than the viscosity

of wetting phase. Specifications of their pore network model are presented in Table 4. To include gravity forces in the simulations, Bond number (Bo), was considered. Bond number is defined as the ratio of gravity forces to capillary forces:

$$Bo = \frac{\Delta\rho g a^2}{\sigma^{nw}} \tag{28}$$

in which, ρ is the density and a is the length scale (lattice spacing of a pore network). According to Løvoll et al. (2005), percolation theory can predict a scaling law for this displacement as follows:

$$w = (Bo - Ca)^{-a} = (Bo - Ca)^{-\upsilon/1+\upsilon} \tag{29}$$

To have a stable width evolution, $(Bo - Ca)$ should be positive. It means that width will increase with time until reaching a steady state. They showed that the width evolution with time reaches a steady state condition with $(Bo - Ca) > 0$. They found that their simulation results were in qualitative agreement with experiments. Front width increased with time, and when $(Bo - Ca) > 0$ a steady-state condition was reached. With increasing $(Bo - Ca)$ values, the required time to reach the steady-state front width decreased.

Another aspect of the macroscopic interface dynamics is related to the average interfacial velocity, which was studied by Nordhaug et al. (2003), and Joekar-Niasar and Hassanizadeh (2011), and Joekar-Niasar et al. (2010a). Nordhaug et al. (2003) studied interface movement in a three-dimensional lattice pore-network model with circular cross sections using a single-pressure algorithm. To save computational time and memory, they did not track the menisci within pore throats (i.e., spontaneous pore throat filling was assumed). They simulated stable and unstable displacement mechanisms during drainage under Dirichlet boundary conditions (during simulation capillary number varied between 10^{-3} and 10^{-2}) for three different viscosity ratios ($M = 0.1, 1, 10$). They estimated interface velocity for stable displacement as well as viscous fingering regime. Since it was assumed that the pore throats are filled spontaneously, they could not calculate menisci velocity in the pore throats. However, they calculated the magnitude of a local velocity in pore bodies based on time-rate change of local saturation, as follows:

$$\|v_i^{nw}\| = l_{ij}\frac{\Delta S_i^n}{\Delta t}, \quad ij : \text{pore throat including the traveling interface} \tag{30}$$

in which $\|v_i^{nw}\|$ is the menisci velocity in pore body i, and l_{ij} denotes the length of pore throat ij through which the entering interface travels plus the diameter of the pore body i. To define the direction of the velocity, they averaged the directions of total inflow and total outflow in pore body i. Equation 30 has a shortcoming in definition; in Equation 30 it is assumed that velocity is calculated only based on one pore throat including the travelling

interface. If simultaneously more that one interface is moving toward the pore body i with different velocities, it is not clear how the menisci interface in a pore body should be calculated.

To upscale the velocity from pore body to REV scale, they averaged local velocities weighted with local interfacial area:

$$v^{nw} = \frac{\sum_{i=1}^{\#pb} a_i^{nw} v_i^{nw}}{\sum_{i=1}^{\#pb} a_i^{nw}} \tag{31}$$

This definition has also a drawback; the term $a_i^{nw} v_i^{nw}$ does not represent a physical quantity and is not additive. They averaged fluid velocities weighted with local saturation. Since it was not possible to compare their simulation results with experiments, they compared the results with a simplified equation derived from thermodynamic theory developed for multiphase flow in porous media by Hassanizadeh and Gray (1990, 1993). They found that when the trapped interfaces were included in the calculation of total interfacial area, results of the simulation will underestimate the menisci velocity compared with the thermodynamic-based equations. As expected, their results were in better agreement with theory for stable displacement ($M = 10$) compared with viscous fingering regime ($M = 0.1$) as shown in Figure 23. Nordhaug et al. (2003) found that regardless of displacement regime, under constant pressure boundaries, interface velocity decreased nonlinearly with decrease of wetting fluid saturation during drainage; with the major drop in velocity happening in the saturation range from 1.0 to 0.8. Qualitatively a similar behavior for average interface velocity versus saturation was found by Lam and Horváth (2000) in pore-network modeling of primary imbibition. Velocity of interfaces in the case of unfavorable viscosity ratio were higher than the case of favorable viscosity ratio. In their model, there were some simplifications that might affect results significantly. For instance, capillary

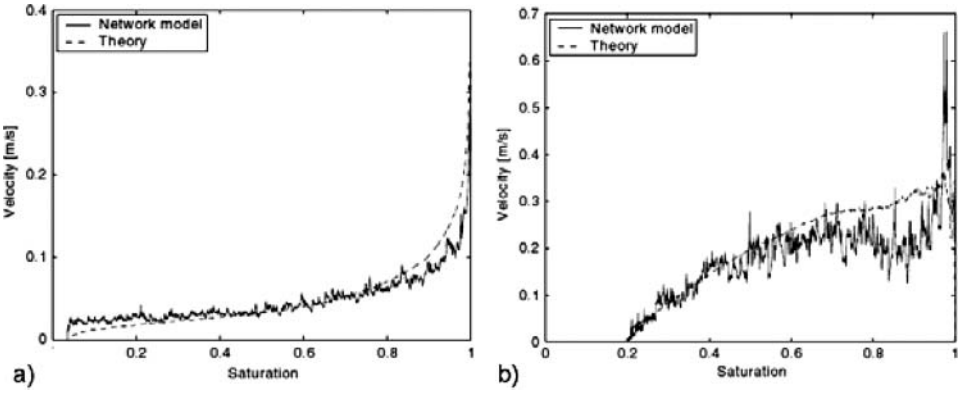

FIGURE 23. Comparison between velocity of interface resulted from model and theory for (a) $M = 10$ and (b) $M = 0.1$ (Nordhaug et al., 2003).

diffusion through corner flow, local capillary pressures at pore bodies, and tracking of interface in pore throats were not included in the model.

In a recent study, Joekar-Niasar et al. (2010a) studied variation of specific interfacial area (as the ratio of total fluid-fluid capillary interfaces to the total volume of the sample) with saturation under different boundary pressures. They simulated the drainage process under five different global pressure differences and three different viscosity ratios (M =0.1,1, 10). Viscosity of the wetting fluid was kept constant in all simulations. They calculated the specific interfacial area under dynamic conditions and compared it with the quasistatic simulations. It was shown that with the decrease of invading fingers, the area associated with the main fluid-fluid interfaces will decrease as shown in Figure 24. Furthermore, they showed that the production rate

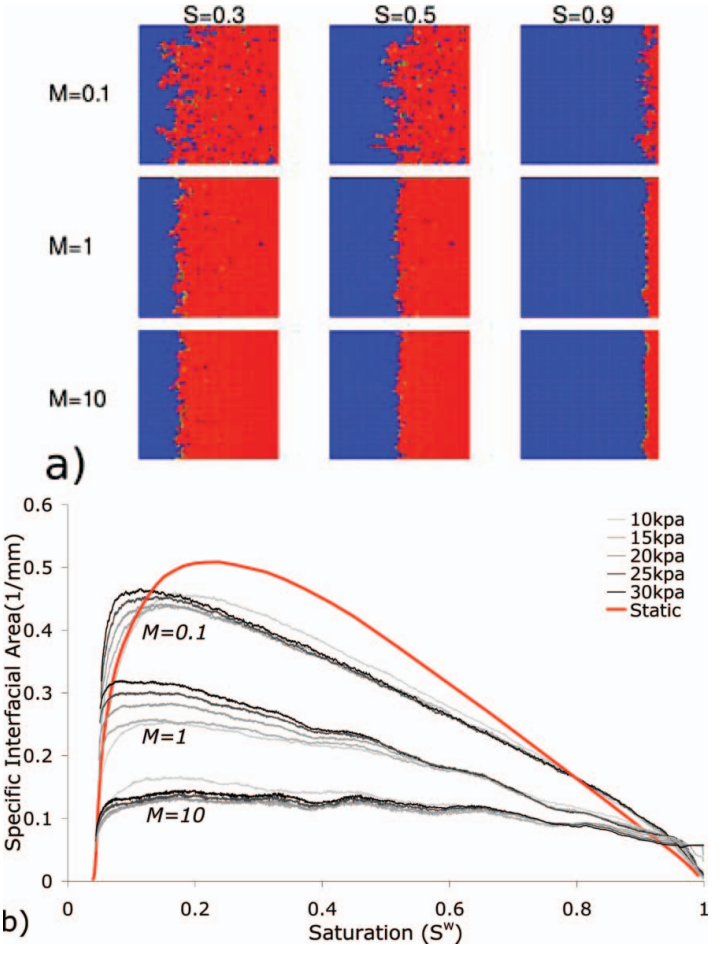

FIGURE 24. (a) Qualitative comparison of macroscopic interface topology for $M = 0.1, 1$ and 10 in a 2D (70 × 70) network at three different saturations, (b) Quantitative comparison between quasistatic and dynamic specific interfacial area-saturation curves for the same fluid-solid properties as (a) and boundary conditions mentioned (Color figure available online).

of specific interfacial area has a linear function with $\frac{\partial s^w}{\partial t}$ and production rate of interfacial area decreases with decrease of s^w during drainage.

7. GANGLIA FLOW DYNAMICS

As mentioned in Section 4, during both drainage and imbibition processes, the receding phase can be entrapped in the domain. However, the trapping mechanisms are more significant during imbibition than drainage. In reservoir engineering, at the end of a secondary flooding, a large ratio of oil remains entrapped in the reservoir. The residual oil exists in the form of discrete oil ganglia that can occupy 25 to 50% of the pore space. The size of an individual ganglion is typically ranging from one to fifteen pore volumes (Payatakes et al., 1980). A picture of trapped ganglia in a micromodel is shown in Figure 25 (from Avraam and Payatakes, 1995a).

Based on visual observations and flow rate measurements, Avraam et al. (1994), and Avraam and Payatakes (1995) found that the disconnected oil movement contributed substantially to the flow of oil during imbibition. (Avraam et al., 1994; Avraam and Payatakes, 1995) stated that over a large range of system parameters (in the range of practical interest) the flow of oil takes place solely through the movement of ganglia and/or droplets. Based on their experiments, two-phase flow behavior can be roughly classified into four flow regimes: large ganglion dynamics (Figure 26a), small ganglion dynamics (Figure 26b), drop traffic flow (Figure 26c), and connected-path flow (Figure 26d). In the first three classes, oil flow is due to the motion of disconnected bodies of oil. This is the case even in the connected-path flow

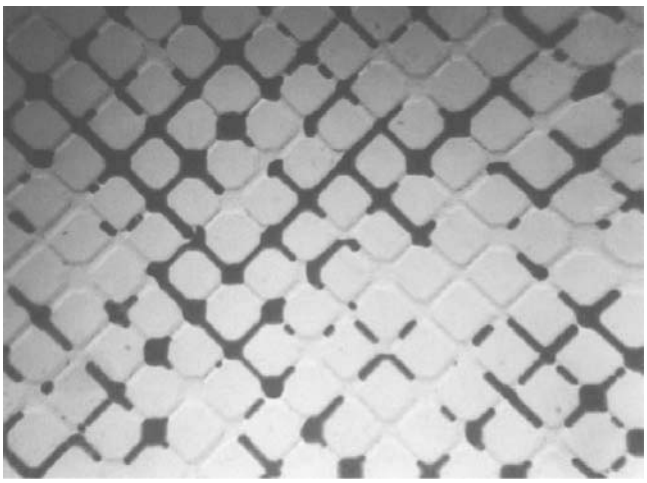

FIGURE 25. Snap-shot of ganglia trapped in a micromodel under steady-state flow conditions (Avraam and Payatakes, 1995a).

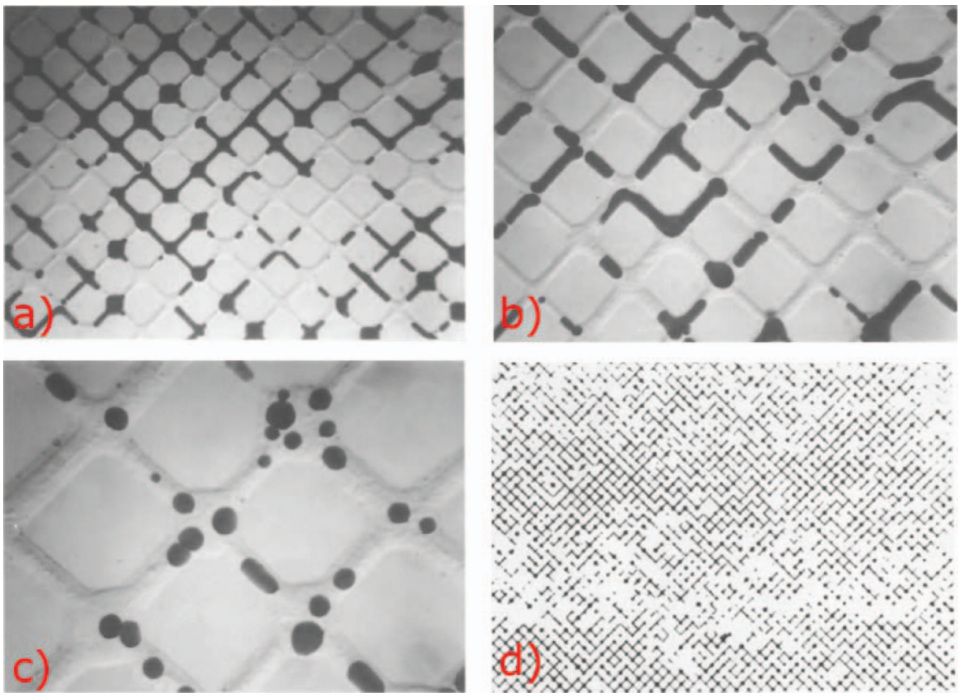

FIGURE 26. Ganglia flow regimes (a) Large ganglia dynamics (b) Small ganglia dynamics (c) Droplet traffic flow (d) Connected-path flow (Avraam and Payatakes, 1995a) (Color figure available online).

regime (high values), where many droplets and ganglia move at the fringes of connected pathways. Nonlinearity in the relative permeability depends on the pressure gradient, which is related to the creation, motion, fission, and coalescence of ganglia/droplets or menisci/interfaces. Observations showed that, for a wide range of variables ($10^{-8} \leq Ca \leq 10^{-6}$;$0.6 \leq M \leq 3.4$; $0.2 \leq S_w \leq 0.8$), oil is disconnected in the form of ganglia or droplet.

One of interesting issues—investigated extensively—is the fate of trapped ganglia under different dynamic conditions.

Most pore-network models assume that at any flow rate, disconnected ganglia are immobile. In addition, it has been assumed that the intertwined pathways of the two fluids are nearly independent of the flow rate within a wide range of flow rates. This assumption leads to the result that the phase velocity is a linear function of macroscopic pressure gradient. However, in experiments the phase velocity is nonlinearly dependent on macroscopic pressure gradient. A number of pore-network models have been developed by Payatakes and coworkers for ganglia movement. They have investigated different aspects of ganglia movement and its contribution to the nonlinearity observed in relative permeabilities in several publications. The use of pore network modeling for studying ganglia movement has been reported in

Ng and Payatakes (1980), Payatakes (1982); Payatakes et al. (1980), Dias and Payatakes (1986a, 1986b), Hinkley et al. (1987), Constantinides and Payatakes (1991, 1996), Avraam et al. (1994), Avraam and Payatakes (1995); Avraam and Payatakes (1995a), Vizika et al. (1994), Valvanides et al. (1998); Valvanides and Payatakes (2001), Dahle and Celia (1999), Al-Gharbi and Blunt (2005), and Bravo et al. (2007).

At pore scale, various mechanisms can act on ganglia, such as breakup (of a ganglion into two smaller ganglia), mobilization (of an entrapped ganglion within the pore space), stranding, and coalescence (if two or more ganglia join to form a new bigger ganglion). To investigate the effect of these pore-scale phenomena at macroscale, Payatakes and his coauthors adopted the following steps, implemented in several publications from 1980 to 2001 (see the previous list):

- Defining system parameters for a single pore, such as geometry, conductivity, and entry capillary pressure.
- Simulating ganglia dynamics in a pore-network model at meso-scale ($\sim 10^3$ pores) to calculate system factors; such as the mean time-averaged ganglion velocity, the stranding and breakup coefficients, the mode of ganglion breakup, the probability of stranding of a newly formed ganglion, and the mean and maximum length of a ganglion for a given volume (Valvanides et al., 1998).
- Development of population-dynamic equations and using the system factors acquired in the previous step to investigate the effect of ganglia dynamics at macroscale for steady-state conditions.

The main findings are described below in section 7.1.

7.1. Microscale Phenomenology of Ganglia Dynamics

Ng and Payatakes (1980) have developed an approach for determining the fate of an immiscible ganglion in a granular porous medium under quasistatic displacement. In other words, ganglia flow stage was not simulated in their model. Since they studied quasistatic displacement of a ganglion, no pressure field was computed. They considered three mechanisms for a solitary ganglion in porous medium, namely, breakup, mobilization and stranding (but not coalescence).

To summarize their approach, a ganglion with an arbitrary volume was considered in the network model and the exact geometry of the ganglion was captured. Then, mobilization-breakup criterion was applied to all interfaces to determine advancing/receding interfaces at that capillary number. Simulations were terminated when stranding or breakup occurred. To understand the mechanisms more clearly, several realizations in each class of capillary number and ganglion volume were implemented. Finally,

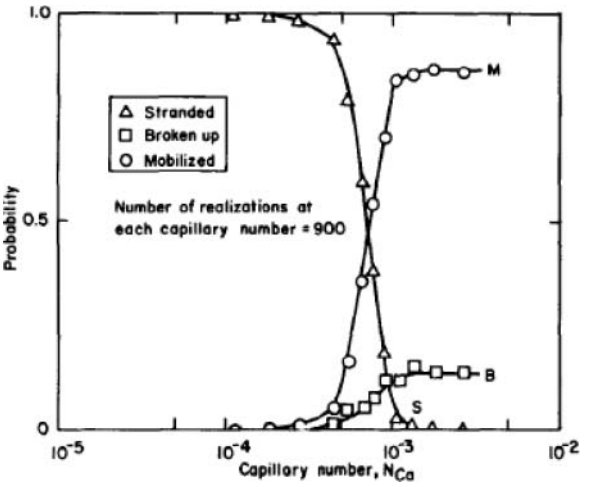

FIGURE 27. Probability of mobilization (M), breakup (B) and stranding (S) per rheon for a ganglion versus. capillary number (Ng and Payatakes, 1980).

probability functions were produced for the fate of a solitary ganglion based on quasistatic conditions as shown in Figure 27. This figure shows variations of occurrence probability in a capillary number range of 10^{-4} to 10^{-2}. Ng and Payatakes (1980) showed that the threshold capillary number for moving the stranded ganglia is 10^{-4}. It decreases form 10^{-4} to 10^{-3} from probability of 1 to zero. But probability of two other phenomena, namely breaking up and mobilization, increases. However, mobilization increases to the probability of 0.85 and breakup probability increases to almost 0.15. When stranding of ganglia begins to decrease, probability of mobilization begins to increase.

These three mechanisms are functions of ganglion volume and capillary number; larger ganglia have higher probability for breakup and less probability for stranding as shown in Figure 28. Ng and Payatakes (1980) introduced the concept of Conceptual Element Void Space (CEVS), which is the volume assigned to the pore elements surrounded by circles in Figure 11. In the simulations, they observed that in the absence of coalescence, the ganglia would be immobile. Thus it was necessary to study the role of coalescence in producing large ganglia.

All results shown previously were obtained from a quasistatic pore-network model. However, dynamics of ganglia is more complex. It has been observed in experiments that in viscous-dominated flows, ganglia can move through several pores simultaneously. Due to the lack of this feature in quasistatic models, there were two major shortcomings in such simulations. First, it was observed that tendency for alignment and elongation in experiments was less, compared with simulations. Second, if downstream part of a ganglion encounters small pores, it cannot advance into them quickly. Thus, the ganglion may grow a new branch at some appropriate site along its body

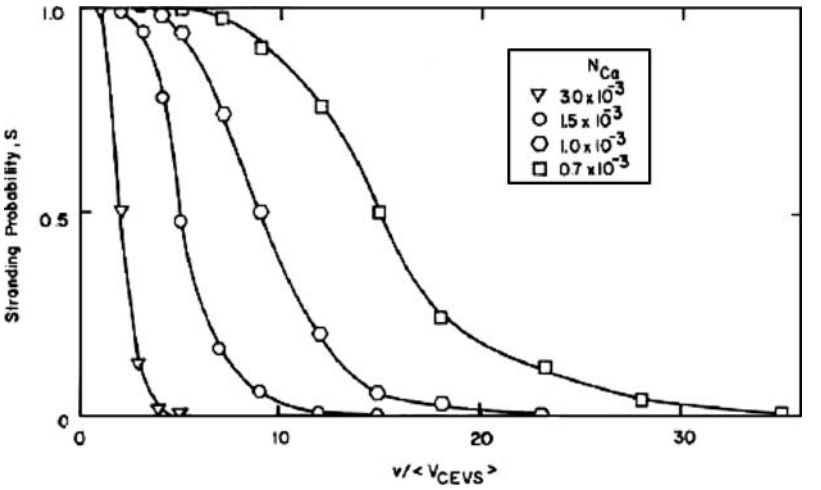

FIGURE 28. Probability of stranding (S) per rheon for a ganglion volume of ganglion for different capillary number (CEVS; Ng and Payatakes, 1980).

to bypass the elongation (Payatakes, 1982). Since Payatakes and coworkers were interested in using the microscale results for macroscale simulations based on population-dynamics formulation, they had to define coefficients representing microscale mechanisms, such as stranding (λ), breakup (ϕ), and coalescence (Co). The first two ones were defined as follows:

$$\lambda = -\frac{1}{n}\frac{\partial n}{\partial z}\Big|_{\text{due to stranding}} \tag{32}$$

$$\phi = -\frac{1}{n}\frac{\partial n}{\partial z}\Big|_{\text{due to break-up}} \tag{33}$$

in which n is the total number of ganglia and $\frac{\partial n}{\partial z}$ is the variation of n in z direction. But, the coalescence factor was not as straight-forward as breakup and stranding factors. Coalescence factor of ganglia was investigated by Constantinides and Payatakes (1991). Coalescence at pore scale depends on many factors including pore geometry, physical properties of fluids, interfacial tension, interface velocity, double ionic layer interactions, initial positions of interfaces, and pressure difference between oil bodies. Constantinides and Payatakes (1991) tried to quantify the coalescence parameter using their porenetwork model. The model consisted of two components, simulating bulk motion of ganglia in a porenetwork, and simulating drainage of a water film trapped between two colliding menisci at each pore (Figure 29).

Both parts were coupled together at different time scales. The time scale of the inner component (water film simulator) was much smaller than the outer one. They simulated the film flow using a criterion for critical

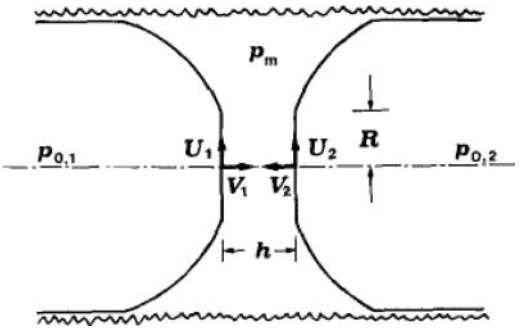

FIGURE 29. Schematic presentation of two-component model for simulating coalescence (Constantinides and Payatakes, 1991).

thickness of film. When the thickness of the film is larger than the critical value, the interfaces are non-interacting. However, in very small thickness (in this work $\sim<$ 100Å), London-van der Waals forces are considered using the Hamaker constant (Sheludko, 1967). Constantinides and Payatakes (1991) defined a probability rate for coalescence for two ganglia with different sizes and found a range of 0.03−0.15. Coalescence probability would increase gradually with the increase of capillary number, but it increased significantly with the decrease of contact angle.

Figure 30 shows plots of stranding and breakup coefficients against the ganglia volumes for different wetting-phase saturations resulted from dynamic pore-network modeling, while coalescence probability (Co) was set equal to 0.15 (Valvanides et al., 1998). According to Figure 30, with the increase of ganglia volume, breakup coefficient increases while stranding coefficient decreases nonlinearly. Furthermore, with the increase of

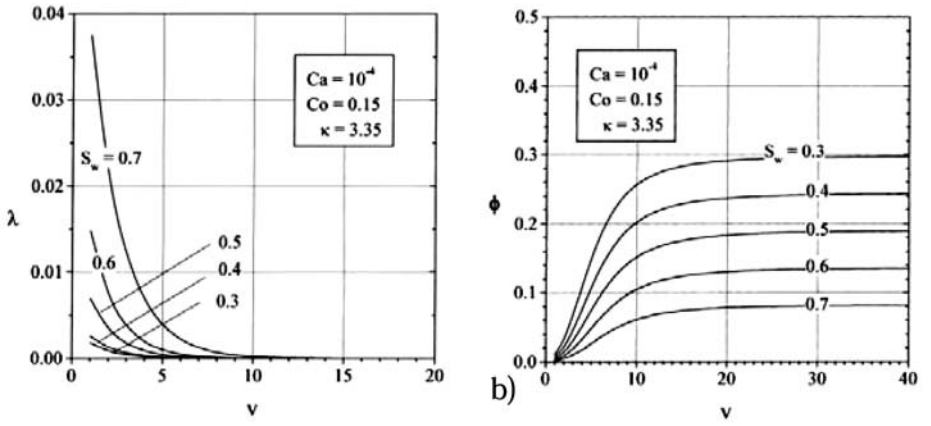

FIGURE 30. Dependency of (a) stranding coefficient, λ and (b); break-up coefficient ϕ on the ganglion volume, v, and the water saturation, S_w, for $Ca = 10^{-4}$, $\kappa = \frac{\mu_n}{\mu_w} = 3.35$, $Co = 0.15$, $\theta_a = 45$, $\theta_r = 35$ (Valvanides et al., 1998).

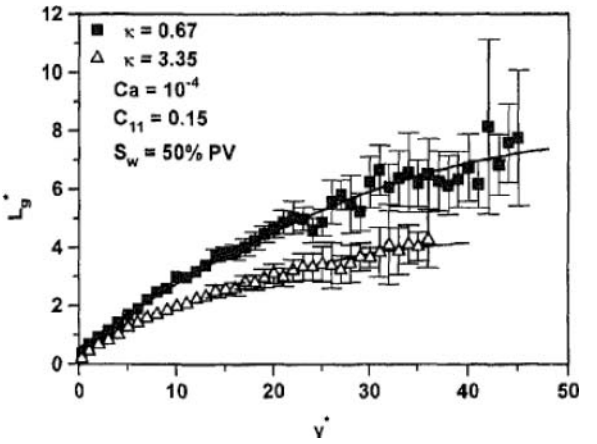

FIGURE 31. Length of ganglia (normalized by mean lattice spacing length) for different ganglia volume and two viscosity ratios ($\kappa = 1/M$; Constantinides and Payatakes, 1996).

wetting phase saturation, stranding coefficient increases and breakup coefficient decreases.

Length of ganglia under different dynamic conditions is another system factor that should be determined for macroscale modeling of ganglia dynamics. For $M > 1$ during imbibition, length of ganglia aligned to the direction of macroscopic flow is relatively high (Figure 31). But, for $M < 1$ length of ganglia decreases in direction of flow (Figure 31), and it prefers to follow a path composed of large pores. With the decrease of water saturation, interstitial velocity and local pressure gradient increase, which increases dynamic ganglion displacement. Thus, with decrease of saturation, tendency of ganglia to become long and aligned with the macroscopic flow direction increases. Thus ganglia displace not only in the direction of the macroscopic flow, but also in other directions due to the population density. As Valvanides et al. (1998) have observed, stranding of ganglia decreases as *Ca* or ganglia size increases and breakup increases. With the increase of viscosity ratio (decrease of κ) during imbibition, time rate of stranding decreases and breakup rate decreases (Constantinides and Payatakes, 1996), although the first one is stronger. In addition, with the decrease of M ganglia volume decreases. Effect of viscosity ratio on the size of ganglia is significant at large wetting phase saturations.

Another system factor required for macroscale modeling is the average velocity of ganglia for different ganglia volumes. To understand the dynamics of ganglia, Payatakes (1982) reviewed data from a micro-model experiment done by Rapin (1980). Rapin (1980) investigated the velocity of ganglia using visualization techniques in experiments. His results are shown in Figure 32, where u_z/V_f is the normalized velocity of a ganglion defined as the velocity of the centroid of a ganglion (u_z) divided by the superficial velocity of

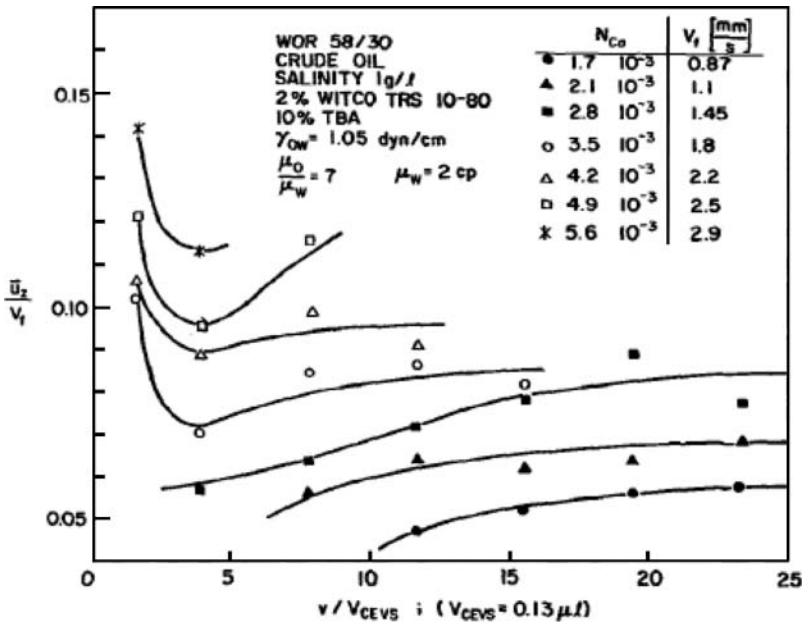

FIGURE 32. Average ganglion velocity (normalized by superficial fluid velocity) versus ganglion volume (normalized by volume of CEVS) for several typical capillary number values. Here, the viscosity ratio is $\mu_n/\mu_w = 7$ (Payatakes, 1982). Data are from Rapin (1980).

the flooding (V_f). According to Figure 32, for a given volume of ganglia, the normalized velocity is a monotonically increasing function of capillary number. Near a critical mobilization capillary number, the normalized velocity increases monotonically with volume, reaching an asymptotic value for volume of ganglia. The asymptotic value of ganglia is about 15∼20 CEVS volume. However, when the value of capillary number exceeds critical mobilization value, velocity will have a minimum in range of 3∼5 CEVS volume. Later, Dias, and Payatakes (1986a, 1986b) and Valvanides et al. (1998) developed a dynamic pore-network model to investigate velocity of ganglia and its dependencies on system parameters. Simulation results shown in Figure 33 are qualitatively comparable with the experiments. Figure 33 shows velocity of a ganglion versus its volume for different viscosity ratios. For viscosity ratio smaller than 1 ($M = 1/\kappa$, $\kappa > 1$), the time-averaged ganglion velocity of oil is smaller than the average velocity of the water. If viscosity ratio is larger than 1 ($\kappa < 1$), this ratio will be larger than 1. Obviously, ganglia velocity increases with the increase of *Ca*.

An interesting result from these simulations is that for a ganglion with a given volume, with the increase of *Ca*, ganglia velocity can reach an asymptotic value for $M < 1$. However, this is not found to hold for $M > 1$. This means that when the wetting fluid is less viscous than the nonwetting fluid, the blobs of the nonwetting phase can move faster and they are less

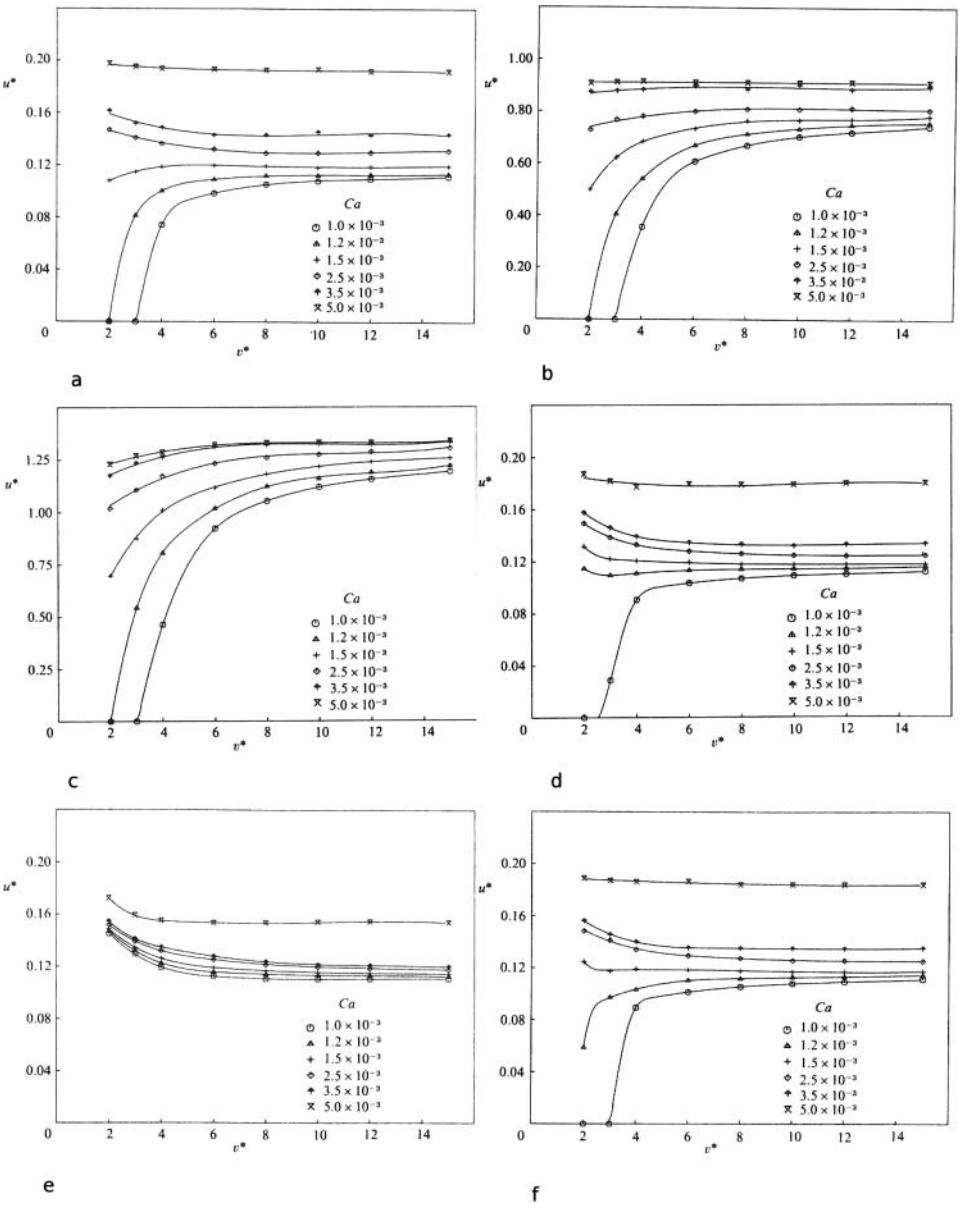

FIGURE 33. Normalized time-averaged ganglion velocity, $u^* = u_z/V_f$, versus the normalized ganglion volume v^* (ganglia volume divided by the volume of a CEVS), in a 15 × 30 network for various *Ca* values, u_z is the velocity of the centroid of a ganglion, and V_f is the superficial velocity of the flooding. (a) $\kappa = 7, \theta_e = \theta_a = \theta_r = 0$. (b) $\kappa = 1, \theta_e = \theta_a = \theta_r = 0$. (c) $\kappa = 0.6, \theta_e = \theta_a = \theta_r = 0$. (d) $\kappa = 7, \theta_e = \theta_a = \theta_r = 10$. (e) $\kappa = 7, \theta_e = \theta_a = \theta_r = 30$. (f) $\kappa = 7, \theta_e = 10\theta_a = 11.4\theta_r = 0$, $\kappa = \frac{\mu_n}{\mu_w}$ (Dias and Payatakes, 1986b).

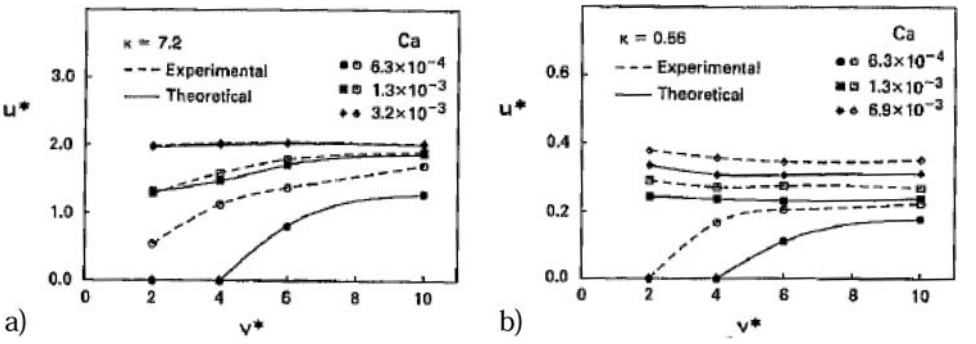

FIGURE 34. Comparison between experimental and theoretical values of the normalized time-averaged ganglion velocity, $u^* = u_z / V_f$, versus the ganglion volume (normalized by the volume of a CEVS), v^*, for various capillary numbers and viscosity ratios. (a) κ =7.2. (b) κ = 0.56, $\kappa = \frac{\mu_n}{\mu_w}$ u_z is the velocity of the centroid of a ganglion and V_f is the superficial velocity of the flooding (Hinkley et al., 1987).

constrained by the invading phase. Based on these simulations, hysteresis in contact angle cannot significantly affect the trend of time-average velocity especially for large ganglia and large *Ca* values.

Hinkley et al. (1987) compared results of the pore-network modeling of Dias and Payatakes (1986a) with the micro-model experiments. They performed some two-dimensional micromodel experiments to investigate the velocity of ganglia for different viscosity ratios and capillary numbers. The model was made of one layer of grains sandwiched between two Plexiglass sheets. Resulting pores were completely regular and uni-size. Comparison between simulation and experimental results is shown in Figure 34. The agreement is very good large capillary numbers, since nonlinearity of the multiphase flow system is not significant. With the decrease of capillary number and increase of viscosity ratio (decrease of κ), the agreement decreases significantly, due to the increase of nonlinearity of the system. The difference can be due to the fact that ganglion motion depends on the initial shape and orientation of the ganglion, the local characteristics of the porous medium, and the distribution of the two phases in the nearby region (Valvanides et al., 1998). In any case, despite the quantitative difference, the same behavior for ganglia dynamics observed by Rapin (1980) was captured by the model.

7.2. Macroscale Ganglia Dynamics

Based on the system factors resulted from pore-network modeling and proposing population dynamics balance equations developed for macro scale ganglia dynamics, Payatakes et al. (1980), Constantinides and Payatakes (1996) and Valvanides et al. (1998) studied macroscale dynamic motion of the ganglia in porous media.

Main assumptions of this model include (a) oil is totally disconnected in the form of ganglia of various sizes (b) the macroscopic flow is one-dimensional (c) the longitudinal dispersion of ganglia is neglected (d) gravity is neglected (e) in the integration of the population balance equations, the ganglia are considered as points coinciding with their mass centers; and (f) specific assumptions are made for the calculation of the dimensionless collision rate.

The resulted populations dynamics equations for moving and stranded ganglia were integro-differential type of equations that were solved numerically. For sake of space the equations and their explanations have not been mentioned in this review. Complete explanation can be found in Payatakes et al. (1980) and Valvanides et al. (1998). Using the population dynamics equation, Valvanides et al. (1998) investigated fate of stranded as well as moving ganglia with space and time for two different types of regime: steady-state fully developed (SSFD) and steady-state non-fully developed (SSnFD). Under SSFD conditions, number concentrations of moving and stranded ganglia are independent of time and space. However, under SSnFD conditions, number concentrations of moving and stranded ganglia are only independent of time.

8. RELATIVE PERMEABILITY

One of the major applications of pore-network models has been in the investigation of relative permeability curves especially for predictive purposes. However, relative permeability curves have been mostly produced by quasistatic pore-network models. To use quasistatic pore-network models for relative permeability simulation, it is assumed that flow paths of both phases are frozen at a given saturation (or a grain global capillary pressure). Thus, dynamic effects on the flow path are ignored. But, Hughes and Blunt (2000) showed that the contact angle, initial wetting saturation, and flow rate can affect significantly the displacement pattern and consequently the relative permeability curves. Extensive experimental and theoretical investigations have shown that the relative permeabilities are strong functions of a large number of parameters, including S_w, Ca, flow rates ratio r, viscosity ratio M, advancing and receding contact angles θ_a and θ_r, coalescence factor, Bond number (Bo), and the flow history (Avraam et al., 1994; Avraam and Payatakes, 1995; Constantinides and Payatakes, 1996; Valvanides et al., 1998).

$$k_{ro} = k_{ro}(S_w, Ca, r, M, \cos\left(\theta_r^0\right), \cos\left(\theta_a^0\right), Co, Bo, \text{flow history}) \qquad (34)$$

Payatakes and co-authors, carried out extensive experimental and numerical studies, using micro-models and pore-network models, to investigate the

effect of ganglia movement on relative permeability (Avraam et al., 1994; Avraam and Payatakes, 1995).

Constantinides and Payatakes (1996) developed a dynamic pore-network model, including dynamics of ganglia, to investigate relative permeability curves at steady-state flow for different saturations. To calculate relative permeability, they used the following equation:

$$\frac{q^{\alpha}}{A} = -k_{r\alpha}\frac{k}{\mu^{\alpha}}\frac{\Delta P^{\alpha}}{L}, \alpha = w, n \tag{35}$$

in which q^{α} is the total flux for α phase, A is the cross section of pore-network model normal to the flow direction, $k_{r\alpha}$ is the relative permeability of α-phase, k is the intrinsic permeability of the pore-network, μ^{α} is the viscosity of phase α, L is the length of the pore network in flow direction, w and n denote wetting and nonwetting phases, respectively, and ΔP^{α} is the pressure drop of phase α. The approach for defining boundary conditions in pore-network model developed by Constantinides and Payatakes (1996) was explained in section 3.4. To prevent effect of initial condition on simulation results, they continued the simulations so that the time-averaged relative permeability became constant. Results for relative permeability of oil are shown in Figure 35. The same behavior was found for relative permeability of water, and macroscopic pressure drop for nonwetting and wetting phase. Oscillations in relative permeability values of oil are small for large ganglion dynamics. But, they are significant for connected-path flow regime. The wetting phase relative permeability oscillations were minimal for small ganglion dynamics.

Constantinides and Payatakes (1996) calculated relative permeability curves for different viscosity ratios and capillary numbers, including ganglia dynamics effect. Figure 36a shows the effect of viscosity ratio on relative permeability curves. With the increase of viscosity ratio (decrease of $\kappa = \frac{\mu^n}{\mu^w}$), relative permeability decreases. It is clear that relative permeability of nonwetting phase is more sensitive to the viscosity ratio. Constantinides and Payatakes (1996) postulated that with the decrease of M $(= \frac{\mu^w}{\mu^n})$, both phases tend to segregate and create their own separate flow paths. Nonwetting phase tends to flow through big pores, which causes an increase of its permeability. This segregation reduces viscous dissipation in the system. However, these results differ from the findings of Lefebvre du Prey (1973) and Fulcher et al. (1985), who observed experimentally that with the decrease of M, relative permeability of nonwetting phase increased but relative permeability of wetting phase decreased. Constantinides and Payatakes (1996) conjectured that this contradiction may be due to the fact that in those experiments, different fluids and porous media were used, which may indeed affect contact angle and consequently relative permeabilities.

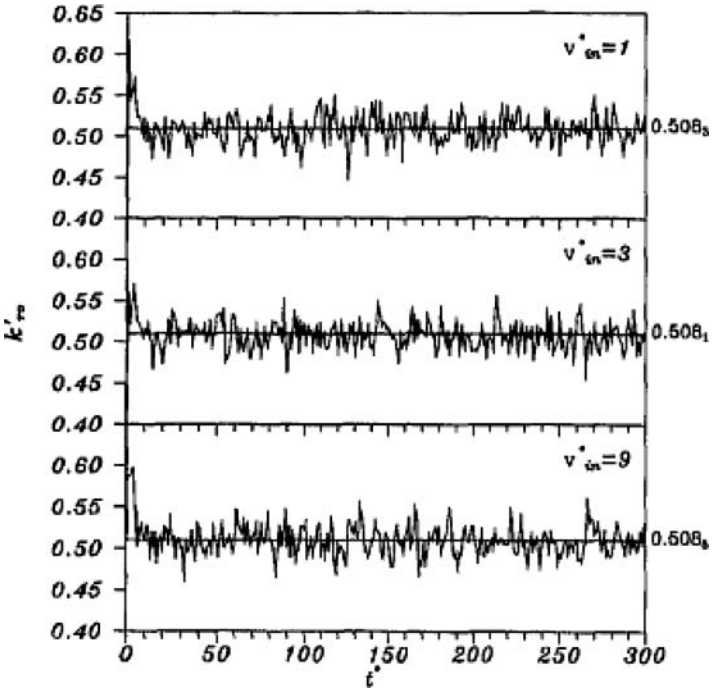

FIGURE 35. Time series of the instantaneous relative permeability of oil, k'_{ro} for (a) Ganglia with 1 CEVS volume (b) Ganglia with 3 CEVS volume (c) Ganglia with 9 CEVS volume ($\kappa = 3.35$, $Ca = 10^{-4}$, $C_{11} = 0.15$, $S_w = 0.5$ pore-volume, $\theta_a^0 = 45°$, $\theta_r^0 = 35°$ Constantinides and Payatakes, 1996).

Figure 36b shows the effect of capillary number on relative permeability. With the increase of capillary number, relative permeability increases as well. Constantinides and Payatakes (1996) found that at medium and high *Ca* values, the two fluids tend to become more segregated compared

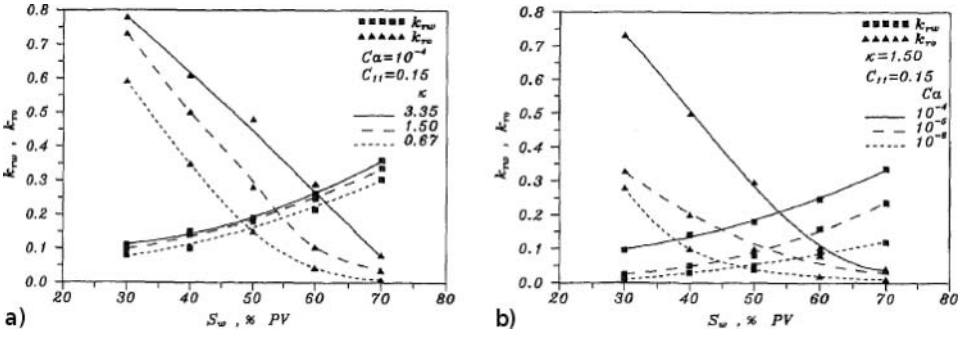

FIGURE 36. Dependency of steady; state relative permeability of both fluids (k_{rw} and k_{ro}) on water saturation (a) for different $\kappa = \frac{\mu_n}{\mu_w}$ ($\kappa = 0.67, 1.5, 3.35$, $Ca = 10^{-4}$, $\theta_{advancing} = 45°$, $\theta_{receding} = 35°$) (b) for different capillary number values *Ca* ($Ca = 10^{-4}, 10^{-5}, 10^{-6}$, $\theta_{advancing} = 45°$, $\theta_{receding} = 35°$ Constantinides and Payatakes, 1996).

with small capillary number values. This causes an increase of both relative permeabilities.

Avraam et al. (1994) observed the same behavior in two-dimensional and quasi-three-dimensional (consisting of two layers of pores) micro-models under steady-state conditions. They found that relative permeability of oil correlates strongly with the flow regimes and dynamic parameters of the system such as capillary number and viscosity ratio. Avraam and Payatakes (1999) showed that the lubrication effect can be significant for strongly wetting systems. They observed experimentally that for small capillary numbers ($Ca \leq 10^{-6}$), flow of oil takes place through the motion of ganglia and/or droplets. For larger capillary numbers ($Ca > 10^{-6}$), connected pathways for the flow of oil can form, but the disconnected flow can also lubricate the flow of ganglia.

Avraam et al. (1994) and Avraam and Payatakes (1995) also investigated relative permeability curves using micro-model experiments. Their micro-model had a square lattice structure with node-to-node distance of 1221 μm. Macroscopic flow direction was parallel to one of the diagonals. The network consisted of 11300 chambers and 22600 throats. Mean diameters of chambers and pore throats were 560 μm and 112 μm, respectively. Maximum depth of pores was almost uniform equal to 140 μm. Cross section of pore throats was almost eye-shaped with a planer porosity of 0.25. To study the effects of different physical parameters such as viscosity ratio and interfacial tension, three different fluid sets were used. In each experiment, simultaneous injection of the two fluids was continued (at a constant rate) until steady-state conditions was reached. Avraam and Payatakes (1995) observed that at the pore scale this mechanism is transient but at mesoscale it is almost stationary, such that it can be identified as steady state.

Based on the experimental data reported by Avraam and Payatakes (1995), Avraam and Payatakes (1995a) implemented some optimization calculations to study the behavior of viscous coupling coefficients ($k_{r\alpha\beta}$, $k_{r\beta\alpha}$) introduced in the following extended Darcy's law.

$$v_\alpha = -\frac{kk_{r\alpha}}{\mu_\alpha}\frac{\Delta P_\alpha}{L} - \frac{kk_{r\alpha\beta}}{\mu_\beta}\frac{\Delta P_\beta}{L}$$
$$v_\beta = -\frac{kk_{r\beta}}{\mu_\beta}\frac{\Delta P_\beta}{L} - \frac{kk_{r\beta\alpha}}{\mu_\alpha}\frac{\Delta P_\alpha}{L} \tag{36}$$

The cross-coupling terms are needed to describe the macroscopic flow when a disconnected fluids is present. Avraam and Payatakes (1995a) used their pore-network model to study changes of the coefficients with S_w, Ca, and M. Conventional and generalized relative permeabilities were determined based on B-spline functions combined with standard

constrained optimization techniques. They found that the cross coefficients were not equal ($k_{r\alpha\beta}/\mu_\beta \neq k_{r\beta\alpha}/\mu_\alpha$). These coefficients as well as conventional coefficients were found to depend on the flow conditions and the corresponding flow mechanics.

Relative permeabilities $k_{r\alpha}$ and $k_{r\beta}$ are increasing functions of the saturation of the respective fluid. $k_{r\alpha}$ and $k_{r\beta}$ increase as Ca increases (shown in Figure 37a-f). The behavior of $k_{r\alpha}$ is more complicated. In most cases $k_{r\alpha}$ increases as S_α increases, but in certain cases the opposite behavior has been observed. Roughly speaking, as Ca increases, all the generalized coefficients increase.

Afterwards, Valvanides and Payatakes (2001) developed a continuum two-phase flow model, which included the nonlinear dependence of permeability coefficients. Their model was based on the decomposition of a two-phase system into two subdomains: connected-oil path domain and ganglion dynamics domain. The main goal in their model was to save computation time to have a mesoscale predictive model that for practical applications. The model results were compared with experimental results done in a two-dimensional micro-model by Avraam and Payatakes (1995a). They founded fairly good to good agreement with experimental results for low capillary numbers ($Ca = 10^{-6}$) at different viscosity ratios (Fig. 37b,e). It seems that for high capillary numbers, where ganglia dynamics can be important, the model was not fully successful and there was a need for further improvement before it could be used for predictive purposes (Fig. 37c).

Bravo et al. (2007) followed the same approach as Avraam and Payatakes (1995,a) did, to study coupling coefficients in extended Darcy's law. They used a dynamic pore-network model for simulating disconnected gas and oil flow. What they presented is very similar to the results of Avraam and Payatakes (1995a) for very limited cases. They studied the effect of disconnected gas bubbles on relative permeability curves for different bubbles sizes, but only in the viscous-dominated flow regime. They assumed that gas bubbles were incompressible, which is a good approximation when the relative variations of absolute pressures of gas bubbles due to the pressure gradient in water phase and also capillary pressure differences are negligible. However, at least at pore-scale, this assumption is no valid, because absolute pressure is known to fluctuate with time and space as Constantinides and Payatakes (1996) showned.

Bravo et al. (2007) found that when relative permeability of oil increases, when the viscosity of gas bubbles is smaller than that of oil, and even relative permeabilities larger than 1 can be obtained. In addition, they showed that the effect of gas bubble size at different gas saturations on relative permeability is not monotonic. There is a peak of relative permeability in the intermediate bubble size. In another study Wang and Mohanty (2000) investigated the relative permeability in gas-condensate systems. Similar to Avraam and Payatakes (1995a) as shown in Figure 26, Wang and Mohanty

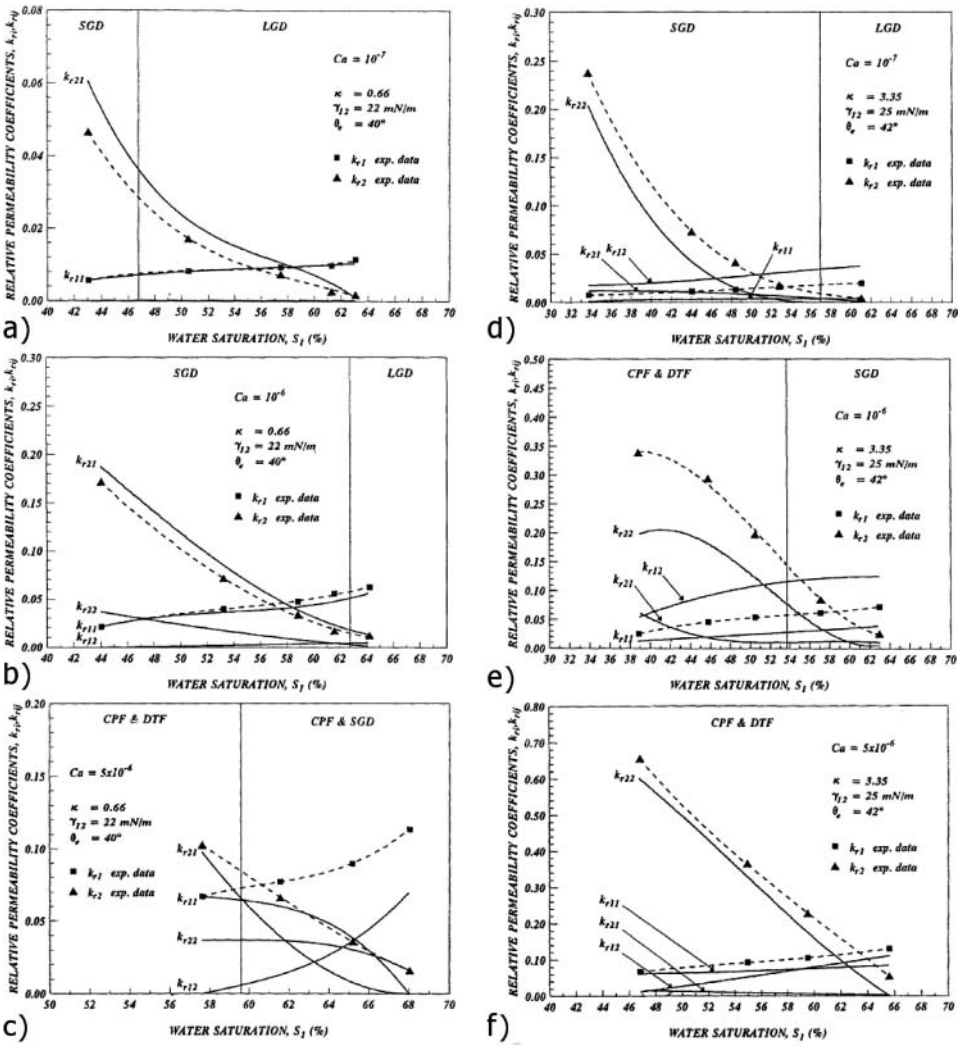

FIGURE 37. Conventional (broken lines) and generalized (solid lines) relative permeability coefficients for $\kappa = 0.66$ (left column) and $\kappa = 3.35$ (right column). (a,d) $Ca = 10^{-7}$. (b,e) $Ca = 10^{-6}$. (c,f) $Ca = 5 \times 10^{-5}$, given $\kappa = \frac{\mu_n}{\mu_w}$ (Avraam and Payatakes, 1995a).

(2000) illustrated that gas and condensate can have their separate path, or gas can flow with condensate as ganglia or it can flow as small droplets if the capillary number increases enough. In another study Jamiolahmady et al. (2003) developed an irregular lattice porenetwork with circular cross sections to investigate the effect of velocity on relative permeability, which was reported in gas-condensate core experiments by Herderson et al. (2001). To adapt the network structure to a Berea sandstone, the pore throats were deleted randomly to illustrate average coordination number of 3. To include

the tortuosity, bends, expansion, and contraction of real porous media in the idealized network, a hydraulic length was considered for calculation of the pressure drop. They observed that with increase of the injection velocity, the relative permeability of gas increases.

Using a dynamic pore-network model, and assuming a constant injection rate for drainage, Singh and Mohanty (2003) showed that for low capillary numbers, flow in the wetting phase flow includes only 1% of the total flow. Based on their results, saturation-relative permeability relationship is a function of capillary number, viscosity ratio and distribution of the pores as shown already by Blunt and King (1990) and Blunt and King (1991). Their model is based on the pore-network model developed by King (1987). However, King (1987) did not consider capillary pressure in the setup of equations. Later, Blunt and King (1991) added capillary pressure as a function of local pore size and showed that at the same saturation, relative permeability of the receding phase in low capillary numbers is below those with high capillary number as shown in Figure 38. But for the invading phase, both cases may occur. They explanation was that at very high rates, flow can proceed through all parts of the network, including the very small tubes. As *Ca* decreases, flow is blocked in some places due to capillary forces. This will tend to decrease the relative permeability of both injected and displaced fluids. At low rates, the injected fluid moves through only the widest channels, which means an increase of its permeability relative to the displaced fluid. Thus, at a given saturation, $k_{r\alpha}$ must decrease with the decrease of flow rate, while $k_{r\alpha}$ may either increase or decrease. This explanation works for different mobility ratios, so that with the decrease of mobility ratio, relative permeability of the invading phase will decrease. In addition, nonlinearity of relative permeability-saturation curve increases with the increase of interfacial tension.

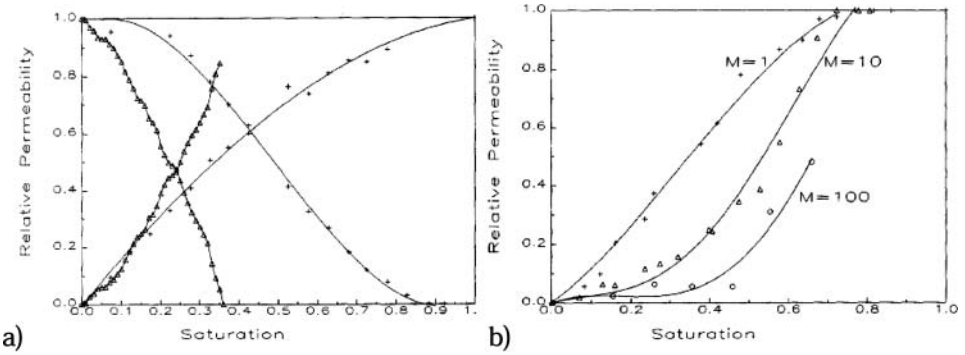

FIGURE 38. Relative permeability-saturation curves for different values of (a) *Ca* number and (b) viscosity ratios (Blunt and King, 1991).

9. DISCUSSION AND SUMMARY

9.1. Current State of Dynamic Pore-Network Models

9.1.1. Dynamic Pore-Network Modeling as an Investigation Tool

In this review, we have given an overview of various aspects of dynamics of two-phase flow in porous media, investigated using dynamic pore-network models. Table 4 presents a list of major dynamic pore-network models, their applications, and their technical specifications (such as size, simulated process, pressure algorithm, network geometry, and topology). These models can provide physicallybased insights into various processes and their dependencies that may be difficult to obtain through laboratory experiments. They have been used for understanding various aspects of dynamics of two-phase flow, such as

- pressure field development and evolution of capillary forces and viscous forces with change of saturation at Darcy scale.
- scaling of invasion patterns (mostly viscous fingering).
- crossover from capillary fingering to viscous fingering and from viscous fingering to compact flow.
- effect of capillary number and viscosity ratio on residual nonwetting phase saturation
- effect of geometry (aspect ratio) and topology (coordination number) on residual nonwetting phase saturation.
- nonequilibrium capillarity effects and dependencies of nonequilibrium capillarity coefficient.
- dynamic effects on relative permeability and viscous-coupling coefficients.
- dynamics of ganglia such as mobilization, stranding, breakup, and coalescence. Contribution of dynamics of ganglia to nonequilibrium effects in relative permeability.
- dynamic effects in fluid-fluid interfacial area and macroscopic interfacial velocity.

9.1.2. Computational Aspects of Dynamic Pore-Network Models

We have also presented and discussed technical details of dynamic pore-network models, such as network structure, governing equations, numerical problems, and boundary conditions.

The major computational issue in the dynamic pore-network modeling is related to the pressure field calculation. There are two different algorithms for solving the pressure fields, namely single-pressure and two-pressure approaches. The single-pressure algorithm is basically applicable to the networks with pore elements that have circular cross sections. In such networks, a pore element is occupied by only one fluid at any given time. To adapt

the single-pressure algorithm to the networks with angular cross sections, effective resistance of all pores are calculated using Kirchhoff's rule for electrical resistors. Then, instead of solving the pressure field in a network filled with physical fluids, it is solved for a network filled with an equivalent fluid phase (which is not physical). This approach has some shortcomings that are explained subsequently.

The pressure field is obtained by solving the linear system $\mathbf{K}P = B$. The coefficient $\mathbf{K}$ is composed of conductances of pores. In single-pressure algorithms for angular cross sections, the effective conductance is calculated from the geometry, regardless of the bulk flow direction or corner flow in a pore throat. This assumption influences the ability of the model in reproduction of some pore-scale mechanisms. For instance, pore-scale countercurrent flow in a pore throat cannot be reproduced. Thus, the capillary diffusion (through the corner) and its effect on relaxation of the interface are not modeled properly. It has been observed that during drainage, with the invasion of nonwetting fluid into a new pore, local imbibition in other pores behind the macroscopic front may occur. This happens due to the connection of wetting phase through the corners and local countercurrent flow in the pores. Such a mechanism cannot be modeled by the single-pressure approach. If the two-pressure algorithm is employed, flow directions of both nonwetting and wetting fluids are determined by local pressure gradient within each phase; this results in the reproduction of detailed pore-scale mechanisms.

The second computational issue is related to the numerical instability. In particular, the strong nonlinearity at the pore scale causes severe stability problems in dynamic pore-network models. This has been observed under capillary-dominated regimes as well as unfavorable viscosity ratios. This problem, referred to as "capillary pinning" has been reported in many studies such as Aker et al. (1998 1998b,a); Koplik and Lasseter (1985) and Løvoll et al. (2005). To remove the nonlinearity caused by capillary forces, in most studies, such as Aker et al. (1998a, 1998b) and Løvoll et al. (2005) capillary deactivation zones at both ends of pore throats were defined. Based on this assumption, capillary pressures at the ends of pore throats were forced to be zero. This assumption was imposed without any physical explanation. However, Joekar-Niasar et al. (2010a) showed that the combination of a semi-implicit saturation update (instead of explicit saturation update) and defining entry capillary pressure as well as snap-off capillary pressure would remove this numerical problem without any ad hoc assumption. Using this approach, Joekar-Niasar et al. (2010a) showed that results obtained from multistep pressure dynamic simulations are consistent with results of quasistatic simulations. However, they stated that the simulations were too time-consuming. Furthermore, they have mentioned that simulation time is highly dependent on capillary number and viscosity ratio in dynamic pore-network models.

9.1.3. Complex Invasion Mechanisms at Pore Level

As explained in section 3.6, pore-scale invasion mechanisms under imbibition is more complex than under drainage. Piston-like movement, snap-off, and cooperative filling are invasion processes that may occur under imbibition. The significance of these mechanisms is highly dependent on the pore geometry (angularity of cross sections, aspect ratio; Wardlaw and Yu, 1988). For instance, in domains with small aspect ratio, cooperative filling will be the dominant invasion mechanism, which cannot be simulated by pore-network models accurately. Thus, application of network models for predictive purposes for high porosity domains will fail (Joekar-Niasar et al., 2009). Furthermore, in such media, it is hard to clearly identify pore bodies and pore throats. With such geometrical complexities, dynamic pore-network models are less promising for predictive purposes. Thus, application of dynamic pore-network models for investigation of two-phase flow in fibrous material (such as Thompson [2002] who simulated air-liquid flow in paper) is only qualitatively, and not quantitatively, useful.

Other complexities in dynamics of two-phase flow, which are absent in quasistatic models, are related to the mobilization of a disconnected phase. This issue was studied extensively by Payatakes and his coworkers from 1980 to 2002. Generally, they focused on the mobilization of a disconnected phase (ganglia) and its contribution to dynamic effects in relative permeability curves. Despite the substantial works they performed, there are some major shortcomings in their approach such as the following:

- Their micromodels and pore-network models had idealized and regular geometries. Thus, effects of topological and geometrical properties of porous media were not investigated. Since pore-scale phenomena (snap-off, invasion, corner flow) are highly dependent on pore geometry, shape factor, and aspect ratio, the results of their micromodels and network models are not directly applicable to most natural porous media.
- Their pore-network model was based on the single-pressure algorithm for circular cross sections. Thus, effects of corner flow, snap-off, capillary diffusion, and interface relaxation behind the invading interface could not be studied.
- Valvanides et al. (1998) and Valvanides and Payatakes (2001) used dynamic pore-network models to obtain statistical relationships for coalescence, breakup, and mobilization of ganglia as a function of ganglia size and flow velocity. They obtained statistical kernel functions and employed them in macroscopic equations of population dynamics of ganglia for one-dimensional systems. However, they did not clarify how this approach can be followed in a three-dimensional system. Moreover, due to complexities of their approach, as well as dependence of kernel functions on geometry

and topology of porous media, it seems that their methodology cannot be used for practical purposes.

- From a practical point of view, according to Al-Gharbi and Blunt (2005), the range of capillary numbers considered in the works of Payatakes and his co-workers are much larger than the range encountered in reservoir engineering; under small capillary numbers, mobilization of disconnected phase is not significant.

9.2. Outlook and Challenges

Compared to the extensive applications of quasistatic pore-network models, dynamic models have been developed and employed much less frequently. This has been due to strong numerical instability and tractability, computational costs, limited verification possibility in a three-dimensional domain, complexities of physics at pore level, and difficulties in casting the pore-level physics into network models. Some of the major issues that potentially can improve applicability of dynamic pore-network models are discussed subsequently.

Network geometry and topology: None of the dynamic pore-network models have been developed for natural porous media, which have complex topology and geometry. While complex quasistatic pore-network models with mixed-cross-sectional pores and unstructured irregular networks have been developed (e.g., Øren and Bakke, 2002), network structures of dynamic models are still quite simple.

Up to now, most works are dedicated to investigation of effect of dynamic parameters (capillary number and viscosity ratio) on dynamics of two-phase flow. Except for Mogensen and Stenby (1998), effect of network topology on dynamics of two-phase flow has never been studied. Although Mogensen and Stenby (1998) studied effect of coordination number on residual saturation under dynamic conditions, they did not provide any analysis how they have generated an irregular network (variable coordination number). Furthermore, they used only one realization of network for each coordination number distribution. It means that no analysis regarding the sensitivity of results to network generation is provided.

Computational costs: As we have explained, to compare results of dynamic network models with continuum-scale theories, the local entities should be averaged over the domain. However, The size of the pore network should be large enough to represent at least one REV size. The most common fashion for determining REV is to simulate capillary pressure – saturation (P^c-S^w) or relative permeability – saturation (k_r^α-S^w) curves in networks with different sizes for fixed statistical parameters. If with increase of the size of the network, the characteristic curves do not change significantly, that minimum size of network for those curves can represent the REV size. This issue was discussed in Joekar-Niasar et al. (2010b) in detail. In some

works such as Gielen et al. (2005); Joekar-Niasar et al. (2010b) the REV size for the pore network can be a cube with 30–35 pore bodies in each direction. However, one should note that with increase of variance of pore size distribution as well as the correlation length, the REV size will increase.

The analysis of REV size in many works is absent and as shown in Table 4, many dynamic network models are too small to provide results representative for REV scale or Darcy scale. For instance, the dynamic model developed by Al-Gharbi and Blunt (2005) had only 9×9 pore units. Thus their simulation results were highly influenced by boundary conditions. Another example of boundary effects on the results can be found in the work of Nordhaug et al. (2003) on the computation of interfacial velocity. There is a velocity overshoot at high saturations, which seems to be a boundary effect. Applying constant flux and fully periodic boundary conditions, applied by Constantinides and Payatakes (1996) and later on by Knudsen and Hansen (2002), can eliminate the effects of boundary and initial conditions on simulation results. However, since the simulations need to be continued until steady-state is reached, simulations may be too time-consuming.

The largest pore-network model run on a single-processor computer reported in the literature, using a dynamic pore-network model, has around 150000 nodes (Joekar-Niasar and Hassanizadeh, 2011) which has been used for capillary numbers from 10^{-5} to 10^{-7} and viscosity ratio of $M = 1$.

Furthermore, it should be noted that in most dynamic pore-network models, interfaces are not tracked within the pore throat. It means that the implicit assumption is made that the time associated with the pore throat filling is much smaller than the time required for pore body filling. Although this assumption may be valid for granular media, it is probably not reasonable for porous media with long pore throats. Tracking the interfaces within pore throats will be computationally too expensive. It should be noted that the simulation time of dynamic pore-network models is highly dependent on viscosity ratio and capillary number. Simulation of a capillary-dominated regime takes much more time compared with viscous fingering, and viscous fingering much more time than stable invasion (Joekar-Niasar et al., 2008). Up to now, no dynamic pore-network model has been developed for parallel computation. One of the major limitations of dynamic pore-network models is related to the pore filling residence time. Since at each time step, the minimum residence time is selected, one can guess why dynamic pore-network models are computationally too expensive. Adapting the discretized equations to be independent of local residence time, similar to the algorithm developed by Dahle et al. (2005), may improve the computational aspect of these model.

Limited possibility for direct comparison with experiments: As the reviewed works illustrate, none of the dynamic pore-network models has been validated against experiments in three-dimensional natural porous media. Monitoring local (pore-scale) real time measurements in three-dimensional

TABLE 4. Summary of the developed dynamic pore-network models and their applications, specifications

Model Developer	Structure	Network elements	Application	Boundary Condition	Dimension Size	Structure	Pressure solver
Aker et al. (1998 1998b)	2-D, S, R	Circular comp.	Drainage, flow regime patterns, front width as a function of *Ca*	Cons. Flux	60 × 80	A	one-pressure
Aker et al. (1998a)	2-D, S, R	Circular comp.	Drainage, Pressure field evolution with time, effect of trapping on permeabilities	Cons. Flux	60 × 80 40 × 40 25 × 35	A	one-pressure
Al-Gharbi and Blunt (2005)	2-D, S, R	Triangular comp.	Drainage, flow regime patterns, residual saturation vs. *Ca*	Cons. Flux	9 × 9	A	one-pressure
Blunt and King (1990)	2-D,3-D, Irr UnS., Iso.	Circular p.th. Spherical p.b.	Drainage, invasion patterns fractional flow vs. *Ca* and *M*, relative permeabilities	Cons. Flux	80000 in a sphere	B	one-pressure
Bravo et al. (2007)	2-D, S, R	Square p.th. No p.b.	Disconnected gas flow in oil flow	Cons. Flux	50 × 50	A	one-pressure
Chaouche et al. (1994)	2-D, S, R	Circular p.th. Spherical p.b.	Drainage, Effect of heterogeneity on saturation distribution	Cons. Flux	100 × 21 100 × 60	B	one-pressure
Constantinides and Payatakes (1991)	3-D, S, Dist.R.	Circular comp. dependency on topology	Imbibition, coalescence system dynamics	Cons. Flux	100 × 7 × 2	A	one-pressure
Constantinides and Payatakes (1996)	3-D, S, Dist.R.	Circular comp.	Imbibition, steady-state relative permeabilities vs. system dynamics	Cons. Flux	30 × 20 × 5	A	one-pressure
Dahle and Celia (1999)	3-D, S, R	Circular p.th. No p.b.	Drainage, P^c-S curve	Cons. Flux	17 × 17 × 29	A	one-pressure
Dias and Payatakes (1986a)	2-D, S, R	Circular comp.	Imbibition, effect of *Ca* and *M* on residual one-pressure saturation and interface dynamics	Cons. Flux	15 × 40	A	
Dias and Payatakes (1986b)	2-D, S, R	Circular comp.	Imbibition, effect of *Ca* and *M* on ganglia mobilization, stranding, and breakup	Cons. Flux	15 × 40	A	one-pressure

(Continued on next page)

TABLE 4. Summary of the developed dynamic pore-network models and their applications, specifications *(Continued)*

Model Developer	Structure	Network elements	Application	Boundary Condition	Dimension Size	Structure	Pressure solver
Ferer et al. (2005, 2004, 1993) Ferer and Smith (1994)	2-D, S,. R	Circular p.th. Spherical p.b.	Drainage, cross over invasion regimes	Cons. Flux.	90 × 300 96 × 640	A	one-pressure
Hughes and Blunt (2000)	2-D, 3-D, S, R	Angular p.th. Angular p.b.	Imbibition, effect of *Ca*, aspect ratio, contact angle, initial saturation on invasion regime and its pattern	Cons. Flux	128 × 128 20 × 20 × 20	B	one-pressure
Gielen et al. (2004, 2005)	3-D, S,. R	Circular p.th. Spherical p.b.	Drainage, nonequilibrium effects in phase pressures difference	Cons. Pres.	30 × 30 × 40 10 × 10 × 82	B	one-pressure
Joekar-Niasar et al. (2010a)	3-D, S., R	Square p.th. Cubic p.b.	Drainage, Non-equilibrium effects on phase pressures difference and interfacial area	Cons. Pres.	35 × 35 × 35	B	two-pressure
Joekar-Niasar and Hassanizadeh (2010)	3-D, S., R	Square p.th. Octahedon p.b.	Drainage & Imbibition, Non-equilibrium effects on phase pressures difference	Cons. Pres.	45 × 35 × 35	B	two-pressure
King (1987)	2-D, Uns., Irr	Circular p.th.	Drainage, Fractal nature of invasion front	Cons. Pres.	N.A.	A	one-pressure
Knudsen and Hansen (2002) Knudsen et al. (2002)	2-D, R, S	Circular comp.	Countercurrent flow, nonequilibrium relative permeabilities	Closed boundaries	20 × 40 40 × 80	A	one-pressure
Koplik and Lasseter (1985)	2-D, UnS., Irr	Circular p.th. Spherical p.b.	Imbibition, Effect of *Ca* on residual saturation, snap-off and piston-like movement	Cons. Flux	10 × 10	–	one-pressure
Lam and Horváth (2000)	2-D, S, R	Circular p.th., no p.b.	Imbibition, scaling fronts	Periodic boundaries	1000 × 200	A	one-pressure
Løvoll et al. (2005)	2-D, S, R	Circular p.th., no p.b.	Drainage, gravity and viscous forces on invasion pattern boundaries	Cons. Press.	N.A.	A	one-pressure

Mogensen and Stenby (1998)	3-D, S, Irr	Square p.th., Cubic p.b.	Imbibition, Effect of *Ca*,*M*, aspect ratio, coordination no., on snap-off & piston-like movement	Cons. Flux	25 × 25 × 25	C	one-pressure
Nguyen et al. (2004, 2006)	3-D, UnS, Irr	Triangular p.th. Cubic p.b.	Imbibition, effect of contact angle, *Ca*, aspect ratio on relative permeabilities	Cons. Flux.	12349 p.b. 26146 p.th.	C	one-pressure
Nordhaug et al. (2003)	3-D, S, R	Circular p.th. Spherical p.b.	Drainage, interface velocity for different regimes	Cons. Press.	10 × 10 × 50	B	one-pressure
Payatakes (1982)	2-D, S, R	Circular comp. Spherical p.b.	Imbibition, ganglia movement	Cons. Flux	15 × 30	A	one-pressure
Pereira et al. (1996)	2-D, S, R	Eye-shaped p.th. Spherical p.b	Drainage, three-phase flow	Cons. Press.	50 × 50	B	Three-phase pressure
Singh and Mohanty (2003)	3-D, S, R	Square p.th. Cubic p.b.	Drainage, Effect of *Ca* on residual saturation	Cons. Flux.	30 × 8 × 8	B.	one-pressure
Thompson (2002)	3-D, S, R	Angular. p.th. Cubic p.b	Imbibition, Effect flow rate on water invasion in paper	Cons. Flux.	2000		two-pressure
Touboul et al. (1987)	2-D, S, R	Circular p.th. Spherical p.b.	Drainage, Effect of pressure on fingering and stable movement	Cons. Flux.	100 × 100	A	one-pressure
Valvanides et al. (1998)	3-D, S, R	Circular comp.	Imbibition, large and small ganglia dynamics	Cons. Flux.	30 × 20 × 5	A	one-pressure
Van der Marck et al. (1997)	3-D, S, R	Circular p.th. Spherical p.b.	Drainage, Pressure field evolution vs. saturation	Cons. Flux.	25 × 25 × 2	B	one-pressure
Vizika et al. (1994)	3-D, S, R	Circular comp.	Imbibition, Effect of *M* and *Ca* on residual saturation	Cons. Flux.	12 × 5 × 2	A	one-pressure

S: Structure, UnS:Unstructured, R:Regular, Irr: Irregular, Comp.:composite, p.th.:pore throat, p.b.:pore body.

A: No pore body is assumed, resistance and volume are assigned only to pore throats.

B: No resistance is assigned to pore bodies and no volume is assigned to pore bodies.

C: Volume and resistance are assigned to either pore throats or pore bodies.

domains is still challenging and too difficult. Imaging techniques for obtaining real-time pore-scale information in which fluid interfaces are moving have yet to be developed. It seems that simulations can be only validated against measurements outside the porous media (such as outflow boundary pressures).

Complexities of physics of two-phase flow dynamics: Comparison between experiments and quasistatic simulations show that Young-Laplace equations can be used successfully to describe the invasion process where only capillary forces are dominant. However, different issues may be of importance under dynamic conditions. For instance, pore-scale simulations of a single tube show that dynamics of contact angle is important (e.g Blake and Haynes, 1969). Also, computational analyses have shown that inertia effect in highly dynamic conditions are important (e.g., Ridgway et al., 2002). Up to now, most dynamic models have employed the Washburn equation without inertia effects. These effects need to be incorporated in dynamic pore-network models for capturing pore-scale mechanisms, such as Haines jump.

ACKNOWLEDGEMENTS

The authors would like to acknowledge the reviewer, Dr. Rink van Dijke from Heriot-Watt University, for his very useful comments and suggestions. The authors are members of the International Research Training Group NUPUS, financed by the German Research Foundation (DFG) and The Netherlands Organization for Scientific Research (NWO). This research was financed by Utrecht Centre of Geosciences.

REFERENCES

Aker, E.K., Maloy, K.J., and Hansen, A. (1998b). Simulating temporal evolution of pressure in two-phase flow in porous media. *Physical Review E* 58, 2217–2226.

Aker, E., Maloy, J., Hansen A., and Batrouni, G.G. (1998a). A two-dimensional network simulator for two-phase flow in porous media. *Transport in Porous Media* 32, 163–186.

Al-Futaisi, A., and Patzek, T.W. (2003). Extension of hoshenkopelman algorithm to non-lattice environments. *Physica A* 321, 665–678.

Al-Gharbi, M.S., and Blunt, M.J. (2005). Dynamic network modeling of two-phase drainage in porous media. *Physical Review E* 71, 016308–016308.

Avraam, D.G., Kolonis, G.B., Roumeliotis, T.C., Constantinides, G.N., and Payatakes, A.C. (1994). Steady-state two-phase flow through planar and non-planar model porous media. *Transport in Porous Media* 16, 75–101.

Avraam, D.G., and Payatakes, A.C. (1995). Flow regimes and relative permeabilities during steady-state two-phase flow in porous media. *Journal of Fluid Mechanics* 293, 207–236.

Avraam, D.G., and Payatakes AC. (1995a). Generalized relative permeability coefficients during steady-state, two-phase flow in porous media and correlation with the flow mechanisms. *Transport in Porous Media* 20, 135–168.

Avraam, D.G., and Payatakes, A.C. (1999). Flow mechanisms, relative permeabilities and coupling effects in steady-state two-phase flow in porous media. the case of strong wettability. *Industrial and Enginerring Chemistry Research* 38, 778–786.

Barenblatt, G., Patzek T., and Silin, D. (2003). The mathematical model of nonequilibrium effects in water-oil displacement. *SPE Journal* 8, 409–416.

Berentsen, C.W.J., and Hassanizadeh, S.M. (2006). *On the equivalence of measured and averaged pressures in porous media*. Paper presented at the 16th International Conference on Computational Methods in Water Resources, Copenhagen, Denmark.

Blake, T.D., and Haynes, J.M. (1969). Kinetics of liquid/liquid displacement. *Journal of Colloid and Interface Science* 30, 421–423.

Blunt, M.J. (2001). Flow in porous media—pore-network models and multiphase flow. *Current Opinion in Colloid & Interface Science* 6, 197–207.

Blunt, M., Jackson, M.D., Piri M., and Valvatne, P.H. (2002). Detailed physics, predictive capabilities and macroscopic consequences for pore-network models of multiphase flow. *Advances in Water Resources* 25, 1069–1089.

Blunt, M., and King, P. (1990). Macroscopic parameters from simulations of the pore scale flow. *Physical Review A* 42, 4780–4788.

Blunt, M., and King, P. (1991). Relative permeabilities from two- and three- dimensional pore- scale network modeling. *Transport in Porous Media* 6, 407–433.

Blunt, M., King P., and Scher, H. (1992). Simulation and theory of two-phase flow in porous media. *Physical Review A* 46, 7680–7702.

Blunt, M., and Scher, H. (1995). Pore-level modeling of wetting. *Physical Review E* 52, 6387–6403.

Bondino, I., McDougall S., and Hamon, G. (2009). A pore-scale modeling approach to the interpretation of heavy oil pressure depletion experiments. *Journal of Petroleum Science and Engineering* 65, 14–22.

Bosanquet, C.H. (1923). On the flow of liquids into capillary tubes. *Philosophical Magazine Series 6* 45, 525–531.

Bottero, S. (2009). *Advances in theories of capillarity in porous media*. PhD thesis, Utrecht University, the Netherlands.

Bottero, S., and Hassanizadeh, S.M. (2006). *Experimental and numerical study to investigate dynamic capillary pressure effect in two-phase flow in porous media*. Paper presented at the 16th International Conference on Computational Methods in Water Resources, Copenhagen, Denmark.

Bravo, M.C., Araujo M., and Lago, M.E. (2007). Pore network modeling of two-phase flow in a liquid-(disconnected) gas system. *Physica A* 375, 1–17.

Brooks, R.H., and Corey, A.T. (1964). *Hydraulic properties of porous media*. Tech. Rep. Hydrol. Pap. No. 3, Colorado State University.

Camps-Roach, G., O'Carroll, D.M., Newson, T.A., Sakaki T., and Illangasekare, T.H. (2010). Experimental investigation of dynamic effects in capillary pressure: Grain size dependency and upscaling. *Water Resources Research* 46, W08544.

Celia, M.A., Reeves, P.C., and Ferrand, L.A. (1995). Recent advances in pore scale models for multiphase flow in prous media. *Reviews of Geophysics* 33, 1049–1058.

Chaouche, M., Rakotomalala, N., Salin, D., Xu, B., and Yortsos, Y.C. (1994). Capillary effects in drainage in heterogeneous porous media: continuum modeling, experiments and pore network simulations. *Chemical Engineering Science* 49, 2447–2466.

Chen, J.D., and Wilkinson, D. (1985). Pore-scale viscous fingering in porous media. *Physical Review Letters* 55, 1892–1896.

Constantinides, G.N., and Payatakes, A.C. (1991). A theoretical model of collision and coalescence of ganglia in porous media. *Journal of Colloid and Interface Science* 141, 486–504.

Constantinides, G.N., and Payatakes, A.C. (1996). Network simulation of steady-state two-phase flow in consolidated porous media. *AIChE Journal* 42, 369–382.

Constantinides, G.N., and Payatakes, A.C. (2000). Effects of precursor wetting films in immiscible displacement through porous media. *Transport in Porous Media* 38, 291–317.

Cormen, T.H., Leiserson, C.E., Rivest, R.L., and Stein, C. (2009). *Introduction to algorithms* (3rd ed.). Cambridge, MA: MIT Press.

Dahle, H.K., and Celia, M.A. (1999). A dynamic network model for two-phase immiscible flow. *Computational Geosciences* 3, 1–22.

Dahle, H.K., Celia, M.A., and Hassanizadeh, S.M. (2005). Bundle-of-tubes model for calculating dynamic effects in the capillary-pressure-saturation relationship. *Transport in Porous Media* 58, 5–22.

Das, D., Gauldie R., and Mirzaei, M. (2007). Dynamic effects for two-phase flow in porous media: Fluid property effects. *AIChE Journal* 53, 2505–2520.

Das, D.B., Mirzaei M., and Widdows, N. (2006). Non-uniqueness in capillary pressure–saturation–relative permeability relationships for two-phase flow in porous media: Interplay between intensity and distribution of random micro-heterogeneities. *Chemical Engineering Science* 61, 6786–6803.

Dias, M.M., and Payatakes, A.C. (1986a). Network models for two-phase flow in porous media part 1. immiscible microdisplacement of non-wetting fluids. *Journal of Fluid Mechanics* 164, 305–336.

Dias, M.M., and Payatakes, A.C. (1986b). Network models for two-phase flow in porous media part 2. motion of oil ganglia. *Journal of Fluid Mechanics* 164, 337–358.

DiCarlo, D.A. (2006). Quantitative network model predictions of saturation behind infiltration fronts and comparison with experiments. *Water Resource Research* 42, W07408.

Du, C., and Yortsos, Y. (1999). A numerical study of the critical gas saturation in a porous medium. *Transport in Porous Media* 35, 205–225.

Dullien, F.A.L. (1992). *Porous media: Fluid transport and pore structure*. (2nd Rev. ed.), San Diego, CA: Academic Press.

Entov, V.M. (1980). Theory of nonequilibrium effects associated with the flow of nonuniform fluids in porous media. *Fluid Dynamics* 15, 365–369.

Fatt, I. (1956). The network model of porous media, i. capillary pressure characteristics. *Petroleum Trans. AIME* 207, 144–159.

Fenwick, D.H., and Blunt, M.J. (1998). Network modeling of three-phase flow in porous media. *SPE Journal* 3, 86–97.

Ferer, M., Bromhal, G.S., and Smith, D.H. (2005). Two-phase flow in porous media: Crossover from capillary fingering to compact invasion for drainage. *Physical Review E* 71, 026303.

Ferer, M., Ji, C., Bromhal, G.S., Cook, J., Ahmadi G., and Smith, D.H. (2004). Crossover from capillary fingering to viscous fingering for immiscible unstable flow:experiment and modeling. *Physical Review E* 70, 016303.

Ferer, M., Sams, W.N., Geisbrecht, R.A., and Smith, D.H. (1993). Crossover from fractal to compact flow from simulations of two-phase flow with finite viscosity ratio in two-dimensional porous media. *Physical Review E* 47, 2713–2723.

Ferer, M., and Smith, D.H. (1994). Dynamics of growing interfaces from the simulation of unstable flow in random media. *Physical Review E* 49, 4114–4120.

Fernández, J.F., Rangel R., and Rivero, J. (1991). Crossover length from invasion percolation to diffusion-limited aggregation in porous media. *Physical Review Letters* 67, 2958–2961.

Figus, C., Le Bray, Y., Bories S., and Prat, M. (1999). Heat and mass transfer with phase change in a porous structure partially heated continuum model and pore network simulations. *International Journal of Heat and Mass Transfer* 42, 2557–2569.

Frette, O.I., Måløy, K.J., J. S., and Hansen, A. (1997). Immiscible displacement of viscosity matched fluids in two-dimensional porous media. *Physical Review E* 55, 2969–2975.

Fulcher, R.A., Ertekin, T., and Stahl, C.D. (1985). Effect of capillary number and its constituents on two-phase relative permeability curves. *Journal of Petroleum Technology* 37, 249–260.

Gielen, T.W.J. (2007). *Upscaling multiphase transport processes in porous media*. PhD thesis, Delft University of Technology, Delft, the Netherlands.

Gielen, T., Hassanizadeh, S.M., Celia, M.A., Dahle, H.K., and Leijnse, A. (2004). *A pore-scale network approach to investigate dynamic effects in multiphase flow*. Paper presented at the XVth International Conference on Computational Methods in Water Resources (CMWR XV). Chapel Hill, NC, USA.

Gielen, T., Hassanizadeh, S.M., Leijnse A., and Nordhaug, H.F. (2005). Dynamic effects in multiphase flow: A pore-scale network approach. In D.B. Das and H.S.M. (eds.), *Upscaling multiphase flow in porous media*, Amsterdam, the Netherlands: Springer (pp. 217–236).

Hashemi, M., Dabir B., and Sahimi, M. (1999). Dynamics of two-phase flow in porous media: Simultaneous invasion of two fluids. *AIChE Journal* 45, 1365–1382.

Hassanizadeh, S., Celia M., and Dahle, H. (2002). Dynamic effects in the capillary pressure-saturation relationship and their impacts on unsaturated flow. *Vadose Zone Journal* 1, 38–57.

Hassanizadeh, S.M., and Gray, W.G. (1990). Mechanics and thermodynamics of multiphase flow in porous media including interphase boundaries. *Advances in Water Resources* 13, 169–186.

Hassanizadeh, S.M., and Gray, W.G. (1993). Thermodynamic basis of capillary pressure in porous media. *Water Resources Research* 29, 3389–3405.

Hassanizadeh, S.M., Oung, O., and Manthey, S. (2004). Laboratory experiments and simulations on the significance of non-equilibrium effect in the capillary

pressure-saturation relationship. In T. Schanz (ed.), *Unsaturated soils: Experimental studies. Proceedings of the International Conference: From experimental evidence towards numerical modeling of unsaturated soils* (vol. 1). Berlin, Germany: Springer Verlag.

Held, R.J., and Celia, M.A. (2001). Modeling support of functional relationships between capillary pressure, saturation, interfacial area and common lines. *Advances in Water Resources* 24, 325–343.

Herderson, G., Danesh A., and Tehrani, D. (2001). Effect of positive rate sensitivity and inertia on gas condensate relative permeability at high velocity. *Petroleum Geoscience* 7, 45–50.

Hinkley, R.E., Dias, M.M., and Payatakes, A.C. (1987). On the motion of oil ganglia in porous media. *Physicochemical Hydrodynamics* 8, 185–211.

Horváth, V.K., and Stanley, H.E. (1995). Temporal scaling of interfaces propagating in porous media. *Physical Review E* 52, 5166–5169.

Hughes, R.G., and Blunt, M.J. (2000). Pore scale modeling of rate effect in imbibition. *Transport in Porous Media* 40, 295–322.

Impey, M.D., Grindrod, P., Takase H., and Worgan, K.J. (1997). A capillary network model for gas migration in low-permeability media. *SIAM Journal on Applied Mathematics* 57, 597–608.

Jamiolahmady, M., Danesh, A., Tehrani D., and Duncan, D. (2003). Positive effect of flow velocity on gascondensate relative permeability: Network modeling and comparison with experimental results. *Transport in Porous Media* 52, 159–183.

Joekar-Niasar, V., and Hassanizadeh, S.M. (2011). Specific interfacial area: the missing state variable in two-phase flow equations?, *Water Resources Research* 47, w05513; DOI: 10.1029/2010 WR009291.

Joekar-Niasar, V., and Hassanizadeh, S.M. (2011). Effect of fluids properties on non-equilibrium capillarity effects; dynamic pore-network modeling. *International Journal of Multiphase Flow* 37, 198–214.

Joekar-Niasar, V., Hassanizadeh, S.M., and Dahle, H.K. (2010a). Non-equilibrium effects in capillarity and interfacial area in two-phase flow: Dynamic pore-network modeling. *Journal of Fluid Mechanics* 655, 38–71.

Joekar-Niasar, V., Hassanizadeh, S.M., and Leijnse, A. (2008). Insights into the relationships among capillary pressure, saturation, interfacial area and relative permeability using pore-network modeling. *Transport in Porous Media* 74, 201–219.

Joekar-Niasar, V., Hassanizadeh, S.M., Pyrak-Nolte, L.J., and Berentsen, C. (2009). Simulating drainage and imbibition experiments in a high-porosity micromodel using an unstructured pore network model. *Water Resources Research* 45, W02430.

Joekar-Niasar, V., Prodanović M, Wildenschild, D., Hassanizadeh SM. (2010b). Network model investigation of interfacial area, capillary pressure and saturation relationships in granular porous media. *Water Resources Research* 46, W06526.

Kalaydjian, F., and Marle, C.M. (1987). Thermodynamic aspects of multiphase flow in porous media. *Collection colloques et séminaires—Institut français du pétrole* 45, 513–531.

King, P.R. (1987). The fractal nature of viscous fingering in porous media. *Journal of Physics.A, Mathematical and General* 20, L529–L534.

Knudsen, H.A., Aker E., and Hansen, A. (2002). Bulk flow regimes and fractional flow in 2d porous media by numerical simulations. *Transport in Porous Media* 47, 99–121.

Knudsen, H.A., and Hansen, A. (2002). Relation between pressure and fractional flow in two-phase flow in porous media. *Physical Review E* 65,1–10.

Knutson, C.E., Werth, C.J., and Valocchi, A.J. (2001). Pore-scale modeling of dissolution from variably distributed nonaqueous phase liquid blobs. *Water Resources Research* 37, 2951–2963.

Koplik J., and Lasseter, T.J. (1985). Two-phase flow in random network models of porous media. *Society of Petroleum Engineers Journal* 25, 89–110.

Lam, C., Horváth VK. (2000). Pipe network model for scaling of dynamic interfaces in porous media. *Physical Review Letters* 85, 1238–1241.

Lefebvre du Prey EJ. (1973). Factors affecting liquid-liquid relative permeabilities of a consolidated porous medium. *Society of Petroleum Engineering Journal*, Vol.13, DOI: 10.2118/3039-PA.

Lenormand, R. (1990). Liquids in porous media. *Journal of Physics: Condensed Matter* 2, SA79–SA88.

Lenormand, R., Touboul E., and Zarcone, C. (1988). Numerical models and experiments on immiscible displacements in porous media. *Journal of Fluid Mechanics* 189, 165–187.

Lerdahl, T.R., Øren, P.E., and Bakke, S. (2000). *A predictive network model for three-phase flow in porous media*. Paper presented at the SPE Symposium on Improved Oil Recovery. Tulsa, OK.

Lewalle, J., Singh K., and Bambacht, J. (1994). Analysis of the wet pressing of paper pulp. *International Journal of Multiphase Flow* 20, 415–437.

Liu, M., Meakin P., and Huang, H. (2006). Dissipative particle dynamics with attractive and repulsive particle-particle interactions. *Physics of Fluids* 18, 017101.

Løvoll, G., Méheust, Y., Maløy, K.J., Aker E., and Schmittbuhl, J. (2005). Competition of gravity, capillary and viscous forces during drainage in a two-dimensional porous medium, a pore scale study. *Energy* 30, 861–872.

Lu, T., Nielsen D., and Biggar, J. (1995). Water movement in glass bead porous media. 3. theoretical analysis of capillary rise into initially dry media. *Water Resources Research* 31, 11–18.

Ma, S., Mason G., and Morrow, N.R. (1996). Effect of contact angle on drainage and imbibition in regular polygonal tubes. *Colloids and Surfaces A* 117, 273–291.

Manthey, S., Hassanizadeh, S.M., and Helmig, R. (2005). Macroscale dynamic effects in homogeneous and heterogeneous porous media. *Transport in Porous Media* 58, 121–145.

Manthey, S., Hassanizadeh, S.M., Oung O., and Helmig, R. (2004). *Dynamic capillary pressure effects in two-phase flow through heterogeneous porous media*. Paper presented at the 15th International Conference on Computational Methods in Water Resources, Chapel Hill, North Carolina, USA.

Martys, N.S., and Hagedorn, J.G. (2002). Multiscale modeling of fluid transport in heterogenous material using discrete bolzmann methods. *Materials and Structures* 35, 650–659.

Mason, G., and Morrow, N.R. (1991). Capillary behavior of a perfectly wetting liquid in irregular triangular tubes. *Journal of Colloid and Interface Science* 141, 262–274.

Mayer, R.P., and Stowe, R.A. (1965). Mercury porosimetry-breakthrough pressure for penetration between packed spheres. *Journal of Colloid Science* 20, 891–911.

Mirzaei, M., and Das, D.B. (2007). Dynamic effects in capillary pressure-saturations relationships for two-phase flow in 3d porous media: Implications of microheterogeneities. *Chemical Engineering Science* 62, 1927–1947.

Mogensen K., and Stenby, E.H. (1998). A dynamic two-phase pore-scale model for imbibition. *Transport in Porous Media* 32, 299–327.

Ng, K.M., and Payatakes, A.C. (1980). Stochastic simulation of the motion, breakup and stranding of oil ganglia in water-wet granular porous media during immiscible displacement. *AIChE Journal* 26, 419–429.

Nguyen, V.H., Sheppard, A.P., Knackstedt, M.A., and Pinczewski, W.V. (2004). A dynamic network model for imbibition. *SPE Annual Technical Conference and Exhibition*, 26–29 September 2004, Houston, Texas, USA.

Nguyen, V.H., Sheppard, A.P., Knackstedt, M.A., and Pinczewski, W. (2006). The effect of displacement rate on imbibition relative permeability and residual saturation. *Journal of Petroleum Science & Engineering* 52, 54–70.

Nordhaug, H.F., Celia M., and Dahle, H.K. (2003). A pore network model for calculation of interfacial velocities. *Advances in Water Resources* 26, 1061–1074.

O'Carroll, D.M., Phelan, T.J., and Abriola, L.M. (2005). Exploring dynamic effects in capillary pressure in multistep outflow experiments. *Water Resources Research* 41, W11419.

Øren, P.E., and Bakke, S. (2002). Process based reconstruction of sandstones and prediction of transport properties. *Transport in Porous Media* 46, 311–343.

Øren, P.E., Bakke S., and Arntzen, O.J. (1998). Extending predictive capabilities to network models. *SPE Journal* 3, 324–336.

Oung, O., Hassanizadeh, S.M., and Bezuijen, A. (2005). Two-phase flow experiments in a geocentrifuge and the significance of dynamic capillary pressure effect. *Journal of Porous Media* 8, 247–257.

Pan, C., Hilpert M., and Miller, C.T. (2004). Lattice-boltzmann simulation of two-phase flow in porous media. *Water Resources Research* 40, W01501.

Patzek, T.W., and Silin, D.B. (2001). Shape factor and hydraulic conductance in noncircular capillaries: I. one-phase creeping flow. *Journal of Colloid and Interface Science* 236, 295–304.

Payatakes, A.C. (1982). Dynamics of oil ganglia during immiscible displacement in water-wet porous media. *Ann. Review Fluid Mechanics* 14, 365–393.

Payatakes, A.C., Ng, K.M., and Flumerfelt, R.W. (1980). Oil ganglion dynamics during immiscible displacement: model formulation. *AIChE Journal* 26, 430–442.

Pereira, G.G., Pinczewski, W.V., Chan DYC, Paterson, L., and Øren PE. (1996). Pore-scale network model for drainage-dominated three-phase flow in porous media. *Transport in Porous Media* 24, 167–201.

Porter, M.L., Schaap, M.G., and Wildenschild, D. (2009). Lattice-boltzmann simulations of the capillary pressure-saturation-interfacial area relationship for porous media. *Advances in Water Resources* 32, 1632–1640.

Prat, M. (2007). On the influence of pore shape, contact angle and film flows on drying of capillary porous media. *International Journal of Heat and Mass Transfer* 50, 1455–1468.

Princen, H.M.J. (1969a). Capillary phenomena in assemblies of parallel cylinders i. Capillary rise between two cylinders. *Colloid and Interface Science* 30, 69–75.

Princen, H.M.J. (1969b). Capillary phenomena in assemblies of parallel cylinders ii. Capillary rise in systems with more than two cylinders. *Colloid and Interface Science* 30, 359–371.

Princen, H.M.J. (1970). Capillary phenomena in assemblies of parallel cylinders iii. Liquid columns between horizontal parallel cylinders. *Colloid Interface Science* 34, 171–184.

Prodanović, M., and Bryant, S.L. (2006). A level set method for determining critical curvatures for drainage and imbibition. *Journal of Colloid and Interface Science* 304, 442–458.

Ransohoff, T.C., and Radke, C.J. (1988). Laminar flow of a wetting liquid along the corners of a predominantly gas-occupied noncircular pore. *Journal of Colloid and Interface Science* 121, 392–401.

Rapin, S. (1980). *Behavior of non-wetting oil ganglia displaced by an aqueous phase*. Master's thesis, University of Houston, Houston, Texas.

Reeves, P.C., and Celia, M.A. (1996). A functional relationship between capillary pressure, saturation, and interfacial area as revealed by a pore-scale network model. *Water Resources Research* 32, 2345–2358.

Ridgway, C.J., Patrick A.C.G., and Schoelkopf, J. (2002). Effect of capillary element aspect ratio on the dynamic imbibition within porous networks. *Journal of Colloid and Interface Science* 252, 373–382.

Roof, J.G. (1970). Snap-off of oil droplets in water-wet pores. *SPE Journal* 10, 85–90.

Sheludko, A. (1967). Thin liquid films. *Advances in Colloid Interface Science* 1, 391–464.

Singh, M., and Mohanty, K.K. (2003). Dynamic modeling of drainage through three-dimensional porous materials. *Chemical Engineering Science* 58, 1–18.

Sinha, P.K., and Wang, C. (2007). Pore-network modeling of liquid water transport in gas diffusion layer of a polymer electrolyte fuel cell. *Electrochimica Acta* 52, 7936–7945.

Sorbie, K.S., Zhang, H.R., and Tsibuklis, N.B. (1995). Linear viscous fingering: New experimental results, direct simulation and the evaluation of averaged models. *Chemical Engineering Science* 50, 601–616.

Stauffer, F. (1978). Time dependence of the relations between capillary pressure, water content and conductivity during drainage of porous media. Proceeding of Symposium of International Association for Hydro-Environment Engineering (IAHR). Thessaloniki, Greece.

Tartakovsky, A., and Meakin, P. (2005). Simulation of unsaturated flow in complex fractures using smoothed particle hydrodynamics. *Vadose Zone Journal* 4, 848–855.

Thompson, K.E. (2002). Pore-scale modeling of fluid transport in disordered fibrous materials. *AIChE Journal* 48, 1369–1389.

Touboul, E., Lenormand R., and Zarcone, C. (1987). Immiscible displacements in porous media: Testing network simulators by micromodel experiments. *SPE Annual Technical Conference and Exhibition* 27–30.

Valvanides, M.S., Constantinides, G.N., and Payatakes, A.C. (1998). Mechanistic model of steady-state two-phase flow in porous media based on ganglion dynamics. *Transport in Porous Media* 30, 267–299.

Valvanides, M.S., and Payatakes, A.C. (2001). True-to-mechanism model of steady-state two-phase flow in porous media, using decomposition into prototype flows. *Advances in Water Resources* 24, 385–407.

Van der Marck, S.C, Matsuura T., and Glas, J. (1997). Viscous and capillary pressures during drainage: Network simulations and experiments. *Physical Review E* 56, 5675–5687.

van Dijke, M.I.J., and Sorbie, K.S. (2006). Existence of fluid layers in the corners of a capillary with non-uniform wettability. *Journal of Colloid and Interface Science* 293, 455–463.

Vidales, A.M., Riccardo, J.L., and Zgrabli, G. (1998). Pore-level modeling of wetting on correlated porous media. *Journal of Physics D, Applied Physics* 31, 2861–2868.

Vizika, O., Avraam, D.G., and Payatakes, A.C. (1994). On the role of viscosity ratio during low-capillary-number forced imbibition in porous media. *Journal of Colloid and Interface Science* 165, 386–401.

Vogel, H.J., and Roth, K. (2001). Quantitative morphology and network representation of soil pore structure. *Advances in Water Resources* 24, 233–242.

Wang, X., and Mohanty, K.K. (2000). Pore-network model of flow in gas/condensate reservoirs. *SPE Journal* 5, 426–434.

Wardlaw, N.C., and, Yu, L. (1988). Fluid topology, pore size and aspect ratio during imbibition. *Transport in Porous Media* 3, 17–34.

Wilkinson, D. (1984). Percolation model of immiscible displacement in the presence of the buoyancy forces. *Physical Review A* 30, 520–531.

Wilkinson, D. (1986). Percolation effects in immiscible displacement. *Physical Review A* 34, 1380–1391.

Zhou, D., Blunt, M.J., and Orr, F.M. (1997). Hydrocarbon drainage along corners of noncircular capillaries. *Journal of Colloid and Interface Science* 187, 11–21.